CELL ENVELOPE REGULATORY TWO-COMPONENT SYSTEMS IN *BRUCELLA OVIS*

By

Xingru Chen

A DISSERTATION

Submitted to
Michigan State University
in partial fulfillment of the requirements
for the degree of

Microbiology and Molecular Genetics – Doctor of Philosophy

2024

ABSTRACT

The bacterial cell envelope is a multi-layered structure that serves as a barrier between the interior of cells and the exterior environment. Accordingly, the envelope protects the cells from different physical and chemical stressors in the environment. Two-component signal transduction systems (TCS) are a common regulatory mechanism that bacteria use to control expression of genes that determine the cell envelope structure and function. A typical TCS consist of a histidine kinase that can sense certain signals from the environment and a response regulator that can bind to DNA and regulate gene expression. To identify TCS genes that are important for cell envelope regulation in the intracellular ovine pathogen, *Brucella ovis*, I generated a library of TCS mutants where I made in-frame deletions of all non-essential TCS genes and subjected the mutant library to several cell envelope stressors. Through this initial screen, I identified 9 TCS genes that are important for different aspects of cell envelope regulation.

Three of these TCS genes had similar phenotypes on all stress conditions tested. Through genetic, biochemical, and multi-omics analyses, I determined that CenR, a known cell envelope regulator, and EssR-EssS, a previously uncharacterized TCS pair, function in the same pathway and depend on one another for function and protein stability to regulate cell envelope integrity and support *B. ovis* replication in the intracellular niche. The two response regulators, CenR and EssR, interact via their receiver domains. This interaction is important for the protein stability of both proteins and serves to regulate the phosphorylation of EssR by its cognate histidine kinase, EssS. This is a novel regulatory mechanism for cross-regulation between TCSs.

My TCS mutant screen further revealed an uncharacterized HWE histidine kinase – BOV_1602 – that strongly impacted resistance to the detergent, SDS. Though, the cognate response regulator(s) of this kinase are unknown, RNA-seq studies and proteomic analysis of outer membrane protein fractions revealed that BOV_1602 regulates many genes with cell envelope functions and influences the outer membrane protein composition of *B. ovis*. I have further shown that BOV_1602 deletion influences cell shape and size. Combining genetics with

proteomics, I further present evidence that genes encoding the type IV secretion system and an SPFH protein, which are commonly found in lipid rafts, are regulated by BOV_1602 in a post-transcriptional manner and that both classes of these proteins contribute to detergent resistance.

ACKNOWLEDGEMENTS

First and foremost, I would like to thank Sean and Aretha for taking me in as a student, training me, and giving me the freedom to decide which TCS genes that I wanted to work on, which led to the discovery the CenR-EssRS system. I also want to thank them for always believing in me and for sharing their words of encouragement, especially Sean's famous quotes. I would like to give Aretha a special thanks for guiding me through the Next-generation sequencing and my first attempt at radioactive experiments.

I want to thank my thesis committee, Rob, Teresa, Steph, and Yann for their thoughtful inputs at every committee meeting. Their excitement for my project is such a good validation and motivation that helped me through my thesis work. Their suggestions have made me a better scientist and I am grateful for their support outside of committee meetings as well.

I could not have finished this thesis work without my wonderful and talented lab mates. They have answered so many questions and helped me with experiments over the years. I want to give especial thanks to my lab siblings, Hunter, Tom, and Sergio. We joined the lab around the same time and have gone through the same challenges together. Being in the office with all of you has been one of my favorite moments in graduate school.

I also have a network of friends outside of lab that I need to give thanks to. I could not have gone through graduate school without my roommate, Ana. For the past five years, we have shared so much personal growth and memories together. I also want to thank Ana's family for inviting me to their home when I couldn't go back to China during the pandemic. Christophe, I want to thank you for sharing so many adventures, long conversations, helping me taking care of Coco, and believing in me always. I want to thank my best friend, Roseann. Thank you for opening your farm to me and letting me live my farm girl dream. I also owe you many thanks for helping me throughout the last five years. I also want to thank my friends Morgen, Marcela, Noah, Morgan, Mackenzie, David, Jab, and Josh and many others for being good friends over the years, especially this last year. I also want to say a big thank you to MMG/MGI at MSU for letting me

grow and providing many opportunities for me to develop my organization skills and all the help and support from Jessica and Jessie.

I want to give a big shoutout to my dog and biggest supporter, Coco. She joined my PhD journey in the second year and has witnessed all my big milestones and breakdowns. She is a constant motivation and source of joy for me. She is also the one that forces me to take breaks and go for a walk, no matter the weather.

Lastly, I want to thank my family. Being literally on the other side of the world from all my family members is hard. It is even hard to not be able to go home for the first four years of graduate school. However, their constant support and love, despite the difficult time difference, made this journey less hard. I can’t express enough how grateful I am and how lucky I am tohave them as my family. I love you all.

TABLE OF CONTENTS

Chapter 1: Introduction

Bacteria, either free living or inside a host, are constantly encountering different signals from the environment and responding to them. For example, they need to sense nutrient level, pH, temperature, attacks from the host immune system, and many more. A common molecular mechanism that bacteria use to sense and respond to different signals is through the two-component signal transduction systems (TCS). In this dissertation, I specifically focus on TCSs that are important for maintaining the cell envelope in the facultative intracellular pathogen, *Brucella ovis,* as the cell envelope acts as a physical barrier between the bacterium and its outside environment. In this introductory chapter I will describe the genus *Brucella* and its unique cell envelope structure, different variations of TCS in *Brucella*, and will describe cell envelope stress regulatory systems that have been identified in other Gram-negative bacteria. In chapters two, three, and four I will describe the previously uncharacterized TCS genes that I have identified and demonstrated to be important for cell envelope regulation in *B. ovis*.

The genus *Brucella*

The genus *Brucella* are Gram-negative, intracellular pathogens that belong to the *Alphaproteobacteria* class. *Brucella* was first isolated by Sir David Bruce in 1877 as the causative agent of Malta Fever in humans (1), which now is referred to as Brucellosis. Symptoms of the disease often include fever, joint pain, weight loss among others. In severe cases, arthritis, endocarditis, and swelling of the liver and spleen can also occur. The genus *Brucella* consists of an evolving list of subspecies as new species are constantly being discovered. The six *Brucella* species that were first identified in animals are referred to as “the classical *Brucella* group.” They are determined based on their specific host tropism: *Brucella melitensis* (sheep and goats), *Brucella abortus* (cattle), *Brucella suis* (pigs), *Brucella ovis* (sheep), *Brucella canis* (dogs), and *Brucella neotomae* (desert rats). In recent years, at least seven more *Brucella* species have been isolated in infected animals including dolphins, seals, primates, and frogs, as well as human

breast implants (2). This shows how adaptable *Brucella* are at infecting a wide variety of hosts. Despite having specific host preferences, *Brucella* species have very high genome similarities, between 85-97% DNA similarity between species (3). How exactly the *Brucella*'s host preference is determined despite the highly similar genome Is not yet known, but researchers believe that differences in genome degradation, insertion/deletion due to mobile elements, SNPs (single nucleotide polymorphisms), and VNTR (variable number of tandem repeats) may play a role in host preference (3-5).

In my graduate work, I used the ovine facultative intracellular pathogen, *Brucella ovis,* as a model system to study TCS regulatory systems that regulate the *Brucella* cell envelope. *B. ovis* are only found in sheep and are the etiological agents of ovine epididymitis in rams and can also cause abortion in pregnant ewes. *B. ovis* can be transmitted sexually, through birth or contact with infected aborted fetus and placenta (Buddle, 1956). Infections in ewes are usually less persistent than in male sheep. It has been noted that infections usually do not last longer than a pregnancy or two months in the vagina while they are much harder to clear in rams and usually leave life-long effects on fertility.

Even though *B. ovis* shares a large portion of its genome with the other *Brucella* species, it stands out as an outlier for a few reasons. At the time of its discovery in the 1950s in New Zealand, *B. ovis* was thought as a "*Brucella* mutant" due to its "non-smooth type," which we now know is due to the lack of the O-chain on its lipopolysaccharide (LPS). *B. canis* is the only other *Brucella* species that also do not have an O-chain, making it and *B. ovis* the only two naturally "rough" species of *Brucella*. This is an important distinction because the O-chain is an important virulence factor in other smooth *Brucella* species. In fact, rough mutants of naturally smooth *Brucella* strains have shown high attenuation in infection models and show clinical potential as vaccine candidates (6-8). Additionally, *B. ovis* along with *B. neotomae* are the only two non-zoonotic species among the classical *Brucella* group while the other ones are considered either highly or moderately zoonotic and can infect humans (9-11). The third reason for *B. ovis* being an

outlier is that it shows a high level of genome degradation compared to the zoonotic *Brucella* species. There are 244 pseudogenes, 38 IS711 mobile elements, and 4 large deletions identified specifically in the *B. ovis* ATCC 25840 genome. Many of the pseudogenes encode various transporters, outer membrane proteins, enzymes involved in a range of metabolic processes (3, 12). Rearrangement of IS711 mobile elements lead to some gene disruption and a 25-kb genomic island on chromosome II in *B. ovis* that is not found in the any other classical *Brucella* species. Among the genes in the deletion regions are ones encoding glycosyltransferases that are essential for LPS biosynthesis, which is the cause for the rough LPS phenotype in *B. ovis*, which I will discuss more in detail below. Overall, despite sharing high genome similarity with the other classical *Brucella* species, *B. ovis* is an outlier due to its rough LPS, non-zoonotic capability and its high genome degradation.

The Intracellular life cycle of *Brucella*

The classical *Brucella* species infect domestic animals and the major routes of transmission include sexual intercourse, exposure to aborted fetus, semen from infected males, vaginal secretion from infected females, consumption of contaminated milk and *in utero* (13). Once inside the host, *Brucella* reside in professional and non-professional phagocytes through phagocytosis (14). Upon entry into a host cell, *Brucella* reside in *Brucella*-containing vacuoles (BCVs), which interact with the early endosome, late endosome, and partially fuse with the lysosome to eventually form endosomal BCVs (eBCVs). As the BCVs mature to eBCVs, which is within the first 8 hours of infection, pH decreases to around pH 4-4.5, which induces expression of the type IV secretion system (T4SS) in *Brucella* (15). *Brucella* does not start its replication Inside the eBCVs. The development of T4SS promotes further maturation of the BCV into the replicative BCVs, (rBCVs) which interact with endoplasmic reticulum and has a slight acidic to neutral pH. This occurs around 8-12 hours post entry and is where *Brucella* replicates (16). Lastly, autophagic BCVs (aBCVs) form from rBCVs and promotes the last step of the Brucella intracellular life cycle through bacterial egress (13, 14, 16).

The *Brucella* LPS

The LPS of Gram-negative bacteria is made of three components: lipid A, core oligosaccharide, and O-polysaccharide chain. Lipid A contains various lengths of fatty acids and is the LPS anchor to the outer membrane due to its hydrophobicity. It is also referred to as endotoxin and it is the component recognized by Toll-like receptor 4 (TLR-4) (17). In many bacteria, such as *Escherichia coli*, lipid A is composed of C12-C14 fatty acids and glucosamine backbone sugars. However, the *Brucella* lipid A is made of diaminoglucose backbones and very long chain fatty acids (VLCFAs), ranging from C16 to C28 (18, 19). This unique structure makes it bulkier than lipid A In other bacteria and It Induces less host Innate Immune response than other gram-negative bacteria (20). The core oligosaccharide is made of sugars that covalently link lipid A and the O-polysaccharide chain. Although there are variabilities in the core polysaccharide among different species and strains in gram-negative bacteria, the 3-deoxy-D-manno-2-octulosonic acid (Kdo) sugar has been discovered as essential for Gram-negative bacterial viability and therefore highly conserved (21). *Brucella* has two Kdo sugars connecting to lipid A. Unlike other bacteria, *Brucella* has two branches in its core oligosaccharide stemming from each of the Kdo sugars, one connects to the O-PS and a side branch that does not (22). It has been shown that the side branch is important for hindering host immune recognition (23), survival inside the host, and resistance to complement and antimicrobial peptides (24). Lastly, the presence or absence of O-PS is what differentiates the smooth and rough species. In *Brucella*, unlike other bacteria, the smooth strains share high similarity in their O-PS composition, possibly due to their niche in the host (25). The Brucella O-PS is composed of N-formyl-perosamine (26). The genes involved in O-PS biosynthesis are in *wbo* and *wbk* genetic regions. *wboA* and *wboB* encode two O-PS glycosyltransferases and they are on a 15kb-genomic island on chromosome I that *B. ovis* lacks (3, 27). However, *B. canis*, the only other naturally rough *Brucella* species, has *wboA* and *wboB*. The *wbk* region includes genes that encode for perosamine synthesizing enzymes, O-PS glycosyltransferases, and genes for bactoprenol priming and O-PS translocation (28). Both

naturally rough strains have mutations in gene(s) involved in bactoprenol priming, but in different ways. *B. ovis* has a frameshift mutation in *wbkF* while *B. canis* has a deletion that expands between *wbkF* and *wbkD* (29). This difference in mutation(s) suggests that *B. ovis* and *B. canis* evolved into rough strains independently. Multiple studies have shown that the O-PS is an important component for protection in smooth strains against host complement and antimicrobial peptides as well as inhibition of fusion with lysosomes which is important for survival inside the host (30-32). Interestingly, the naturally rough strains have also shown resistance to complement and antimicrobial peptides (33), suggesting a different mechanism of resistance. Moreover, there have been instances where smooth strains spontaneously turn “rough” in both lab settings and infected animals (34, 35). This suggests that sometimes there are extra advantages for not having the O-PS, likely for energy conservation and lower detection from the host immune system.

The *Brucella* outer membrane proteins

Another key component of the cell envelope is the outer membrane proteins. As the name suggests, these are proteins located on the outer membrane of gram-negative bacteria. These proteins differ vastly in size and functions, and many have been studied for decades. It is known that they are important for outer membrane stability and some also provide protection against host immune system (36). It is also important to note that the composition of outer membrane proteins is different in each *Brucella* species, regardless of their LPS. In fact, outer membrane protein composition is used as a serological identification tool. A current hypothesis in the *Brucella* field is that the different outer membrane protein profiles could be a reason for different host preferences and difference in virulence. Martín-Martín and colleagues analyzed the major outer membrane proteins, Omp25 and Omp31, in the six classical *Brucella* species and found that the expression pattern is different in each of the six *Brucella* species. Moreover, they found that the composition of the outer membrane proteins does not depend on the presence or absence of the O-PS (33). For example, *B. ovis* and *B. canis* show different banding patterns for *omp31, omp25,* and *omp25c*, despite both being naturally rough strains (37). Additionally, not all outer membrane

proteins are expressed in each *Brucella* species. For example, in the conditions they tested, *B. ovis* does not express *omp25b*, *B. abortus* does not express omp31, and *B. canis* has very minimal expression of *omp31b, omp25c, omp25d*, and *omp22*.

In *B. ovis*, due to its lack of the O-polysaccharide chain, the outer membrane proteins are more exposed at the bacterial surface and to the extracellular environment. In the Martín-Martín et al. study from 2011, they showed that the six classical *Brucella* species have different outer membrane-related properties. For example, *B. ovis* is more sensitive to detergents whereas *B. abortus* is more sensitive to polymyxin B (33), which is a cationic antimicrobial peptide that targets the outer membrane. There are also differences in sensitivity to acidic pH, non-immune human serum, and hydrogen peroxide among the six species. The sensitivity does not correlate with their LPS phenotype, suggesting that these cell membrane-related phenotypes are not related to the O-PS presence or absence (33).

The outer membrane proteins are not only Important for membrane Integrity and stability but also virulence. Studies have shown that Omp22 and Omp25d are required for entry and replication in murine macrophage for rough *Brucella* spp. (38) while they are not required in smooth strains (39). *B. ovis omp25d* and *omp22* mutants also have reduced spleen colonization in mice. Omp22 is also important for fitness during the stationary phase and protection to nonimmune serum (40).

B. ovis has mutations in two outer membrane protein-encoding genes: *omp2a* and *omp31* (3). Omp2a is one of the two Omp2 porins, along with Omp2b. *omp2a* and *omp2b* are the most variable outer membrane protein genes among the classical *Brucella* species and have been used for species identification (41). In *B. abortus* and *B. melitensis*, *omp2a* has around 100bp deletion in the middle of the gene, compared to *omp2b*. *omp2b* has been reported to be the only expressed gene of the two in lab settings (42). In *B. ovis,* instead of a deletion in the middle of the gene, omp2a has an early stop due to a nonsense mutation, making it 63-bp shorter than *omp2b*. The mutation in *omp31* is also a nonsense mutation that leads to a truncated protein.

Two-component signal transduction systems

Two-component signal transduction systems (TCSs) are a major mechanism that bacteria use to sense their environment and respond to them quickly and accordingly. In canonical TCS, there is a sensor histidine kinase (HK) and a response regulator (RR) (**Figure 1.1**). The HK usually autophosphorylates at the conserved histidine residue through ATP hydrolysis upon sensing an environmental cue. Next, it will transfer the phosphoryl group onto its cognate RR at a conserved aspartate residue. This phosphorylation of RR leads to its homodimerization and a switch to its active form. The homodimer of RR then binds to the target DNA and regulates gene expression in response to the stimulus.

Bacteria have evolved with their TCS genes. Almost all bacterial genomes encode some TCS proteins, ranging from just a few to hundreds. Oftentimes the RR and its interacting HK are encoded adjacent to each other on the genome, which makes it easier to identify cognate pairs. When surveying a large number of bacterial species, there seems to be a correlation between genome size and the number of TCS genes encoded (43). The bioinformatician, Michael Galperin has used the number of signal transduction proteins that a bacterial genome encodes as a measure for “bacterial IQ” (43). Due to the critical role that TCS plays in environmental sensing and regulation, it is not surprising that if a bacterium encounters constantly changing environments, it possesses more TCS genes in its genome. For example, *Myxococcus xanthus* is a soil bacterium with a complex life cycle that ranges from motile single cells to fruiting bodies and sporulation. Because soil are highly heterogenous and often have limited nutrients, *M. xanthus* also needs to sense nutrient levels and signals from its surrounding cells (44) to know when to become dormant. Due to its complex need to sense different signals and adjust to different lifestyles, *M. xanthus* has over 200 TCS genes in its genome (45), one of the highest number of TCS genes in a bacterial genome. In contrast, bacteria that tend to have a more constant and restricted environment have fewer TCS genes. For example, *Rickettsia 7ickettsia* is an obligate intracellular pathogen and only has less than 10 TCS genes. As a facultative

intracellular pathogen, *B. ovis* contains 47 TCS genes in its genome (Genbank accessions NC_009504 and NC_009505). 20 of those encode genes encode histidine kinases, 22 encode response regulators, one encodes a histidine kinase-response regulator hybrid, one encodes a histidine phosphotransferase, and three are pseudogenes due to either a frameshift or nonsense mutation. Notably, 9 of the 47 TCS genes in *B. ovis* are considered essential based on TN-seq data from our lab (46). These make up about 20% of the TCS genes and most of them are important for *Brucella* cell cycle and development and pathogenesis.

Histidine kinases

The overall role for a histidine kinase is to sense a specific signal and either activated or inactivated the cognate response regulator. A typical HK has a sensor domain, a dimerization and histidine phosphotransfer (DHp) domain, and a catalytic ATP-binding (CA) domain (47). Usually, HK proteins function as homodimers. Upon sensing a signal in the sensor domain, each of the two HK monomers will induce phosphorylation at the conserved histidine residue in the DHp domain, in either a *cis*- or *trans*- manner. This process is called the autophosphorylation of HK and it is regulated by ATP hydrolysis of the terminal phosphate group, the γ-phosphate (48). The HK will then transfer the phosphate onto its cognate RR at the conserved aspartate residue and triggers downstream gene regulation. It is important to note that most HKs have both phosphoryl transfer and phosphatase activities. The ability to do both is critical for turning on and shutting off the system quickly.

Most but not all of the orthodox HKs have periplasmic membrane bound sensor domains. In fact, in *B. ovis*, 15 out of 20 HKs are membrane bound (Table 1). There are some HKs that possess additional transmembrane and cytoplasmic sensory domains for their specific functions. For example, putative-ligand sensing (PAS) domains are a common accessory domain in HKs. Depending on the specific types of PAS domains, they can sense changes in light, redox potential, oxygen, and other small ligands (49). In *B. ovis*, 5 HKs (PleC, NtrY, PdhS, DivL, LovhK) and a hybrid HK-RR (CckA) each has a PAS domain.

There are also some extracellular sensory domains found in many types of receptor proteins, including HKs. One common one is the CHASE (cyclase/histidine kinase-associated sensing extracellular) domain. Zhulin and colleagues have discovered and subcategorized different classes of CHASE domains based on their amino acid sequences (50). In *B. ovis*, PhyT has a CHASE3 domain, which is commonly found in HKs and adenylate cyclase (50). Studies done in another Alphaproteobacterial species, *Sphingomonas melonis*, and in the Gammaproteobacterium *Pseudomonas putida* have shown that CHASE3 is a salt sensor (51, 52). However, studies have yet to be done on CHASE3 in PhyT to examine whether it is also a salt sensor. Another common extracellular sensory domain in HKs is CACHE (Ca2+ channel, chemotaxis receptors) domain. In *B. ovis*, BOV_0357 has a CACHE domain but its function is unknown.

Another atypical HK family that are found in *B. ovis* is the HWE (histidine- tryptophan-glutamine) HK family. HWE HKs share similarities with typical HKs as they also contain DHp and CA domains. However, there are conserved motifs that are unique to HWE HKs – Histidine (H) in the N-box and tryptophan-glutamine (WE) near the G1 box of the CA domain (53, 54). Studies on multiple HWE HKs in different species have shown that these HKs form unusual oligomeric state; some function as monomers while some function as hexamers (55, 56). It is also believed that HWE HKs usually do not follow the typical phosphorylation and direct downstream gene regulation pathway. Instead, the pathways are usually multi-component and the RRs involved tend to have non-DNA binding functions, such as binding to anti-sigma factor (PhyR), which I will describe more in detail below. Lastly, many of the HWE HKs found in Alphaproteobacteria are in the general stress response (GSR) regulatory pathway (53, 57, 58). There are three HWE HKs in *B. ovis*: BOV_1602, BOV_1607, and LovhK. LovhK is shown to be part of the GSR and phosphorylates PhyR (59). BOV_1602 and BOV_1607 were not characterized/ their pathways are unknown. In chapter 3 I will discuss how BOV_1602 is important for detergent resistance in *B. ovis*.

Response Regulators

The overall role of a response regulator is to regulate gene expression according to the upstream signal from its cognate HK (60). A typical RR catalyzes the phosphoryl transfer from its phosphorylated cognate HK. Once phosphorylated, the RR is in its active state and undergoes a conformational change that promotes homodimerization. The homodimers bind to its target DNA and regulate downstream gene expression, which usually is the last step of the two-component signal transduction system. Dephosphorylation of RRs is important for turning off the response when needed. Usually, the phosphate group gets transferred to water (61). Sometimes, phosphatases also facilitate the dephosphorylation of RRs.

A typical RR is cytoplasmic and has a receiver domain and a DNA binding domain. Typically, phosphates are transferred from the histidine residue on HKs onto the aspartate residue in the receiver domain of the cognate RRs. This reaction usually happens within seconds between cognate pairs. However, sometimes RRs can also be phosphorylated by small molecule phosphor donors, such as acetyl phosphate, carbamoyl phosphate, imidazole phosphate, and phosphoramidate (62).

Some RRs do not have a DNA-binding domain and therefore, do not directly regulate gene expression. In *B. ovis*, there are four single-domain RRs (SDRRs) (BOV_0099, PhyR, CpdR, DivK), and PleD has a receiver domain and a diguanylate cyclase (GGCEF) domain instead of a DNA binding domain. DivK is involved in the CckA-CtrA multi-component master cell cycle regulatory system. When phosphorylated, DivK sequesters DivL and prevents it from interacting with CckA (63) and initiating the phosphorelay, which I will discuss further below. CpdR is also a part of this system. Instead of binding to DNA, CpdR binds to two other proteins, PopA and RcdA, and regulates CtrA proteolysis. PhyR is another SDRR in *B. ovis* and it is a key component of the alphaproteobacterial general stress response. It possesses a sigma-like domain. Upon activation, PhyR sequesters the anti-sigma factor, NepR, and releases the sigma factor, RpoE1 and allows it to regulate gene expression (64).

Overall, RRs have diverse activities and functions. In Chapter 3 of my thesis, I describe a novel interaction between two RRs, CenR and EssR, along with detailing the mechanism of their interaction and exploring the impact of this interaction on gene regulation in *B. ovis*.

Hybrid histidine kinase and phosphotransferase

As I mentioned above, some signal transduction systems require more than two components and sometimes there are phosphorelays between the proteins. Hybrid histidine kinases (HHKs) and phosphotransferases (HPTs) are often found in these multi-component signal transduction systems. HHKs as the name suggests, is a hybrid between histidine kinase and response regulator and has features of both proteins. In *B. ovis*, there are two HHKs, PrlS and CckA, though *prlS* is a pseudogene due to a frameshift mutation that leads to an early stop codon in the sequence.

HPTs usually act as a shuttle that transfers phosphate groups from one protein to another. They can either act as monomers, such as ArcB in *E. coli* (65), or dimers that resemble histidine kinases, such as Spo0B in *Bacillus subtilis* (66). Even though some HPTs contain a CA domain, no ATP binding activities have been observed from any HPTs (67). In *B. ovis*, there is only one HPT, ChpT, which is part of the CckA-CtrA system (68).

The CckA-CtrA pathway is the master cell cycle regulatory system that is conserved in the Alphaproteobacteria family, and it requires phosphorelays with multiple players. DivL is a histidine kinase and upon localization to CckA, it activates the kinase activity of CckA. CckA is an HHK that has both a kinase domain and a receiver domain. CckA first autophosphorylates in the DHp domain and transfers the phosphate onto its receiver domain. Then the phosphate gets passed on to the DHp domain of an HPT, ChpT. ChpT then transfers the phosphate group to two RRs, CtrA and CpdR (63, 68).

Cell envelope stress regulation in Gram-negative bacteria

The Gram-negative cell envelope is a powerful structure that protects the cells from toxins, antibiotics, and many environmental stresses. The bacteria also are equipped with many other

regulatory systems to respond to various kinds of cell envelope stresses, such as changes in temperature, pH and osmolarity, antimicrobial peptides, toxic metals, oxidative stress, and intrinsic stresses that affect the cell envelope. There have been extensive studies on the mechanism of these regulatory systems, and I will provide a brief summary of 5 major systems, RpoE, Cpx, Rcs, Psp, and OmpR/EnvZ.

The RpoE response

σ^E, also known as the envelope stress sigma factor, responds to the outer membrane stress from misfolded OMPs and mutated LPS (69, 70). In the absence of misfolded OMPs in the periplasm, σ^E is bound to the cytoplasmic domain of its anti-sigma factor, RseA, and is inhibited from interacting with RNA polymerase (71). RseA is an inner membrane protein, with a periplasmic domain, a transmembrane domain, and a cytoplasmic domain. In the non-activating state, RseA also binds to RseB in the periplasm, and this complex prevents another protease, RseP from degrading RseA (72, 73). In the presence of misfolded OMPs, the inner membrane-bound protease, DegS undergoes a conformational change after sensing the unfolded proteins. This will cause DegS to cleave the periplasmic portion of RseA and RseP to cleave the transmembrane portion of RseA, which then releases σ^E. The free σ^E can then bind to RNA polymerase to upregulate OMP folding pathways, genes encoding periplasmic protease to increase protein degradation of unfolded OMPs, LPS biogenesis and transportation, and repress OMP translation to halt more OMP production before homeostasis is restored.

Cpx response

CpxAR (conjugative plasmid expression) is a canonical two-component system that responds to inner membrane stresses (74) and it is important for resistance to many antibiotics (75, 76). CpxAR is activated through a variety of stresses, such as unfolded IMPs (inner membrane proteins), changes in osmolarity (77), pH (78), and phospholipid composition (79), exposure to ethanol and copper, defects in peptidoglycan synthesis, etc.. CpxA, the histidine kinase, detects the stress signal(s) and activates its cognate response regulator, CpxR through

phosphorylation. Next, CpxR binds to promoters of genes and regulates gene expression. Studies have shown that CpxAR upregulates genes involved in protein folding and degradation of misfolded proteins, peptidoglycan modification, efflux pumps to pump out toxins (80, 81). On the other hand, CpxAR represses expression of non-essential IMPs, such as the respiratory proteins, NADH dehydrogenase I and cytochrome bo3 for better adaptation of envelope stresses (82).

Rcs response

Rcs (regulator of capsule synthesis) is a TCS that senses and responds to changes in membrane structure and biogenesis (83). Unlike traditional TCS, Rcs has multiple components. RcsF, a lipoprotein, is bound to the outer membrane and can detect membrane defects. RcsC, the histidine kinase, can then phosphorylate the response regulator, RcsB. RcsB can either form a homodimer or a heterodimer with RcsA and regulate transcription. The regulons are different for the homodimers and heterodimers. RcsB-RcsB homodimer upregulates a small RNA, RprA, which increases the translation of the stationary-phase sigma factor, RpoS (84). RcsB-RcsA heterodimer upregulates genes involved in EPS and represses genes involved in motility (85).

Psp response

The Phage Shock Protein (Psp) response is a multi-protein system that responds to inner membrane damages, which could be a result of many different stresses, such as heat shock, ethanol exposure, detergent treatment, and increase in pH and osmolarity (86) or mislocalized secretins (87). PspB and PspC form an inner membrane complex and once they detect inner membrane damages, PspA is sequestered to the inner membrane complex and PspF upregulated *psp* operon. Unlike the other ESR systems, Psp response only induces expression of the *psp* operon and has no major effect on other genes. Studies have shown that PspA, PspB, and PspC are important for maintaining the proton motive force and relieving the toxicity from mislocalized secretins, though the exact mechanisms are unknown (88).

OmpR-EnvZ response

OmpR-EnvZ are a canonical TCS pair that respond to osmolarity and pH changes in the outer membrane in the environment. At high osmolarity or low pH, EnvZ phosphorylates OmpR and OmpR increases ompC expression and represses ompF expression. At low osmolarity or neutral pH, OmpR represses ompC expression and induces ompF expression. OmpC and OmpF are both outer membrane porins and they differ in pore sizes and the flow rates. This transcriptional change leads to either OmpC or OmpF being the major outer membrane protein and ultimately, balancing the osmolarity in the cell (89).

Conclusion

The facultative intracellular pathogen *Brucella ovis* is a globally important ovine pathogen that stands as an outlier among the classical Brucella species due to its rough LPS, distinct outer membrane protein composition, and high level of genome degradation relative to other *Brucella* species. In this introductory chapter, I have covered some known mechanisms that bacteria use to respond to cell envelope stresses. In this thesis, I will first describe my system-level analysis of all non-essential TCSs in *B. ovis* (Chapter 2). From this initial screen, I then uncovered the molecular mechanisms of a novel three-component system that is important for cell envelope maintenance and intracellular replication (Chapter 3) and a histidine kinase that is important for detergent resistance (Chapter 4).

Figure

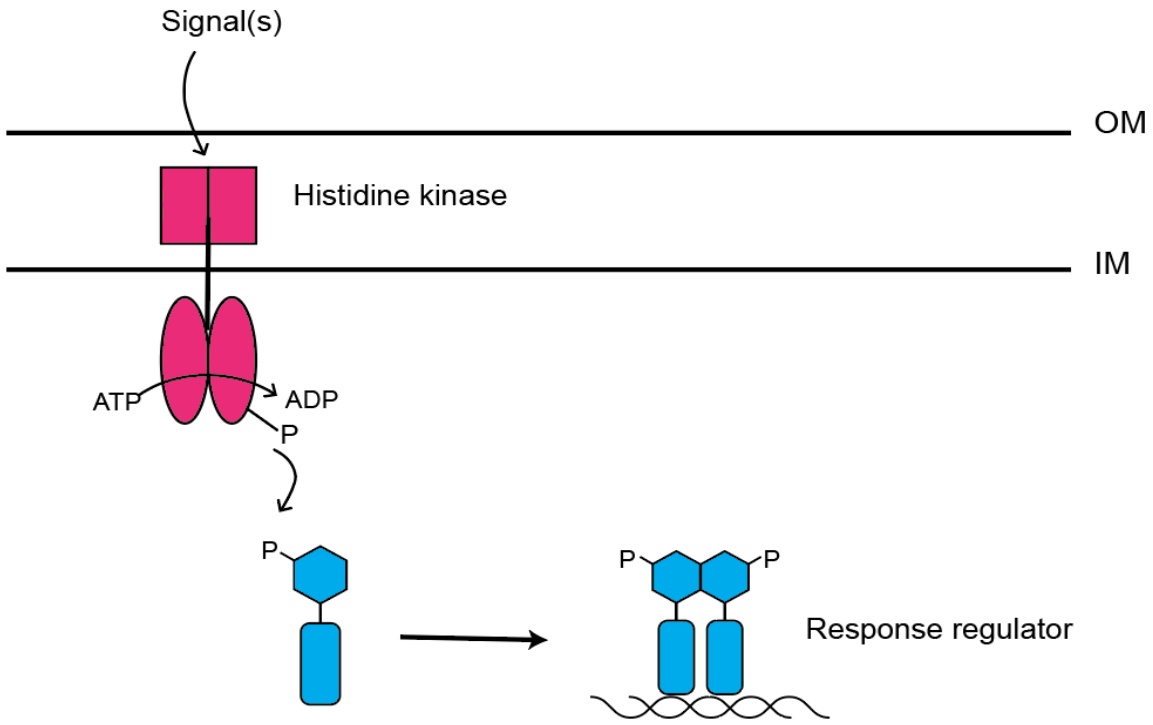

Figure 1.1: schematic of a canonical two-component signal transduction system. The homodimer of HK (pink) is membrane bound and once it senses signals, the homodimers will autophosphorylate via ATP hydrolysis. Then the HK homodimer will transfer the phosphoryl group onto its cognate response regulator (blue). This phosphorylation of RR results in the homodimerization of RR and the RR homodimer bind to its target DNA and regulate gene expression.

Table

Table 1.1: Two-component system (TCS) genes in *Brucella ovis* ATCC 25840

BOV locus	NCBI RefSeq locus	Gene name(s)	Domains	Essential[1]	Mutants generated?
BOV_0099	BOV_RS00485	-	REC	N	Y
BOV_0128	BOV_RS00640	*regB/prrB*	TM-HK	N	N
BOV_0131	BOV_RS00655	*regA*/*prrA*	REC-DBD	N	Y
BOV_0190	BOV_RS18300/ BOV_RS00940[2]	-	Pseudo REC-DBD	N	N
BOV_0289	BOV_RS01475	-	TM-HK	N	Y
BOV_0312	BOV_RS01585	*phoR*	TM-HK	N	Y
BOV_0331	BOV_RS01685	*prlR*	REC-DBD	N	Y
BOV_0332	BOV_RS16185[2]	*prlS*	Pseudo hybrid HK-REC	N	Y
BOV_0357	BOV_RS01805	-	TM-Cache-HK	N	Y
BOV_0358	BOV_RS01810	-	REC-DBD	N	Y
BOV_0577	BOV_RS02880	*divJ*	TM-HK	N	Y
BOV_0603	BOV_RS03015	*feuP*	REC-DBD	N	Y
BOV_0604	BOV_RS03020	*feuQ*	TM-HK	N	Y
BOV_0611	BOV_RS03055	-	REC-DBD	N	Y
BOV_0612	BOV_RS03060	-	TM-HK	N	Y
BOV_0615	BOV_RS03075	*pleC*	TM-PAS-HK	N	Y
BOV_1004	BOV_RS04980	*cckA*	TM-PAS-HK-REC	Y	N
BOV_1073	BOV_RS05335	*ntrX*	REC-AAA+ ATPase-DBD	Y	N
BOV_1074	BOV_RS05340	*ntrY*	TM-PAS-HK	N	N
BOV_1075	BOV_RS05345	*ntrC*	REC-AAA+ ATPase-DBD	N	Y
BOV_1076	BOV_RS05350	*ntrB*	HK	N	Y
BOV_1472	BOV_RS07250	*essR*	REC- DBD	N	Y
BOV_1473	BOV_RS07255	*essS*	TM-HK	N	Y
BOV_1541	BOV_RS07590	*chpT*	HPT	Y	N
BOV_1542	BOV_RS07595	*ctrA*	REC-DBD	Y	N
BOV_1549	BOV_RS07630	*pdhS*	PAS-HK	Y	N
BOV_1602	BOV_RS07885	-	HWE-HK	N	Y
BOV_1604	BOV_RS07895	*phyR*	REC	N	Y
BOV_1607	BOV_RS07910	*phyT*	TM-CHASE3-HWE-HK	N	N
BOV_1929	BOV_RS09460	*cenR*/*otpR*	REC-DBD	N	Y
BOV_2010	BOV_RS09885	*bvrR*	REC-DBD	Y	N
BOV_2011	BOV_RS09890	*bvrS*	TM-HK	Y	N

Table 1.1: (Cont'd)

BOV_2016	BOV_RS09915	*divL*	PAS-HK	Y	N
BOV_2058	BOV_RS10125	*phoB*	REC-DBD	N	Y
BOV_A0037	BOV_RS10530	*nodV*	TM-HK	N	Y
BOV_A0038	BOV_RS10535	*nodW*	REC-DBD	N	Y
BOV_A0040	BOV_RS10545	*cpdR*	REC	N	N
BOV_A0077	BOV_RS10730[2]	-	Pseudo REC-AAA+ ATPase-DBD	N	N
BOV_A0209	BOV_RS11400	-	TM-HK	N	Y
BOV_A0210	BOV_RS11405	-	REC-DBD	N	Y
BOV_A0358	BOV_RS12165	-	REC-DBD	N	Y
BOV_A0412	BOV_RS12435[2]	-	Pseudo HK	N	Y
BOV_A0413	BOV_RS12440	-	REC-DBD	N	Y
BOV_A0554	BOV_RS13160	*lovhK*	PAS-HWE-HK	N	Y
BOV_A0575	BOV_RS13265	*pleD*	REC-GGDEF	N	Y
BOV_A0576	BOV_RS13270	*divK*	REC	Y	N
BOV_A1045	BOV_RS15645	*ftcR*	REC-DBD	N	Y

Abbreviation keys:
TM: transmembrane HWE-HK or HK: histidine kinase
REC: response regulator receiver domain DBD: DNA-binding domain
AAA+ ATPase: sigma 54 activated domain GGDEF: diguanylate cyclase domain
PAS/CHASE3/CACHE: sensory domains HPT: histidine phosphotransferase

[1]Essential genes based on Gumbel and HMM essential gene calculations in TRANSIT(90), using the Tn-Himar sequencing data available at accession SRR19632676 in the NCBI Sequence Read Archive. Genes called essential using both the Gumbel and HMM approaches are noted.
[2]Annotated as pseudogene in RefSeq based on the presence of insertion/deletion or nonsense mutations relative to other *Brucella* species.

Chapter 2: A system-level approach to discover cell envelope regulatory TCS genes in *Brucella ovis*

Preface

The content of this chapter was modified and adapted from its published form:

Chen X, Alakavuklar MA, Fiebig A, Crosson, S. *mBio* (2023).

Introduction

The *Brucella ovis* genome contains 47 genes encoding protein components of two-component signal transduction (TCS) systems. The primary structure of some *B. ovis* TCSs have high identity with previously studied TCSs in other species, and it is assumed that they perform similar functions in *B. ovis*. However, many of TCSs' physiological roles in the cell remain unknown. There also had not been a system-level analysis of all the TCSs in any *Brucella* species. To overcome this lack of knowledge, I performed a system-level analysis of all the non-essential TCSs in *B. ovis*, with the goal of discovering TCSs that regulate cell envelope functions.

The primary strategy involved the creation of mutant strains harboring in-frame deletions of all the non-essential TCS genes and testing the fitness of these mutants under different cell envelope stress conditions. Due to the large amount of cloning that this approach required, and the knowledge that adjacently encoded TCS genes often function together, I chose to delete both response regulator (RR) and histidine kinase (HK) together if they are directly adjacent to each other on the chromosome. For the genes that stand alone on either chromosome, I made single deletions strains.

To focus my directed gene deletion effort, I defined non-essential TCS genes using previously published transposon Tn-seq data in *B. ovis* from our lab (46). Using Hidden Markov model and Bayesian-based analysis (90),9 TCS genes were defined as essential. These include *cckA, ntrX, chpT, ctrA, pdhS, bvrR, bvrS, divL, divK*, and I did not attempt to make deletions of any of these genes. *cpdR* was not considered essential based on the essentiality threshold, but it had fewer insertion counts relative to other non-essential genes. Given the transposon insertion

data and the fact that this gene has been previously studied in *Brucella* I chose not to create a *cpdR* deletion strain due to unlikelihood of success. *ntrX* and *ntrY* are adjacent to each other on the chromosome, and because *ntrX* is essential, I did to not attempt at making either a Δ*ntrX-ntrY* double mutant or a Δ*ntrY* single mutant. *BOV_0190* and *BOV_A0077* have primary structure features of TCS regulators but are both pseudogenes so I also did not make mutants of these genes. Lastly, even though *phyT* and *regB* are considered non-essential based on the Tn-Seq data, I was not able to generate in-frame deletions of these two genes. Altogether, I did not include 15 out of the 47 TCS genes in *B. ovis* in my analysis.

I made deletion mutants of 32 TCS genes (24 strains total), using a double crossover recombination method. The entire mutant panel consists of eight double mutants where I deleted both the RR and HK, and 16 single gene deletion mutants (**Table 1.1**). To assess the impact of these TCS genes on cell envelope stress responses, I examined various stressors targeting different aspects of the cell envelope. The three stressors I chose were: carbenicillin, NaCl, and sodium dodecyl sulfate (SDS). Carbenicillin is a beta-lactam antibiotic that targets the cell wall. High salt concentration is known to induce osmotic stress. SDS is a detergent, which disrupts the cell membranes. Due to the lack of previous studies of on *B. ovis* in the presence of these stressors, I first needed to determine the concentration at which each of the compounds began to impact *B. ovis* growth. The ideal concentration of stressors for my assay is where WT has a slight growth defect when grown on tryptic soy agar supplemented with 5% sheep blood (TSAB) plates containing the stressor compounds relative to WT grown on plain TSA plates. The final concentrations that I identified for each condition were: 2 µg/mL carbenicillin, 0.004-0.0045% SDS, and 200 mM – 225 mM NaCl. It is important to note that the appropriate concentration may change depending on the mutant's phenotype. For example, at 200 mM NaCl, it is easier to distinguish mutants that are more sensitive than WT. However, at 225 mM NaCl, it is easier to distinguish mutants that are more resistant than WT.

Results

Nine cell-envelope regulatory TCS genes identified from the system-level analysis

Out of the 24 mutants, seven of them harboring deletion of 9 TCS genes showed different growth phenotypes in at least one stress condition compared to WT. The remaining mutants did not have any different growth phenotypes compared to WT on all three stress conditions tested. The 9 TCS genes are: *BOV_0577, BOV_0615, BOV_1602, BOV_0311, BOV_0611-0612, BOV_1472-1472, and BOV_1929* (**Figure 2.1**). BOV_0577 and BOV_0615 encode the cell cycle regulators, DivJ and PleC respectively. Both proteins have been studied extensively in the context of cell cycle regulation in *Caulobacter crescentus* and other related Alphaproteobacteria. However, there has not been any previous studies on the importance of DivJ and PleC to cell membrane maintenance and integrity. From my screen, I observed that deletion of *divJ* leads to a slight sensitivity to carbenicillin and deletion of *pleC* leads to an 100-fold growth defect on 200 mM NaCl plate compared to WT (**Figure 2.1**). The deletion of *BOV_1602* (Δ*BOV_1602*) resulted in sensitivity to NaCl and a 4 $\log_{10}$ unit growth enhancement on SDS plates. BOV_0311 encodes a *prlS* (91) homolog and deletion of the gene resulted in minor salt sensitivity. BOV_0611-0612 is an uncharacterized TCS RR/HK pair and deletion of the operon resulted in sensitivity to carbenicillin but had no effect on NaCl or SDS plates. *BOV_1929* has high sequence identity (80-83%) to *cenR* (**c**ell **e**nvelope **r**egulator) in *C. crescentus* and *Rhodobacter sphaeroides*. In both species, it was shown that *cenR* is important for maintaining cell envelope integrity and cell shape (92, 93). The *B. ovis* Δ*cenR* mutant had a 10-fold growth defect on plain TSAB, 1000-fold growth defect on TSAB containing 2 µg/mL carbenicillin, and a 10-fold growth defect on TSAB containing 0.0045% SDS. Lastly, the *BOV_1472-1473* locus encodes an uncharacterized TCS gene pair in which BOV_1472 is the RR and BOV_1473 is the HK. Interestingly, deletion of this pair resulted in very similar phenotypes as Δ*cenR* on all conditions tested. In Chapter 3 I will describe in detail of the molecular connection between CenR and BOV_1472-1473, which will help explain the

congruence in the plate stress phenotype results. In Chapter 4, I will explore the mechanism of detergent resistance in Δ*BOV_1602* mutants.

High throughput screening using barcoded TCS transposon library and Biolog phenotype Microarray

My initial screen successfully identified TCS genes that are important for cell envelope stress responses, which were previously unknown. However, there remain several TCS genes in *B. ovis* that are completely uncharacterized, and it is usually very difficult to identify the signals of each TCS. To leverage the mutant library that I generated and advance efforts of finding possible signals that regulate *Brucella* TCS genes, I decided to transform the initial cell envelope stressor screen into a more high-throughput screening approach that can test all the mutants against hundreds of chemical compounds. Biolog phenotype MicroPlates are a powerful and useful tool to test the phenotype of bacteria in different conditions (94), including various antibiotics, acids, pH, osmotic stress inducers, metal containing compounds, etc. Biolog MicroPlates can also test for growth in different carbon, nitrogen, sulfur, and phosphorous sources. However, because there is currently no minimal media that supports *B. ovis* growth, I was not able to use those Biolog MicroPlates to investigate TCSs that may be important for nutrient uptake and regulation.

Given the large scale of this screen, the initial approach of plating each strain on different plates is not suitable. Instead, I generated a barcoded mutant library in which each of the mutants has a unique barcode integrated at the *glmS* locus using the Tn7 transposon (95). The library has 25 mutants harboring deletion of 32 TCS genes, all of the mutants are the same as in the initial screen, except for Δ*1472-1473*. Instead of using the double mutant, I barcoded Δ*1472* and Δ*1473*, each as a single mutant. I also have included two WT strains with different barcodes as controls. In total, the library contains 27 strains in equal part, each with a unique around 30 bp barcode (**Table 2.1**). I grew the library in seven different Biolog MicroPlates, which are PM9, PM10, PM11C, PM12B, PM13B, PM18C, and PM19. Most of these plates contain a variety of compounds. Additionally, I also grew the library in a plain 96-well plate as a control. I performed PCR on each

well that had growth and amplified the barcodes. To measure the fitness of each mutant strain in each condition, I performed Illumina Next-Generation Sequencing (NGS) on the barcoded region and quantified the reads of each barcode. The script for counting raw reads is attached in the appendix.

There was notable unevenness of amplification of the barcodes in this experiment. For example, the two WT strains should have similar read counts in all conditions. However, barcode 36 was amplified much less than barcode 37. Another concern of this barcoded library is the variability in strain survival during the freezing of the library. All strains should have similar barcode read counts in the no stress condition given that I mixed in equal concentrations of each strain. However, it was obvious that Δ*cenR,* Δ*essR,* and Δ*essS* did not survive during the one-month freezing period which was between when the library was made and when the experiment was conducted. All three strains had very minimal reads of their barcodes in any of the conditions tested. However, many more reads were detected during a trial run a few days after the library was frozen at -80˚C.

Despite the shortcomings of this barcoded library, the results still provided new insights on the possible signals of some TCSs. With a stringent cut-off for significance, 15 TCS mutants showed either sensitivity or resistance to at least one compounds (**Table 2.2**). There are also some interesting patterns between different TCSs. For example, Δ*BOV_A0209-0210,* Δ*BOV_A0575,* Δ*phyR,* Δ*BOV_2058*, Δ*BOV_0577,* and Δ*BOV_0611-0612* all showed resistance to penicillin G, oxacillin, and pheneticillin. There are consistent results between the barcoded library high throughput assay and my initial agar stress assay. For example, in both assays, Δ*pleC* and Δ*BOV_1602* showed sensitivity to NaCl (**Figure 2.1; Table 2.2**).

This barcoded library approach has potentials for identifying potential signals for different TCSs. However, more extensive optimization is needed to improve reproducibility of the results. As I mentioned earlier, the two main areas that future students should focus on for optimization

are 1) how to improve the evenness of amplification 2) how to preserve the viability of certain strains before running the experiment.

Conclusion

I have generated two libraries, the non-essential TCS mutant library and the barcoded transposon mutant library. By screening the mutant library against three cell envelope stressors, I have identified 9 TCS genes that are important for resistance to SDS, carbenicillin, and/or NaCl, some of which are previously uncharacterized TCSs. This mutant library is a useful tool for discovering targets of unknown TCSs or new functions of known TCSs. Although the barcoded transposon library requires more optimization, it has already shown potential for discovering TCSs with similar functions and possibly similar regulatory roles. It also has the potential for identifying sensory signals for TCSs with unknown signals.

Method

Bacterial strains and growth conditions

All *Brucella ovis* ATCC25840 and derivative strains were grown on Tryptic soy agar (BD Difco) + 5% sheep blood (Quad Five) (TSAB) or in Brucella broth at 37˚C with 5% CO_2 supplementation. Growth medium was supplemented with 50 µg/ml kanamycin, 2 µg/mL carbenicillin, 0.0045% sodium dodecyl sulfate (SDS), or 215 mM NaCl when necessary.

All *Escherichia coli* strains were grown in lysogeny broth (LB) or on LB solidified with 1.5% w/v agar. *E. coli* Top10 and WM3064 strains were incubated at 37˚C. WM3064 was grown with 30 µM diaminopimelic acid (DAP) supplementation. Medium was supplemented with 50 µg/mL kanamycin. Primer, plasmid, and strain information are available at (https://doi.org/10.1128/mbio.02387-23; **Table S5**).

Chromosomal deletion strain construction

The double-crossover recombination method was used to generate all *B. ovis* strains bearing in-frame, unmarked gene deletions. Approximately 500 base pair (bp) upstream or

downstream of the target gene, including 9-120 bp of the 3' and 5' ends of the target gene, were amplified by PCR using KOD Xtreme polymerase (Novagen) using primers specific to these regions and the *B. ovis* genomic DNA as template. The DNA fragments were then inserted into the *sacB*-containing suicide plasmid pNPTS138 either through Gibson assembly or restriction enzyme digestion and ligation. The ligated plasmids were first chemically transformed into competent *E. coli* Top10. After sequencing confirmation, plasmids were transformed into chemically competent *E. coli* WM3064 (strain originally produced by W. Metcalf), a DAP auxotroph conjugation-competent donor strain. Plasmids were transferred to *B. ovis* through conjugation. Primary recombinants were selected on TSAB supplemented with kanamycin. After outgrowth in non-selective growth in Brucella broth for 8 hours, clones in which a second recombination removed the plasmid were identified through counter selection with 5% sucrose. Colony PCR was performed on kanamycin-sensitive colonies to distinguish clones bearing the deletion allele from those bearing the WT allele.

Barcoded strain construction

Plasmids containing the barcodes were extracted from the *E. coli* strains carrying the plasmids. Each of the plasmids was transformed into chemically competent *E. coli WM3064* cells. These plasmids were co-conjugated into *B. ovis* strains with a Tn7 integrase expressing suicide helper plasmid, pTNS3. *B. ovis* colonies carrying the integrated mTn7-barcode constructs were selected on TSAB containing kanamycin.

Agar plate growth/stress assays

After 2 days of growth on TSAB or TSAB supplemented with kanamycin, *B. ovis* cells were collected and resuspended in sterile phosphate-buffered saline (PBS) to an OD_{600} = 0.3. Each strain was serially diluted in PBS using a 10^{-1} dilution factor. 5 µl of each dilution was plated onto either TSAB, TSAB containing 0.0045% SDS, 2 µg/ml carbenicillin, or 200 mM NaCl. After 3 days of incubation for TSAB, 4 days for TSAB + 0.0045% SDS and 5 days for TSAB + 2 µg/ml carbenicillin and 215 mM NaCl, growth was documented photographically.

Barcoded mutant library construction

Brucella strains carrying the integrated mTn7-barcode constructs were grown on TSAB containing kanamycin for 2 days. Cells were resuspended in Brucella broth and OD_{600} were adjusted to 1. Five hundred microliter of each normalized culture were mixed together, and a final concentration of 25% glycerol was added to the mixture. The library was stored in 500 µL aliquots at -80˚C.

Biolog Phenotype MicroPlate assay

One aliquot of the barcoded mutant library was thawed on ice and cells were centrifuged at 11,000 x g at room temperature. The supernatant was discarded, and fresh Brucella broth was added. Each well on Biolog plates was resuspended in 100 µL of Brucella broth. The barcoded library was added to each well to a final concentration of OD_{600} = 0.001. For the no stress control, 100 µL of Brucella broth to each well of a 96-well plate. Cells were added to the same concentration as the Biolog plates. Plates were incubated statically at 37˚C with 5% CO_2 supplementation for 4 days. OD_{600} was measured on a Tecan to determine growth after 4 days.

Illumina Next-Generation sequencing amplification of Tn7 barcodes

From the wells that had growth, 2 µL of cell culture was used as DNA template for the first round of Q5 PCR. After PCR program was done, 3 µL of each reaction was mixed with 2.5 µL dH_2O + 0.5 µL ExoSAP to clean up. After the ExoSAP program was done, 2 µL of each ExoSAP reaction was used as DNA template for the second round of Q5 PCR with P5 and P7 indexed primers. Each indexed primer pair is assigned to a specific well on the Biolog Plates. The same ExoSAP step was repeated. The cleaned-up product was quantified using Qubit double stranded DNA kit on a Qubit Fluorometer. DNA sample was diluted to 500 µL of 10 nM in H_2O and then to 100 µL of 1 nM in Resuspension buffer (RSB; Illumina). 5 µL of 1 nM DAN sample was mixed with 5 µL 0.1 N NaOH to denature the DNA; 4 µL 4 nM phiX (Illumina) was mixed with 4 µL 0.1 N NaOH; both mixtures were incubated for 5 minutes at room temperature. 200 µL Tris pH 7 was added to the denatured DNA mixture to neutralize the sample. 985 µL prechilled hybridization

buffer (Illumina) was added to the neutralized DNA sample to dilute the sample. The sample was mixed and quickly centrifuged. PhiX was diluted to 20 pM and the DNA sample was diluted to 5 pM, both with prechilled hybridization buffer. 375 µL 5 pM DNA sample was mixed with 125 µL 20 pM PhiX and the 500 µL mixture was loaded to Illumina reagent cartridge and sequenced using Illumina MiniSeq.

Ilumina Next-Generation sequencing analysis

A sequencing result file was generated from each reaction using a unique indexed primer pair, which was associated with a specific compound from the Biolog Plates. All the sequencing files from Illumina Next-Generation sequencing were run through a script for counting barcodes (attached in Appendix) to get the raw counts of each barcode/mutant in each culture condition. Log_2 (raw reads with stress / raw reads without stress) of each barcode/mutant in each condition was calculated. Due to the noise of the data and uneven amplification of the barcodes, a threshold of significance was set as such: a mutant is considered to be sensitive to a compound if $\log_2 (mutant_{stressed} / mutant_{unstressed}) - \log_2 (WT_{stressed} / WT_{unstressed}) < -2$; a mutant is considered resistant to that compound $\log_2 (mutant_{stressed} / mutant_{unstressed}) - \log_2 (WT_{stressed} / WT_{unstressed}) > 5$.

Figure

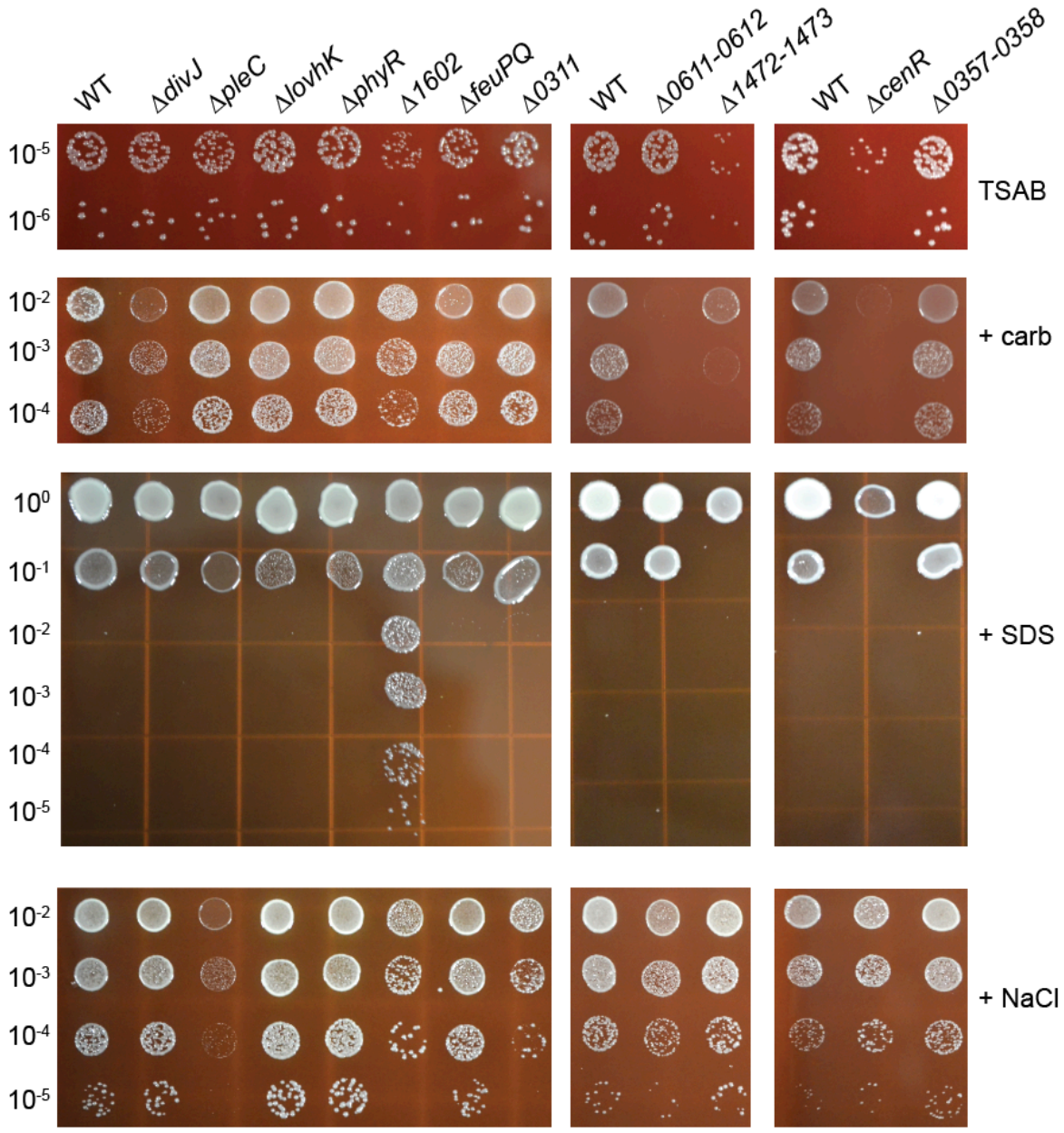

Figure 2.1: system-level analysis of non-essential TCS in *B. ovis* on three cell envelope stressors. Strains harboring in-frame unmarked deletions (Δ) of *B. ovis* TCS gene loci *BOV_0577* (*divJ*), *BOV_0615 (pleC)*, *BOV_A0544* (*lovhK*), *BOV_1604* (*phyR*), *BOV_1602, BOV_0603-0604 (feuPQ), BOV_0311, BOV_0611-0612, BOV_1472-1473, BOV_1929 (cenR), BOV_0357-0358,* plated in $\log_{10}$ dilution series on plain TSA blood agar (TSAB), TSAB containing 2 µg/ml carbenicillin (+carb), TSAB containing 0.0045% SDS (+SDS), or TSAB containing 200 mM NaCl (+NaCl). Dilution plating experiments were repeated at least three times for all strains, and one representative experiment is shown.

Tables

Table 2.1: Mutant strains in the barcoded mutant library and their corresponding

BOV_0131	Barcode #3	TGCGTAACTAGTTTAGTGGTCATGTTTTAA
BOV_0331	Barcode #5	GGAAACATTCTACGCAAGTCTTCCTCCCCA
BOV_0099	Barcode #8	GGATTTTTTTCAATCTGCACGGGGATTTTT
BOV_0577	Barcode #9	CTCGGTGATGTCTCGAATATGGGCGCTTGG
BOV_0615	Barcode #10	CTTATATCTCAGTTCGCGGTGGCTAACCTC
BOV_0357-0358	Barcode #11	TCCCATCGTCATTTCCGGTTAAGGTCTCTA
BOV_0603_0604	Barcode #13	TAGGGCTCTCCGGCAGTCGCGCTGTATCCC
BOV_1075-1076	Barcode #14	CCGATGGTCTCCTAGTCCTTGCCCCGGAGC
BOV_1602	Barcode #15	ACCAGCTAATGGACCGGTGCCGAGTCGATT
BOV_A0037-0038	Barcode #16	CTTAACCCCGTCGGTATGGCCATTTCGATT
BOV_A0412-0413	Barcode #17	CCTATCTCTACCGCGATAAACTCCTGTCTA
BOV_2058	Barcode #18	GACTTAGCGAATCGACGCGATTGCGGATGC
BOV_A0554	Barcode #20	GCGTCCGTCGCGCTGCCCCCTTATTAACTC
BOV_A0209-0210	Barcode #21	TCTTCATGACTCATGGTCAAGGAGAATCC
BOV_A1045	Barcode #22	TTCTTATGTGACTGTCACTACCTTCGCGTC
BOV_1604	Barcode #23	ACTTTAACAGCCATGGGCTTCTCGATTCAT
BOV_0611-0612	Barcode #24	GAAACATTTGGTGCATTTTGTGCCCCTCGG
BOV_1929	Barcode #25	TACGGCGTACCACGACCATGTAATTCCACT
BOV_A0575	Barcode #26	ACTTCACGTAAAGGCGACTCCGGTGCTCCG
BOV_0289	Barcode #27	AGCGTCTAAGGTTTGACTTGGTGATTACTC
BOV_1472	Barcode #28	CTATCGCTTTCTTGCCCCGCCGTCTGTCTG
BOV_1473	Barcode #30	CCTTGATTGGCGTTGCGCGCTTACATCTTA
BOV_3012	Barcode #33	CGTATCTCGAATCTGCCAATATGTGCTAAG
BOV_0332	Barcode #34	TGCTGCTCGCAATCATACTCGCGGTACCCT
WT #1	Barcode #36	ACTTAATATGGTTCTCCGCATATGCCCTAA
WT #2	Barcode #37	TCTAAAGTTTGTCATTCCTACTCGTACTGC

Table 2.2: Biolog phenotype MicroPlate results using barcoded mutant library. Numbers in the parentheses are $\log_2$ ($mutant_{stressed}$ / $mutant_{unstressed}$) - $\log_2$ ($WT_{stressed}$ / $WT_{unstressed}$)

Mutant	Resistant compounds	Sensitive compounds
Δ*BOV_A0209-0210*	Penicillin G (9.85), oxacillin (9.83), pheneticillin (6.27)	Sodium sulfate 4% (-3.80)
Δ*BOV_A0575*	Penicillin G (9.54), oxacillin (9.75), pheneticillin (5.79)	
Δ*phyR*	Penicillin G (9.88), oxacillin (9.81), pheneticillin (5.91), penimepicycline (8.65)	Gallic acid (-3.96)
Δ*BOV_2058*	Penicillin G (10.20), oxacillin (10.53), pheneticillin (5.24), penimepicycline (6.62)	Cloxacillin (-2.43), gallic acid (-2.09), chlortetracycline (-3.05)
Δ*BOV_0577*	Penicillin G (9.91), oxacillin (10.02), pheneticillin (6.8)	NaCl 2% (-2.48), gallic acid (-2.11), sodium sulfate (-4.24)
Δ*BOV_0603-0604*		NaCl 2% (-2.48), sodium sulfate (-2.73)
Δ*BOV_A0412-0413*		Sodium sulfate (-4.00)
Δ*BOV_1075*		Cytosine-1-beta-D-arabinofuranoside (-3.07), semicarbazide (-2.07), sodium sulfate (-5.62)
Δ*BOV_0331*		sodium sulfate (-3.51)
Δ*BOV_0289*		sodium sulfate (-3.31)
Δ*BOV_0611-0612*	Penicillin G (9.53), oxacillin (9.58), pheneticillin (4.51)	Demeclocycline (-2.08), rolitetracycline (-2.00), gallic acid (-7.84), sodium bronate (-2.18)
Δ*BOV_A0037-A0038*		sodium sulfate (-3.58)
Δ*BOV_A0358*		NaCl 2% (-2.04)
Δ*BOV_0131*		Cobalt chloride (-2.69), azathioprine (-4.03), sulfisoxazole (-5.22), tinidazole (-3.13), 2-phenylphenol (-4.09), gallic acid (-9.84)
Δ*BOV_1602*		Bleomycin (-2.25), Cytosine-1-beta-D-arabinofuranoside (-3.90), Cobalt chloride (-2.03), NaCl 1% (-4.20), NaCl 2% (-6.75), sodium sulfate 2% (-5.01), gallic acid (-4.50), sodium sulfate 4% (-5.03)
Δ*BOV_0099*		Sodium sulfate 2% (-3.13), sodium sulfate 4%, (-6.21), semicarbazide (-2.01)

Table 2.2 (Cont'd)

Δ*BOV_0615*		Chlortetracycline (-3.86), bleomycin (-4.44), NaCl 1% (-4.95), NaCl 2% (-4.77), sodium sulfate 2% (-4.29), umbelliferone (-5.76), sodium sulfate 4% (-5.86)
Δ*BOV_0312*		Chlortetracycline (-3.41), cloxacillin (-2.24), sodium sulfate 4% (-7.19)

Chapter 3: Cross-regulation in a three-component cell envelope stress signaling system of *Brucella*

Preface

The content of this chapter was modified and adapted from its published form:

Chen X, Alakavuklar MA, Fiebig A, Crosson, S. *mBio* (2023).

Note: MAA performed the Tn-seq experiment. I performed all the other experiments in this manuscript.

Data sets **Table S1-S5** are available online at https://doi.org/10.1128/mbio.02387-23.

Introduction

Among the 24 TCS mutant strains that I generated (**Table 1.1**), strains lacking the RR encoded by locus *BOV_1929* (BOV_RS09460; *cenR*) or the RR and HK encoded by locus *BOV_1472-73* (BOV_RS07250-55; *essR-essS*) had similar phenotypes under the tested conditions. Through a series of genetic, genomic, and biochemical experiments, I uncovered evidence for direct cross-regulation between these three TCS proteins, which control transcription of a common gene set to support *B. ovis* replication under envelope stress conditions and in the host intracellular niche. Specifically, the conserved alphaproteobacterial cell envelope regulator, CenR (92, 93, 96), stimulates phosphoryl transfer between the cognate RR-HK pair, EssR-EssS, while CenR and EssR regulate the steady-state levels of each other in *B. ovis*. Our results expand understanding of molecular mechanisms of two-component signal transduction and define an unusual mode of TCS cross-regulation in *Brucella* that controls gene expression to support envelope stress resistance and intracellular replication.

Results

Tn-seq identifies a set of candidate essential TCS genes in Brucella ovis

Several histidine kinases and response regulators are reported to be essential in *Brucella* spp. based on previously published Tn-seq data in *B. abortus* (97) and we sought to comprehensively define the essential set of TCS genes in *B. ovis* using *himar* transposon

sequencing. Analysis of Tn-*himar* insertion sites in a collection of approximately 200,000 *B. ovis* mutants revealed ~ 54,000 unique TA dinucleotide insertions in the *B. ovis* genome (98). We used Hidden Markov Model and Bayesian-based approaches (90) to identify candidate essential genes based on this Tn-seq dataset (**Table S1**). As expected, many of the known TCS regulators of *Brucella* cell cycle and cell development (99) are defined as essential using this approach including *ctrA*, *cckA*, *chpT*, *pdhS*, *divL*, and *divK*. Though insertion counts were lower in the developmental/cell cycle regulator *cpdR* relative to local background, this gene did not reach the essential threshold by our analysis. The *bvrS-bvrR* two-component system, which is homologous to the *chvG-chvI* system of other Alphaproteobacteria (100), is also essential. This result is consistent with a report by Martín-Martín and colleagues that the *bvrSR* genes cannot not be deleted in *B. ovis* (101). Notably, the *bvrSR* system is not essential in the smooth strains, *B. melitensis* (100) and *B. abortus* (102). Finally, the *ntrX* regulator is also essential. Considering a recent report of strong genetic interactions between *ntrX*, *chvG*, and *chvI* in *Caulobacter* (103), the essential phenotypes of *bvrS-bvrR* and *ntrX* may be related.

As this study is focused on cell envelope regulation in a rough *Brucella* species, we note that several genes with cell envelope functions were identified as essential in *B. ovis* that are not essential in the smooth species, *B. abortus* (35), including a putative L,D-transpeptidase (*BOV_0757*) and a putative D-alanyl D-alanine carboxypeptidase (*BOV_1129*). Additionally, a DegQ-family serine endoprotease (*BOV_0610*), hydroxymethylpyrimidine phosphate kinase ThiD (*BOV_0209*), the putative magnesium transporter MgtE (*BOV_A0822*), the iron sulfur cluster insertion protein ErpA (*BOV_0886*), and the RNA chaperone Hfq (*BOV_1070*) are essential in *B. ovis* but not in *B. abortus* (35).

A genetic connection between BOV_1472-1473 (essRS) and BOV_1929 (cenR)

There was notable congruence in the agar plate growth defects of the Δ*BOV_1929* and Δ*BOV_1472-1473* strains across the tested conditions, though Δ*BOV_1929* was more sensitive to carbenicillin than Δ*BOV_1472-1473* (**Figure 3.1**). BOV_1929 has high sequence identity to

CenR, which is a known regulator of cell envelope structure in the Alphaproteobacteria (92, 93): *BOV_1929* and *Caulobacter crescentus*, *Rhodobacter sphaeroides*, and *Sinorhizobium meliloti* CenR are reciprocal top-hit BLAST pairs (ranging from 65-80% identity over the full length of the protein). We have thus named *BOV_1929*, *cenR*. Consistent with our data, *Brucella melitensis cenR* (also known as *otpR*) has a reported role in beta-lactam tolerance (104) and acid stress response (105). Studies in *C. crescentus* and *R. sphaeroides* have identified the histidine kinase CenK as the cognate regulator of CenR (92, 93), but the *B. ovis* genome does not encode a protein with high sequence identity to *Caulobacter* or *Rhodobacter* CenK. This is consistent with a previous report that *B. melitensis* does not encode an evident CenK ortholog (106). The *B. ovis* sensor HK most closely related to *C. crescentus* and *R. sphaeroides* CenK is encoded by gene locus *BOV_0289* (33-37% amino acid identity). *BOV_0289* encodes the most likely HK partner for CenR based on a Bayesian algorithm to predict TCS HK-RR pairs (107). However, the Δ*BOV_0289* deletion mutant grew the same as WT in the tested stress conditions and a Δ*BOV_0289* Δ*cenR* double mutant phenocopied the Δ*cenR* single mutant (**Figure 3.1**). These data indicate that BOV_0289 is not an activator of CenR in these conditions.

Given the **e**nvelope **s**tress **s**urvival phenotypes of the Δ*BOV_1472-1473* double deletion mutant, we hereafter refer to the DNA-binding response regulator gene *BOV_1472* as *essR* and the sensor histidine kinase gene *BOV_1473* as *essS*. To our knowledge, EssS and EssR have not been functionally characterized, though EssS is 68% identical to the RL3453 sensor kinase that has been functionally linked to *Rhizobium leguminosarum* plant root attachment (108). EssR is an OmpR-family response regulator, while the EssS sensor kinase has two predicted transmembrane helices and primary structure features that resemble the well-studied CpxA and EnvZ cell envelope regulators (89, 109, 110). To assess phenotypic relationships between the Δ*essR-essS* and Δ*cenR* mutants, we generated *B. ovis* strains harboring in-frame deletions of either *essR* or *essS* and a Δ*cenR* Δ*essR-essS* triple mutant and evaluated growth of these strains on TSAB containing SDS or carbenicillin as above. The Δ*essR* strain phenocopied the Δ*essR-*

essS double mutant in all conditions. The Δ*essS* mutant was indistinguishable from WT in the presence of 0.0045% SDS, however, at a lower SDS concentration (0.004%) Δ*essS* showed an intermediate sensitivity phenotype (**Figure 3.2**). Δ*essS* also showed an intermediate carbenicillin sensitivity phenotype. The Δ*cenR* Δ*essR-essS* triple mutant phenocopied the Δ*cenR* and Δ*essR* single mutants (**Figure 3.1A & 3.2B**). We further evaluated Δ*cenR,* Δ*essR*, and Δ*essS* mutants in three additional stress conditions that perturb the cell envelope in different ways: ethylenediaminetetraacetic acid (EDTA) is a divalent cation chelator that can destabilize the outer membrane (111); polymyxin B is a cationic antimicrobial peptide that targets the outer membrane; and NaCl can function as an osmotic stressor that disrupts envelope integrity. Δ*cenR* and Δ*essR* again phenocopied each other in all three treatment conditions. Both response regulator mutants were more sensitive to EDTA and polymyxin B, and both were more resistant to NaCl compared to wild type. These results provide further support that CenR and EssR function in the same pathway. Like the RR mutants, Δ*essS* was sensitive to EDTA and polymyxin B. However, Δ*essS* was not NaCl resistant (**Figure 3.3**). From these results, we hypothesize that the EssS sensor kinase has distinct regulatory roles in different stress conditions. The sequence relatedness between EssR and CenR is moderate when compared to pairings of all *B. ovis* response regulators with DNA binding domains, with 32% identity and 50% similarity. Specific regions of identity and similarity in their primary structures are presented in **Figure 3.2C**.

Contribution of the CenR and EssR aspartyl phosphorylation sites to stress survival

CenR and EssR are both DNA-binding response regulator proteins, which are typically regulated by phosphorylation of a conserved aspartic acid residue in the receiver domain. To assess the functional role of the CenR aspartyl phosphorylation site (D55), we tested whether expression of non-phosphorylatable ($cenR_{D55A}$) or putative phosphomimetic ($cenR_{D55E}$) alleles of *cenR* could genetically complement the defects of the Δ*cenR* strain in the presence of SDS or carbenicillin. Both mutant alleles of *cenR* restored Δ*cenR* growth/survival to WT levels, indicating that the CenR phosphorylation site does not impact CenR function under these conditions (**Figure**

3.4). We conducted the same experiment for EssR, testing whether *essR*$_{D64E}$ and *essR*$_{D64A}$ could genetically complement the Δ*essR* growth defects. *essR*$_{D64E}$ expression restored wild-type like growth to Δ*essR* on plain TSAB and TSAB-SDS plates but resulted in a strain that was even more sensitive than Δ*essR* to carbenicillin. Expression of *essR*$_{D64A}$ failed to complement Δ*essR* under all conditions (**Figure 3.4**). We conclude that EssR phosphorylation at D64 contributes to *in vitro* stress survival of *B. ovis*.

cenR and essR mutants have equivalent cell size defects

Previous studies of CenR in *C. crescentus* and *R. sphaeroides* have shown that depletion or overexpression of *cenR* leads to large defects in cell envelope structure and/or cell division (92, 93). Considering these results and the sensitivity of *B. ovis* Δ*cenR* to SDS and carbenicillin, we inspected Δ*cenR,* Δ*essR*, and Δ*essS* cells by phase contrast light microscopy and cyro-electron microscopy for defects in cell envelope structure or cell morphology. Deletion of *cenR*, *essR* or *essS* did not result in apparent changes in cell morphology or cell division as assessed by phase contrast microscopy at 630x magnification (**Figure 3.5A**). However, an analysis of cell size revealed that both Δ*cenR* and Δ*essR* mutant cells were larger than WT; the average area of the mutant cells was approximately 12% greater than WT in 2D micrographs ($p<0.0001$) (**Figure 3.5B**). Again, the parallel phenotype of Δ*cenR* and Δ*essR* supports a model in which these two genes execute related functions. An intact phosphorylation site was not required for CenR or EssR to affect cell size, as expression of either phosphorylation site mutant allele of *cenR*(D55) or *essR*(D64) restored cell size to WT levels (**Figure 3.5B**). We did not observe major cell membrane defects in Δ*cenR* and Δ*essR* mutant cells by cryo-EM (**Figure 3.5C**). We conclude that the SDS and carbenicillin resistance defects we observe in the Δ*cenR* and Δ*essR* strains are associated with a defect in cell size control.

B. ovis* Δ*cenR,* Δ*essR, and* Δ*essS strains have equivalent fitness defects in a macrophage infection model

As *B. ovis* is an intracellular pathogen, we sought to examine the importance of *cenR*, *essR* and *essS* in the intracellular niche. The interior of mammalian phagocytes more closely models conditions encountered by the bacterium in its natural host, and many mutants with defects in cell envelope processes are attenuated in infection models (36). Δ*cenR,* Δ*essR*, and Δ*essS* strains had no defect after entry (2h post-infection (p.i.)) or at early stages of infection (6h & 24h p.i.) of THP-1 macrophage-like cells relative to WT. By 48h p.i., recoverable CFU of WT *B. ovis* increased, consistent with adaptation and replication in the intracellular niche; CFU of Δ*cenR,* Δ*essR*, and Δ*essS* did not increase appreciably between 24 and 48h. The 1 $\log_{10}$ unit intracellular replication defect of the Δ*cenR,* Δ*essR*, and Δ*essS* strains at 48h was complemented by expression of the deleted gene(s) from an ectopic locus (**Figure 3.6**). Thus, we conclude that *cenR, essR*, or *essS* do not affect macrophage entry or early survival but all three genes similarly affect replication and/or survival after 24h. These results indicate that *essS*, *essR*, and *cenR* contribute to *B. ovis* fitness after the establishment of the replicative niche inside the *Brucella*-containing vacuole.

Additionally, we tested the infection phenotypes of strains harboring alleles of *essR* and *cenR* in which the conserved aspartyl phosphorylation site was mutated. Expression of $cenR_{D55A}$ or $cenR_{D55E}$ partially - and equivalently - complemented the 48-hour infection defect of Δ*cenR* (**Figure 3.6**). Expression of either $essR_{D64E}$ or $essR_{D64A}$ failed to complement Δ*essR* in this assay (**Figure 3.6**). We conclude that an intact aspartyl phosphorylation site in both the CenR and EssR receiver domains is required for WT levels of replication in a THP-1 macrophage infection model.

cenR, essS and essR mutants are not sensitive to low pH

The Brucella containing vacuole (BCV) is acidified at early time points after infection (1 to 10 hours) in J774 murine macrophages and HeLa cells (112, 113). We observed no defect in recoverable CFU of our mutants at the 2h time point in THP-1 macrophage-like cells (**Figure 3.6**),

which suggested that acid tolerance was not perturbed in Δ*cenR*, Δ*essR*, or Δ*essS*. Nonetheless, we sought to more rigorously test whether sustained exposure to acid impacted the survival of Δ*cenR*, Δ*essR*, and Δ*essS* strains. The acidified BCV has a pH in the 4.0-4.5 range (14), so we tested whether exposure to acidified Brucella broth (pH 4.2) for 2 hours differentially impacted mutant viability. We did not observe significant differences in viability between WT and mutant strains after *in vitro* acid exposure (**Figure 3.7**) and conclude that sensitivity to acid in the BCV cannot alone explain the intracellular defects of *cenR*, *essS* and *essR* mutants. The slower growth rates of *cenR* and *essRS* mutants, which are evident on solid media (**Figures 3.1-3.4**) and in broth (k =0.0028 min^{-1} for WT, 0.0021 min^{-1} for Δ*cenR*, and 0.0022 min^{-1} for Δ*essRS*), could be the primary determinant of their replication defect after 24h. Nonetheless, the more severe defect of the Δ*essS* strain between 24 and 48 hours relative to the other TCS mutants provides evidence that intracellular defects of these TCS mutants are likely complex and multifactorial.

EssR and CenR regulate a common gene set

Considering that TCS proteins typically function to regulate transcription, we used RNA sequencing (RNA-seq) to assess the relationship between EssRS- and CenR-regulated gene sets. The global transcriptional profiles of Δ*cenR* and Δ*essRS* mutant strains were highly correlated (**Figure 3.8**). Filtering genes based on a minimum fold change |2| (FDR p-value < 10^{-4}) revealed 46 transcription units, containing 53 genes, that were regulated by *essR-essS*. Fifty-two transcription units, containing 61 genes, were regulated by *cenR* (**Figure 3.8**; **Table S3**). These gene sets largely overlap: thirty-eight (38) are differentially expressed in the same direction in both datasets. With few exceptions, genes that met the criteria for differential regulation in only one strain showed similar, but more modest, changes compared to WT in the other strain. These results indicate a high degree of functional overlap of EssRS and CenR, with respect to gene expression. One potential explanation for the observed regulatory overlap is that EssR and CenR transcription depend on each other. However, transcript levels of *essR-essS* in a Δ*cenR* background, and *cenR* in Δ*essR-essS* background do not differ significantly from WT (**Table S3**).

We conclude that neither response regulator significantly affects the transcription of the other. Rather, CenR and EssR either independently or coordinately regulate transcription of an overlapping set of *B. ovis* genes.

To further investigate the connection between CenR- and EssR-dependent transcription, we performed chromatin-immunoprecipitation (ChIP)-seq with both EssR and CenR. To promote RR binding to chromosomal target sites, we expressed putative phosphomimetic alleles (D→E) of each RR from their native promoters integrated at the *glmS* locus in each mutant strain; genes were fused to a C-terminal 3xFLAG tag. ChIP of $EssR_{D64E}$-3xFLAG yielded 65 significant peaks across two biological replicates, and ChIP of $CenR_{D55E}$-3xFLAG yielded 47 significant peaks across three biological replicates. Thirty-three peaks were shared between $CenR_{D55E}$ and $EssR_{D64E}$ (**Figure 3.8B** and **Table S4**) providing additional support for a model in which CenR and EssR regulate transcription of a shared gene set, functioning either separately or as a heteromeric complex. We did not observe CenR binding to the *essRS* promoter or EssR binding to the *cenR* promoter in the ChIP-seq data. This is further indication that CenR and EssR do not regulate each other transcriptionally, consistent with the RNA-seq results.

Genes with cell envelope functions are abundant in the CenR-EssRS regulon

The CenR/EssR regulon prominently features genes encoding membrane transport proteins, several of which are contained in co-regulated clusters (**Figure 3.8**). The largest of these clusters encodes carbohydrate metabolism enzymes (BOV_A0354-A0355), transporter subunits (BOV_A0347-A0348; BOV_A0350-A0352), a DapA-family dihydrodipicolinate synthase/N-acetylneuraminate lyase (BOV_A0349), Gfo/Idh/MocA family oxidoreductases (BOV_A0345-A0346), and a FadR-family transcription regulator (BOV_A0353). Transcription of this entire cluster is significantly reduced following *cenR* or *essRS* deletion (**Figure 3.8**; **Table S3**). Expression of *B. melitensis* orthologs of these genes is highly upregulated in supramammary lymph nodes of goats, specifically at late stages of infection (114) suggesting a role in long-term colonization of animal hosts. Homologs of these genes are also regulated by CenR in *R.*

sphaeroides (92) (**Table S3**), providing evidence for conservation of CenR-dependent transcription across Alphaproteobacterial genera.

Other genes with reduced expression upon *cenR* or *essRS* deletion include a third Gfo/Idh/MocA family oxidoreductase (*BOV_0234*) and the secreted BA14K protein (*BOV_A0688*), which is required for normal spleen colonization in a mouse model of *B. abortus* infection (59). Transcripts of three genes immediately adjacent to the general stress response regulator, PhyR, also decreased upon *cenR* or *essRS* deletion including the previously discussed HWE-family sensor kinase, *BOV_1602*, which impacts *B. ovis* SDS resistance (Figure 1). Additionally, the predicted sulfate ABC transport operon, *cysWTP*, decreased significantly in both deletion mutant strains (**Figure 3.8A; Table S3**). Nine genes had significantly higher transcription in Δ*cenR* and Δ*essRS* (**Figure 3.8A; Table S3**) including a site-specific DNA integrase (*BOV_0631*), an ABC transporter (*BOV_A0247*), a C-type lysozyme inhibitor (*BOV_0447*) and LysM-domain protein (*BOV_0448*), envelope integrity protein B (*eipB*; *BOV_1121*), and *BOV_1296*, which is directly regulated by the virulence regulator VjbR under select conditions (115). *BOV_1296* encodes acid shock protein 24 (Asp24), which contributes to virulence in later stages of infection in *B. abortus* and *B. melitensis* (116, 117).

BOV_1399, encoding a periplasmic soluble lytic murein transglycosylase (SLT) enzyme, exhibited the most significant expression difference in our RNA-seq datasets. The promoter of *BOV_1339* is directly bound by CenR and EssR (**Table S4**) and transcript levels were approximately 48 times lower than WT in both Δ*cenR* or Δ*essRS* RNA-seq datasets (**Figure 3.8; Table S3**). To test whether loss of this predicted cell wall metabolism enzyme contributed to the stress survival phenotypes of Δ*cenR* and Δ*essRS*, we deleted *BOV_1399* and subjected this strain to the same agar plate growth assays described above. However, the phenotypes of Δ*BOV_1399* in these assays were indistinguishable from WT. Notably, the promoters of several genes with known cell envelope functions are bound by CenR, EssR, or both but do not exhibit differential transcription in Δ*cenR* or Δ*essRS*. For example, EssR binds to the promoter of

BOV_0115 (Omp25d), which contributes to cell envelope integrity (118, 119), and *B. ovis*-host interaction (38). The outer membrane autotransporters, *bmaA* and *bmaC*, which are important for protein translocation to the cell surface (120) and for host cell adherence (121) are also bound by CenR/EssR but do not change in expression upon *cenR* or *essRS* deletion. Additional studies are necessary to determine what CenR/EssR-bound or regulated genes determine *B. ovis* cell size and support *B. ovis* fitness under envelope stress and in the intracellular niche.

CenR and EssR physically interact via their REC domains in a heterologous system

Genetic, transcriptomic, and ChIP-seq data all indicate that the response regulators EssR and CenR directly control expression of a common gene set in *B. ovis* to enable growth in the presence of SDS and carbenicillin. While the molecular processes that determine signaling via a particular TCS pathway are typically insulated from other TCS proteins (122), we postulated that the congruent genetic and molecular phenotypes of Δ*cenR* and Δ*essR* strains could arise through direct molecular interactions of CenR with either EssS, EssR, or both. In fact, in a systematic analysis of *B. abortus* TCS protein interactions, Hallez and colleagues previously reported the surprising observation that EssR (then, generically annotated as TcbR) and CenR interact in a yeast two-hybrid assay (123). EssR and CenR were the only two *B. abortus* RRs that showed interaction in their genome-scale screen. To test EssR and CenR protein-protein interaction in a heterologous system, we used a bacterial two-hybrid approach based on the T18 and T25 domains of the split adenylate cyclase enzyme (124). CenR and EssR showed strong interactions when fused to either adenylate cyclase domain, while the homomeric CenR-CenR and EssR-EssR combinations showed no evidence of interaction (**Figure 3.9A**).

To test the contribution of the conserved aspartyl phosphorylation sites of CenR and EssR to the observed two-hybrid interaction, we fused putative phosphomimetic (D→E) or non-phosphorylatable (DàA) alleles of either CenR or EssR to the T18 and T25 fragments of adenylate cyclase. Both $EssR_{D64A}$ and $EssR_{D64E}$ interacted with CenR to the same extent as WT EssR (**Figure 3.9B**). $CenR_{D55E}$ had significantly reduced interaction with EssR, while $CenR_{D55A}$

interaction with EssR was not significantly different. These results provide evidence for a model in which CenR phosphorylation attenuates its interaction with EssR. Homomeric CenR-CenR or EssR-EssR interactions were again not observed in our two-hybrid assay for either the D→A or D→E mutants (**Figure 3.9B**).

We used the neural network models of AlphaFold2 (125), as implemented in AF2Complex (126), to develop hypotheses about the structural basis of CenR-EssR interaction. The results of this computation predicted that these two response regulators interact primarily through their receiver (REC) domains rather than their DNA-binding (DBD) domains (Figure 5C). Predicted (1:1) CenR:EssR complex structures showed parallel REC domain heterodimers with significant buried surface area in a region of similar primary structure of CenR and EssR corresponding to the α4-β5-α5 structural face of each protein (**Figure 3.2C**); this is a well-established REC domain interaction interface (127). To test if CenR and EssR interact via their REC domains, we again used a bacterial two-hybrid assay. The measured interaction of the isolated CenR and EssR REC domains was comparable to that of the full-length proteins (**Figure 3.9D**). None of the other DBD-DBD or DBD-REC combinations had significant interactions.

CenR and EssR interact in B. ovis

Given that CenR and EssR strongly interact via their REC domains in a heterologous system, we sought to test whether these two proteins interact in *B. ovis* cells by co-immunoprecipitation. Briefly, we expressed a *cenR-3xFLAG* fusion from the native *cenR* promoter on a low-copy plasmid in strains lacking either endogenous CenR (Δ*cenR*) or lacking both response regulators (Δ*cenR* Δ*essR*) and applied the crosslinked lysates to anti-FLAG magnetic beads. After multiple washing steps we eluted bound protein, reversed the crosslinks, and resolved the eluate by SDS-PAGE. Western blot using polyclonal EssR antiserum revealed clear EssR bands in the lysates of both Δ*cenR / cenR-3xFLAG* and Δ*cenR* vector control strains, but not in Δ*cenR* Δ*essR / cenR-3xFLAG*. Among the three eluate fractions, only the strain expressing both *cenR-3xFLAG* and endogenous *essR* yielded a strong EssR band on the Western blot

(**Figure 3.9E**). These results provide evidence that the CenR-EssR interaction demonstrated by bacterial two-hybrid assay occurs in *B. ovis* cells.

CenR enhances the rate of phosphoryl transfer from EssS to EssR

The related phenotypes of *cenR* and *essR* mutants and the fact that these two response regulators physically interact in cells raised questions about the biochemical consequence(s) of EssR/CenR interaction on histidine kinase autophosphorylation and phosphoryl transfer. The data presented to this point do not clearly establish the identity of a sensor kinase in this system, though we considered EssS to be a strong candidate based on genomic proximity of *essS* and *essR*, and largely overlapping phenotypes between Δ*essS* and Δ*essR* strains. To test this hypothesis, the cytoplasmic kinase domain of EssS (aa 191-488) and full-length EssR and CenR response regulators were purified. The EssS kinase domain autophosphorylated *in vitro*; incubating EssS kinase domain with EssR resulted in rapid loss of phospho-EssS (EssS~P) signal and a concomitant increase in phospho-EssR (EssR~P) signal within 30s, indicating phosphoryl transfer (**Figure 3.10A**). Incubation of EssS with CenR resulted in no detectable phosphoryl transfer by 600s, even when CenR was added in 50 molar excess. We conclude that EssS is the cognate kinase for EssR, and that EssS does not directly phosphorylate CenR.

Though EssS does not phosphorylate CenR *in vitro*, we postulated that CenR may influence activity of the EssS-EssR TCS. To test this idea, we first mixed equimolar EssS and EssR with increasing concentrations of CenR. Supplementing an EssS-EssR reaction mixture with CenR at a 1:1:1 molar ratio resulted in a 20% increase in EssS~P dephosphorylation after 20s relative to a 1:1 EssS-EssR reaction (**Figure 3.11**). Adding CenR to the reaction mixture at 5x molar excess (1:1:5), further enhanced EssS~P dephosphorylation (**Figure 3.11**). The reduction in EssS~P upon addition of CenR coincides with an increase in RR~P. The effect of CenR addition on EssS~P levels (at 20 s) saturated at a 1:1:5 ratio (**Figure 3.11**). Taken together, the data indicate that phosphoryl transfer from EssS to EssR is accelerated by addition of CenR. To further investigate the effect of CenR on the kinetics of phosphoryl transfer between EssS and

EssR, we measured both EssS~P and EssR~P signal over a 1-minute time course. EssS to EssR phosphoryl transfer reactions containing 5-molar excess CenR had an enhanced rate of EssR~P production and an enhanced rate of EssS~P loss compared to reactions with EssS and EssR only (**Figure 3.10B-D**); these experiments do not rule out the possibility that CenR is phosphorylated by EssS when EssR is present as EssR and CenR have similar molecular weights. In the absence of CenR, we observed maximal EssR~P signal after 45-60s. When CenR was present, levels of the band we attribute to EssR~P were maximal by 15s. These results provide evidence that CenR stimulates phosphoryl transfer from EssS to EssR.

EssR and CenR determine protein levels of each other via a post-transcriptional mechanism

Stimulation of phosphoryl transfer from EssS to EssR by the non-cognate CenR protein provides one explanation for the related phenotypes of the Δ*cenR*, Δ*essS* and Δ*essR* mutants. We sought to test whether the CenR protein may have other regulatory effects on the cognate EssS-EssR TCS pair in *B. ovis*. EssR and CenR do not regulate each other's transcription (**Table S3**) but do physically interact (**Figure 3.9**). We hypothesized that CenR interaction with EssR could impact steady-state EssR protein levels through a post-transcriptional mechanism, and vice versa. To test this hypothesis, we measured EssR protein by Western blot in WT and Δ*cenR*. Deletion of *cenR* resulted in a significant reduction (~70%) of EssR protein levels. The Δ*essS* strain also had significantly reduced EssR levels, though the effect was not as large as Δ*cenR* (**Figure 3.12**). The impact of EssS on EssR protein levels is not apparently a consequence of phosphorylation as steady-state levels of EssR, EssR(D64A) and EssR(D64E) did not differ significantly. The mechanism by which CenR affects EssR protein levels is not known, but reduced EssR levels in a Δ*cenR* background provide an additional explanation of the phenotypic congruence of the Δ*cenR* and Δ*essR* strains. The intermediate level of EssR protein in the Δ*essS* strain is consistent with the intermediate phenotype of this mutant in plate stress assays. We further tested whether CenR protein levels are impacted by *essR* by measuring CenR-3xFLAG in

Δ*cenR / cenR-3xFLAG* and Δ*cenR* Δ*essR / cenR-3xFLAG* strains. CenR-3xFLAG was »60% lower in a strain lacking *essR*. We conclude that CenR and EssR regulate each other's protein levels through a post-transcriptional mechanism.

Conclusion

Multiple TCS genes are typically present in bacterial genomes, and the proteins they encode most often function separately to regulate distinct transcriptional responses (122). My systematic analysis of *B. ovis* TCS genes revealed two DNA-binding response regulators, *cenR* and *essR*, that had related morphological, stress resistance, and infection phenotypes when deleted. These results informed the hypothesis that CenR and EssR work together to execute their functions in the cell. RNA-seq and ChIP-seq studies revealed that CenR and EssR regulate similar sets of genes and share many direct binding targets. Contrary to the typical model, co-immunoprecipitation and bacterial two-hybrid experiments provide evidence that CenR and EssR proteins interact both *in vivo* and in a heterologous system. Lastly, through *in vitro* kinase assay, we observed that CenR facilitates a faster phosphoryl transfer between EssS and EssR, though CenR is not directly phosphorylated by EssS. Overall, the data support a model in which CenR and EssRS work together as cell envelope regulators and modulate *B. ovis* intracellular replication and reveal a novel connection between CenR, and a previously uncharacterized TCS in *B. ovis*.

Materials and Methods

Bacterial strains and growth conditions

All *Brucella ovis* ATCC25840 and derivative strains were grown on Tryptic soy agar (BD Difco) + 5% sheep blood (Quad Five) (TSAB) or in Brucella broth at 37˚C with 5% CO_2 supplementation. Growth medium was supplemented with 50 µg/ml kanamycin, 30 µg/ml oxytetracycline, 2 µg/ml carbenicillin, 0.004%-0.0045% sodium dodecyl sulfate (SDS), 2.75 mM EDTA, or 215 mM NaCl when necessary.

All *Escherichia coli* strains were grown in lysogeny broth (LB) or on LB solidified with 1.5% w/v agar. *E. coli* Top10 and WM3064 strains were incubated at 37˚C and BTH101 strains were incubated at 30˚C. WM3064 was grown with 30 μM diaminopimelic acid (DAP) supplementation. Medium was supplemented with 50 μg/ml kanamycin, 12 μg/ml oxytetracycline or 100 μg/ml carbenicillin when necessary. Primer, plasmid, and strain information are available in **Table S5**.

Essential gene calculations using *B. ovis* Tn-himar sequencing data

We constructed a library of *B. ovis* transposon mutants as described previously (128). Briefly, the *E. coli* strain APA752, harboring the pKMW3 mariner transposon library, was conjugated into WT *B. ovis* and transposon bearing strains were selected on TSAB supplemented with 50 μg/ml kanamycin. Following an outgrowth of pooled mutants in 250 ml Brucella broth to $OD_{600} \approx 0.6$, cells were frozen in 25% glycerol in 1 ml aliquots. An aliquot was thawed for gDNA extraction and subsequent insertion site mapping, as described (129). The library contained insertions at over 50,000 unique sites in the genome. Insertion site sequencing data is available in the NCBI sequence read archive under accession SRR19632676. Using the insertion site mapping data from this Tn-seq dataset, we applied the HMM and Gumbel algorithms in the TRANSIT (90) software package to identify candidate essential genes (see Table S1).

Chromosomal deletion strain construction

Same as described in Chapter 2

Complementation strain construction

To engineer genetic complementation constructs, target genes were amplified by KOD polymerase, including ~300 bp upstream and ~50 bp downstream of each target gene. The PCR products were purified and inserted into plasmid pUC18-mTn7 by restriction enzyme digestion and ligation, followed by chemical transformation into *E. coli* TOP10 cells. After sequence confirmation, the mTn7 plasmids were transformed into chemically competent *E. coli* WM3064. These plasmids were co-conjugated into *B. ovis* strains with a Tn7 integrase expressing suicide

helper plasmid, pTNS3, which is also carried by WM3064. *B. ovis* colonies carrying the integrated mTn7 constructs at the *glmS* locus were selected on TSAB containing kanamycin.

Agar plate growth/stress assays

After 2 days of growth on TSAB or TSAB supplemented with kanamycin, *B. ovis* cells were collected and resuspended in sterile phosphate-buffered saline (PBS) to an OD_{600} = 0.3. Each strain was serially diluted in PBS using a 10^{-1} dilution factor. 5 µl of each dilution was plated onto either TSAB, TSAB containing 0.004%-0.0045% SDS, 2 µg/ml carbenicillin, 2.75 mM EDTA, or 215 mM NaCl. After 3 days of incubation for TSAB, 4 days for TSAB + 0.004%-0.0045% SDS and 5 days for TSAB + 2 µg/ml carbenicillin, 2.75 mM EDTA, and 215 mM NaCl, growth was documented photographically.

Polymyxin B stress assay

After 2 days of growth on TSAB supplemented with kanamycin, *B. ovis* cells were collected and resuspended in 1 mL of Brucella broth at an OD_{600} =0.3. Cells were split and one portion was treated with 1 mg/mL polymyxin B, and the other was untreated. Both treated and untreated groups were incubated at 37˚C with 5% CO_2 supplementation for 80 minutes. Each culture was then 10-fold serially diluted in PBS and 5 µl of each dilution was spotted onto TSAB. After 3 days of incubation for untreated group and 4 days for treated group, growth was documented photographically.

Macrophage infection assay

THP-1 cells were grown in Roswell Park Memorial Institute Medium (RPMI) + 10% heat inactivated fetal bovine serum (FBS) at 37˚C with 5% CO_2 supplementation. Three days prior to infection, THP-1 cells were seeded in a 96-well plate at a concentration of 10^6 cells/ml in 100 µl/well of fresh RPMI + 10% FBS with an addition of 50ng/ml phorbol 12-myristate-13-acetate (PMA) to induce differentiation. After three days at 37˚C in 5% CO_2, *B. ovis* cells were resuspended at a concentration of 10^8 CFU/ml (OD_{600} = 0.15) in RPMI + 10% FBS and added to THP-1 cells at a multiplicity of infection (MOI) of 100. The 96-well plate containing *B. ovis* and

THP-1 cells was centrifuged at 150 x g at room temperature for 5 minutes and incubated at 37˚C with 5% CO_2 for 1h. Media was removed and fresh media containing 50 µg/ml gentamicin was added to kill extracellular *B. ovis* that were not internalized. The plate was incubated for another hour at 37˚C with 5% CO_2. Media was removed and fresh media containing 25 µg/ml gentamicin was added to each well except for 2h-p.i. wells. A 2h, 6h, 24h, and 48h post-infection, *B. ovis* were enumerated by removing the media and washing the cells with PBS once and incubating at 37˚C for 10 minutes. Then PBS was removed and 200 µl dH_2O was added to each well and the plate was incubated at room temperature for 10 minutes to lyse the THP-1 cells. *B. ovis* cells were collected and serial diluted with a 10^{-1} dilution factor in PBS and plated on TSAB. Plates were incubated for 3 days and CFU were enumerated.

Acid stress assay

As previously described (64), *Brucella* cells were grown on TSAB for 2 days before being inoculated into 5 mL Brucella broth and shaken for 24h. OD_{600} was adjusted to 1.5 and 50 µl of cells were added to either 5 mL plain Brucella broth or 5 mL Brucella broth pH 4.2 (final OD_{600} = 0.015). After 2h of shaking incubation, cells were serially diluted and plated onto plain TSAB. After 3 days of incubation, CFU/ml were enumerated.

Phase contrast microscopy

Samples of *B. ovis* cells were grown on TSAB supplemented with kanamycin and incubated for 2 days. Cells were resuspended in milliQ H_2O and 1 µl of cells were spotted on an agarose pad on a cover slide and imaged on a Leica DMI 6000 microscope in phase contrast with an HC PL APO 63x/1.4 numeric aperture (NA) oil Ph3 CS2 objective. Images were captured with an Orca-ER digital camera (Hamamatsu) controlled by Leica Application Suite X (Leica). Cell areas were measured from phase contrast images using BacStalk (130).

Cryo-electron microscopy

B. ovis cells were grown on TSAB for 2 days and resuspended in PBS to a $OD_{600} \approx 1$. Five µl of cells were placed on a glow-discharged R 3.51 grid (Quantfoil), blotted for 3.5 s, air dried for

20 s, and plunged into liquid ethane using the Vitrobot robotic plunge freezer (Thermo). Samples were stored in liquid nitrogen before imaging. Cells were imaged on a ThermoScientific Talos Arctica Cryo-EM (Thermo) with a -10.00 µm defocus and 17,500x magnification. Images were captured with a Ceta camera (Thermo) with 2.0 s exposure time.

RNA extraction and sequencing

B. ovis strains were grown in Brucella broth at 37˚C in 5% CO_2 overnight. The next day, cultures were back diluted to OD_{600} = 0.05 in 12 ml Brucella broth and incubated on a rotor at 37˚C with 5% CO_2 for 7h. 9 ml of each culture was harvested by centrifugation, and the pellets were immediately resuspended in 1 ml TRIzol. Samples were stored at -80˚C until RNA extraction. To extract the RNA, samples were thawed and incubated at 65˚C for 10 minutes. 200 µl of chloroform was added to each sample and mixed by vortexing for 15 seconds. Samples were then incubated at room temperature for 5 minutes. Phases were separated by centrifugation at 17,000 x g for 15 minutes at 4˚C. The aqueous layer was transferred into a fresh tube. Sample was mixed with 500 ml of isopropanol and stored at -20˚C for 2h. After thawing, samples were centrifuged at 13,000 x g for 30 minutes at 4˚C to pellet the RNA. Supernatants were discarded and the pellets were washed with 1 ml of ice cold 70% ethanol. Samples were centrifuged at 13,000 x g at 4˚C for 5 minutes. Supernatants were discarded and pellets were air dried. Pellets were resuspended in 100 µl RNAse-free H_2O and incubated at 60˚C for 10 minutes. RNA samples were DNase treated using RNeasy Mini kit (Qiagen). RNA samples were sequenced at Microbial Genome Sequencing Center (Pittsburgh, PA) on an Illumina NextSeq 2000 (Illumina). RNA libraries for RNA-seq were prepared using Illumina Stranded RNA library preparation with RiboZero Plus rRNA depletion.

RNA-seq analysis

All RNA-seq analysis was conducted in CLC Genomics Workbench 21.0.4 (Qiagen). Reads were mapped to reference genome (*Brucella ovis* ATCC 25840, Genbank accessions NC_009504 and NC_009505). Differential expression for RNA-seq default settings were used to

calculate the fold change of all annotated genes in mutant strains versus WT. Raw and processed RNA-seq data are publicly available in the NCBI GEO database at accession GSE229183.

ChIP DNA extraction and sequencing

To build the constructs for ChIP-seq analysis of strains expressing $CenR_{D55E}$ and $EssR_{D64E}$, regions containing each gene (including ~300 bp upstream) were PCR amplified from the *B. ovis* $cenR_{D55E}$ and $essR_{D64E}$ mutant strains with KOD polymerase. Amplified fragments were purified and inserted into plasmid pQF through restriction enzyme digestion and ligation to yield a 3xFLAG fusion at the 3' end of each gene. This C-terminal FLAG fusion plasmid construct was conjugated into *B. ovis* mutants using WM3064 as described above.

Cells were grown on TSAB plates supplemented with 30 mg/ml oxytetracycline for three days and resuspended in Brucella broth. Formaldehyde was added to a final concentration of 1% (w/v) to crosslink, and samples were incubated for 10 minutes on shaker. Crosslinker was quenched by adding 0.125 M glycine and was shaken for an additional 5 minutes. Cells were then centrifuged at 7,196 x g for 5 minutes at 4˚C and pellets were washed 4 times with cold PBS pH 7.5 and resuspended in 900 µl buffer [10 mM Tris pH 8, 1 mM EDTA, protease inhibitor cocktail tablet (Roche)]. 100 µl of 10 mg/ml lysozyme was added to each sample, which were then vortexed and incubated at 37˚C for 30 minutes before adding a final concentration of 0.1% SDS (w/v) to each sample. The samples were then sonicated on ice for 15 cycles (20% magnitude, 20 seconds on/off) and centrifuged at 15,000xg for 10 minutes at 4˚C. Supernatants were collected, Triton X-100 was added to a concentration of 1%, and lysates were added to 30 µl SureBead Protein A magnetic agarose beads (BioRad) equlibrated with binding buffer [10 mM Tris pH 8, 1 mM EDTA pH8, 0.1% SDS, 1% Triton X-100] and incubated for 30 minutes at room temperature; this step has empirically improved signal for our FLAG IP protocols. Beads were collected on a magnetic stand, the supernatant was transferred to a fresh tube, and 5% of each sample supernatant was removed as the input DNA samples. 100 µl of α-FLAG magnetic agarose beads were then washed

three times with binding buffer and incubated overnight at 4˚C shaking in 500 µl binding buffer plus 1% BSA to equilibrate the beads. The following day, α-FLAG beads were washed four times in binding buffer and cell lysates were added to the pre-washed beads and gently vortexed. Samples were incubated for 3h at room temperature with mixing and α-FLAG beads were collected on a magnetic stand and serially washed in 500 µl low-salt buffer [50 mM HEPES pH7.5, 1% Triton X-100, 150 mM NaCl], 500 µl high-salt buffer [50mM HEPES pH 7.5, 1% Triton X-100, 500 mM NaCl], and 500 µl LiCl buffer [10 mM Tris pH 8, 1 mM EDTA pH 8, 1% Triton X-100, 0.5% IGEPAL® CA-630, 150 mM LiCl]. To elute the protein-DNA complex bound to the beads, 100 µl elution buffer [10 mM Tris pH 8.0, 1 mM EDTA pH 8.0, 1% SDS, 100 ng/µl 3x FLAG peptide] was added to the beads and incubated at room temperature for 30 minutes with mixing. The eluate was collected, and the elution step was repeated. Input samples were brought to the same volume as output samples with elution buffer. For RNase A treatment, a final concentration of 300 mM NaCl and 100 µg/ml RNase A were added to each input and output sample and incubated at 37˚C for 30 minutes. Proteinase K was added to a final concentration of 200 µg/ml and the samples were incubated overnight at 65˚C to reverse crosslinks. ChIP DNA was purified with Zymo ChIP DNA Clean & Concentrator kit. The ChIP-seq library was prepared using Illumina DNA prep kit and IDT 10bp UDI indices; DNA samples were sequenced at SeqCenter (Pittsburgh, PA) on an Illumina Nextseq 2000.

ChIP-seq analysis

Output and input DNA sequences were first mapped to the reference genome (*Brucella ovis* ATCC 25840, Genbank accessions NC_009504 and NC_009505) in Galaxy using bowtie2 (131). ChIP-seq enriched peak calls from the mapping output data were carried out in Genrich (https://github.com/jsh58/Genrich) with parameters maximum q-value = 0.05, and minimum AUC (area under the curve) = 20; PCR duplicates were removed. bamCoverage (132) was used to create bigwig file tracks for each replicate, and peaks were visualized in IGB (133). Raw and

processed ChIP-seq data are publicly available in the NCBI GEO database at accession GSE229183.

Bacterial two hybrid β-galactosidase assay

The DNA fragments of the full-length, point mutant, and specific domains of *cenR* and *essR* were PCR amplified by KOD polymerase and cloned into split adenylyl cyclase plasmids (either pKT25 or pUT18c) (124) through restriction digestion and ligation. Each pair of pKT25 and pUT18c plasmids were co-transformed into chemically competent *E. coli* BTH101 cells. BTH101 strains carrying both pKT25 and pUT18c plasmids were grown in LB and incubated at 30˚C overnight while shaking. Fresh LB + 500 μM IPTG was inoculated with 100 μl of overnight culture and incubated at 30˚C until OD_{600} ≈ 0.3-0.4. To assess two-hybrid interaction via reconstitution of adenylyl cyclase activity, 100 μl of culture was mixed with 100 μl chloroform and vortexed vigorously. 700 μl Z buffer (0.06 M Na_2HPO_4, 0.04 M NaH_2PO_4, 0.01 M KCl, 0.001 M $MgSO_4$) and 200 μl ortho-nitrophenyl- β-galactoside (ONPG) was added to each sample. The reactions were stopped with 1 ml of Na_2CO_3 after 7.8 minutes and colorimetric conversion of ONPG was measured at 420 nm (A_{420}) was measured. Miller Units were calculated as MU = A_{420} x 1000 / (OD_{600} x time x volume of cells).

Structure prediction

The heterodimeric structure of CenR and EssR was predicted using the protein complex prediction package AF2Complex (126), which utilizes the neural network models of AlphaFold2 (125). Computations were carried out on the Michigan State University high-performance computing cluster.

EssR-CenR co-immunoprecipitation assay

Strain construction, lysate production, and α-FLAG magnetic agarose beads preparation were the same as described above for ChIP-seq sample preparation. After preparation and centrifugation of the lysates, the supernatants were collected and 50 μl of each sample was mixed with equal amount of SDS loading buffer and stored at -20˚C. For FLAG IP, remaining lysates

were applied to pre-washed α-FLAG beads and incubated at room temperature for 3h with shaking. Beads were washed and eluted as described above, eluate from each sample was incubated at 65˚C overnight to reverse crosslinking, and samples were then mixed with equal volume of SDS loading buffer. All samples collected were heated to 95˚C for 5 minutes before resolving on a 12% mini-PROTEAN precast gel (BioRad). A Western blot using polyclonal EssR antiserum was conducted following the protocol outlined in the Western blot method section below. The membrane was imaged using BioRad ChemiDoc Imaging System (BioRad).

Protein purification

DNA fragments that encode full length CenR and EssR, and EssS residues 191-488 (EssS for short) were PCR amplified by KOD polymerase and inserted into a pET23b-His6-SUMO expression vector through restriction digestion and ligation. Vectors were transformed into chemically competent *E. coli* BL21 Rosetta (DE3) / pLysS. All strains were grown in LB medium at 37˚C and induced with 0.5 mM isopropyl β-D-1-thiogalactopyranoside (IPTG) at $OD_{600} \approx 0.5$. Cell pellets were harvested after 2h of induction at 37˚C and stored at -80˚C until purification.

For protein purification, cell pellets were resuspended in 25 ml of lysis buffer (25 mM Tris pH8, 125 mM NaCl, 10 mM imidazole) with the addition of 1mM phenylmethylsulfonyl fluoride (PMSF) and 5 μg/ml DNase I. Samples were lysed through sonication on ice (20% magnitude, 20 seconds on/off) until the lysates were clear. Lysates were centrifuged, and the supernatant was added to 3 ml of Ni-nitrilotriacetic acid (NTA) superflow resin (Qiagen) and the mixture was applied onto a gravity drip column. The resin was washed with 20 ml of lysis buffer, 50 ml of wash buffer (25 mM Tris pH8, 150 mM NaCl, 30 mM imidazole) and the proteins were collected in 20 ml of elution buffer (25 mM Tris pH8, 150 mM NaCl, 300 mM imidazole) at 4˚C. For CenR and EssR, the elution was dialyzed and the His6-SUMO tags were cleaved with ubiquitin-like-specific protease 1 (Ulp1) overnight at 4˚C in dialysis buffer (25 mM Tris pH8, 150 mM NaCl). The next day, the digested protein was mixed with NTA superflow resin. The mixture was applied onto a gravity column and

the purified and cleaved protein was collected from the flow through. His6-SUMO-EssS was dialyzed in dialysis buffer overnight at 4˚C and collected. All proteins were stored at 4˚C.

In vitro EssS-EssR phosphoryl transfer assay

Purified His-SUMO-EssS(191-488), CenR, and EssR were diluted to 5 μM with 1x kinase buffer (250 mM Tris pH8, 50 mM KCl, 10 mM $MgCl_2$, 10 mM $CaCl_2$, 1 mM DTT). 5 μl of ATP mix (4.5 μl 250 μM ATP, pH 7, 0.5 μl [32P]-ATP (10 μCi/μl) was added to 45 μl of 5 μM His-SUMO-EssS and the protein was allowed to autophosphorylate for 1h at room temperature. 5 μl of His-SUMO-EssS~P was mixed with 5 μl 1x kinase buffer and SDS loading buffer as the autophosphorylation control. To assess phosphoryl transfer, His-SUMO-EssS~P was mixed with equimolar of CenR, EssR, or a CenR/EssR mixture at various CenR:EssR molar ratios. Each phosphoryl transfer reaction was quenched with equal volume of SDS loading buffer. Reaction samples were loaded onto a 12% mini-PROTEAN precast gel (BioRad) and resolved at 180V at room temperature. The dye front of the gel was cut off and the rest of the gel was exposed to a phosphoscreen for 1-2h at room temperature. The phosphoscreen was imaged on a Typhoon phosphorimager (Cytiva), and gel band intensity was quantified using ImageQuant TL (Cytiva).

Western Blotting of EssR protein

B. ovis strains were grown on plain TSAB or TSAB supplemented with kanamycin for two days. Cells were collected and resuspended in sterile PBS to equivalent densities (measured optically at 600 nm). Cell resuspensions were mixed with an equal volume of SDS loading buffer and heated to 95˚C for 5 minutes. 10 μl of each sample was loaded onto a 12.5% SDS-PAGE gel and resolved at 180V at room temperature. The proteins were transferred to a PVDF membrane (Millipore) using a semi-dry transfer apparatus at 10V for 30 minutes at room temperature. The membrane was blocked in 20 ml Blotto (Tris-buffered saline Tween-20 (TBST) + 5% milk) for 1h at room temperature. The membrane was blocked in 10 ml Blott + polyclonal rabbit α-EssR antiserum (1:1,000 dilution), and the membrane was incubated for 1h at room temperature. The membrane was washed three times with TBST. Goat α-rabbit IgG poly-horseradish peroxidase

secondary antibody (Invitrogen; 1:10,000 dilution) was added to 10 ml Blotto and the membrane was incubated for 1h at room temperature. The membrane was washed three times with TBST, developed with ProSignal Pico ECL Spray (Prometheus Protein Biology Products) and imaged on a BioRad ChemiDoc Imaging System. Bands were quantified using ImageLab Software (BioRad).

Western Blotting of CenR-3xFLAG protein

B. ovis strains carrying pQF plasmids were grown on TSAB supplemented with 30 µg/ml oxytetracycline for three days and samples for Western blot were collected and and prepared as described above. 10 µl of each sample was loaded onto a 12.5% SDS-PAGE containing 0.5% 2,2,2-Trichloroethanol (TCE) and resolved at 180V at room temperature. The gel was imaged on a BioRad Chemi-Doc Imaging system using the stain-free protein gel setting to activate TCE and visualize total proteins in the gel. The proteins were then transferred to a PVDF membrane (Millipore) using a semi-dry transfer apparatus at 10V for 30 minutes at room temperature and imaged under the stain-free blot setting on Chemi-Doc to visualize the total transferred proteins. The membrane was blocked in 20 ml Blotto (Tris-buffered saline Tween-20 (TBST) + 5% milk) for 1h at room temperature, then incubated in 15 ml Blotto + monoclonal α-FLAG antibody (Thermo; 1:10,000 dilution) for 1h at room temperature. The membrane was subsequently washed three times with TBST and goat α-mouse IgG poly-horseradish peroxidase secondary antibody (Thermo; 1:10,000 dilution) was added and incubated for 1h at room temperature. Membrane incubated with secondary antibody was subsequently washed three times with TBST, developed with ProSignal Pico ECL Spray (Prometheus Protein Biology Products) and imaged on ChemiDoc Imaging System. Bands were quantified using ImageLab Software (BioRad).

Figures

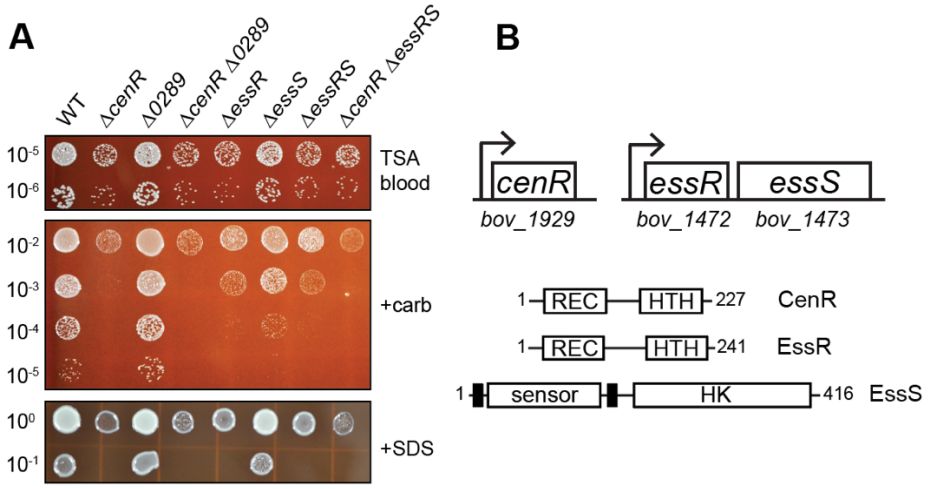

Figure 3.1: Genetic analysis of *cenR, BOV_0289, and essRS*. (A) Strains harboring in-frame unmarked deletions (Δ) of *B. ovis* TCS gene loci *BOV_1929* (*cenR*), *BOV_0289*, *BOV_1472* (*essR*), *BOV_1473* (*essS*), alone and in combination plated in $\log_{10}$ dilution series on plain TSA blood agar (TSAB), TSAB containing 2 µg/ml carbenicillin (+carb) or TSAB containing 0.0045% SDS (+SDS). Genetic complementation of panel B strains using a lower SDS concentration is shown in Figure 3.2. Dilution plating experiments were repeated at least three times for all strains, and one representative experiment is shown. (B) (top) Cartoon of the *cenR* and *essR-essS* genetic loci with *bov* gene locus numbers. (bottom) Protein domain models of CenR, EssR, and EssS with number of amino acid residues in each protein. Domains are labeled as follows: REC - receiver domain; HTH - helix-turn-helix DNA binding domain, sensor - extracellular sensor domain, HK - histidine kinase domain. Predicted transmembrane helices flanking the sensor domain are indicated by heavy black lines.

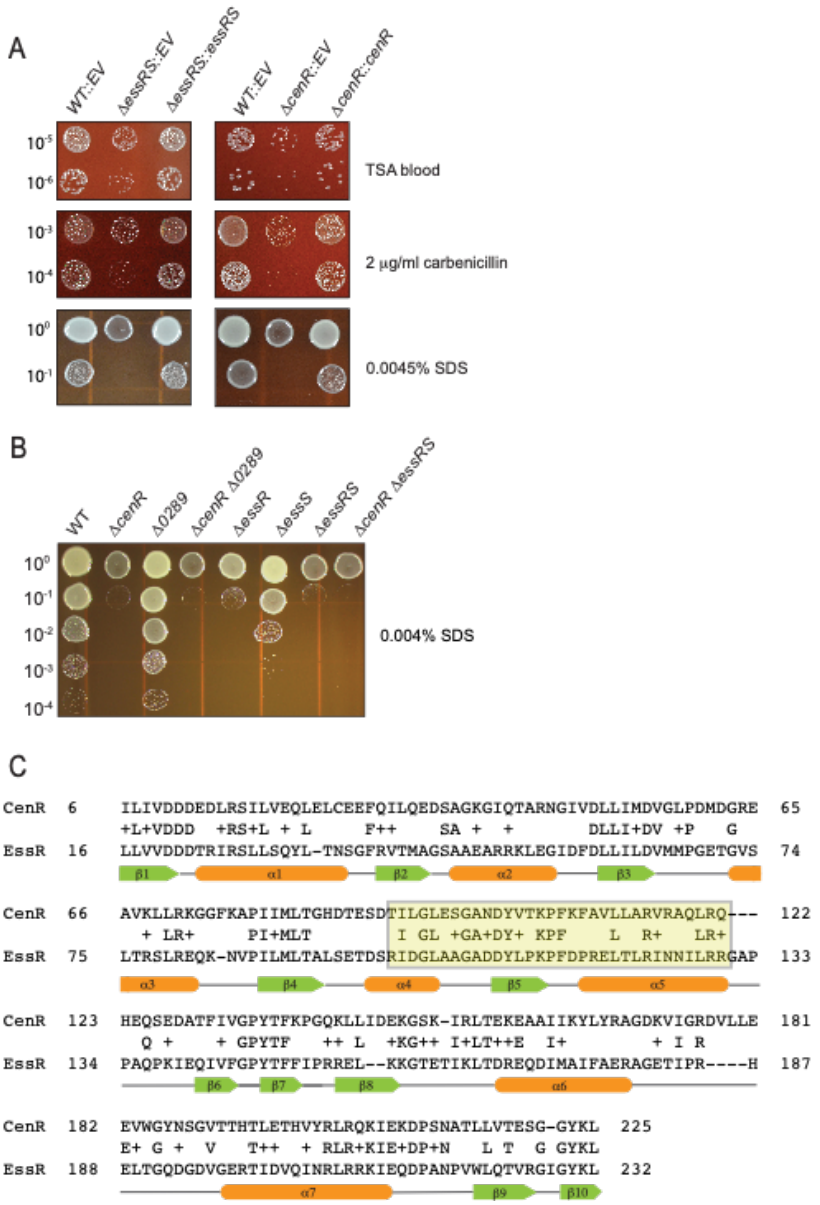

Figure 3.2: Genetic complementation of Δ*essRS* and Δ*cenR* mutants; SDS sensitivity assay at a reduced SDS concentration, and CenR-EssR sequence alignment. (A) Genetic complementation of Δ*essRS* and Δ*cenR* carbenicillin and SDS phenotypes. Complementing copies of the deleted genes were inserted into the ectopic *glmS* locus using Tn7. Dilution plating experiments were repeated at least three times for all strains. One representative experiment is shown. (B) SDS resistance phenotypes of strains harboring in-frame unmarked deletions (D) of *B. ovis* TCS gene loci *BOV_1929* (*cenR*), *BOV_0289*, *BOV_1472* (*essR*), *BOV_1473* (*essS*), alone and in combination show a larger dynamic range at an SDS concentration of 0.004% compared to 0.0045% (as presented in Figure 1). Dilution plating experiments were repeated at least three times for all strains, and one representative experiment is shown. (C) Amino acid sequence alignment of CenR and EssR. Amino acids highlighted in yellow show the primary structure of the α4-β5-α5 protein-protein interaction interface predicted by AFComplex2 (see Figure 5C). Protein secondary structure is presented above the alignment (helix in orange; strand in green).

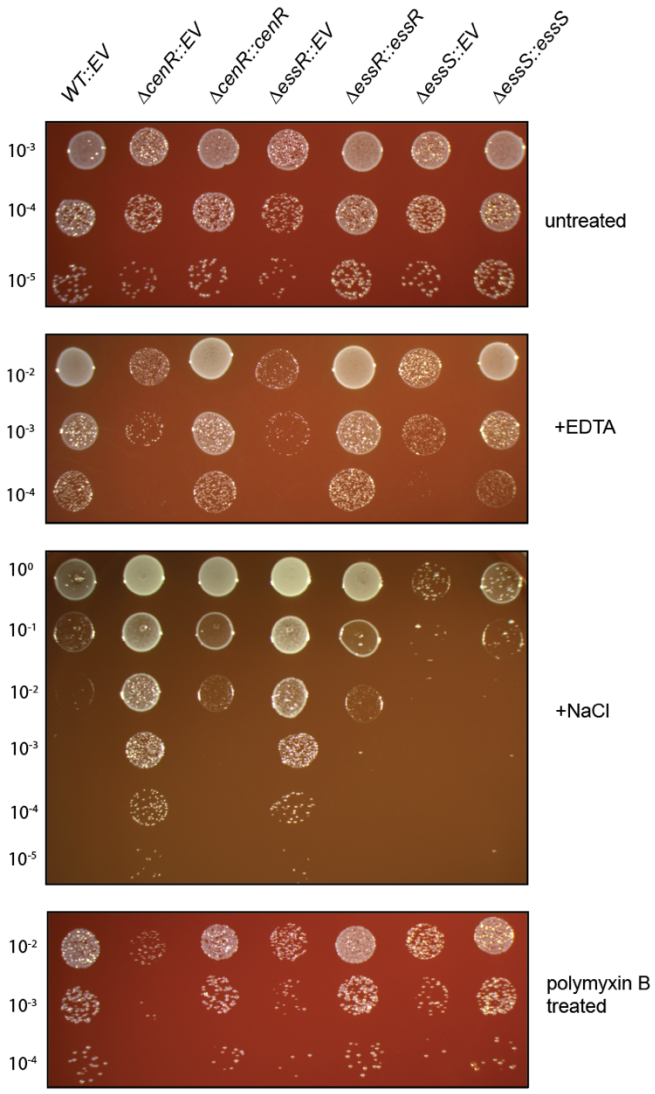

Figure 3.3: *cenR, essR,* and *essS* contribute to cell survival in the presence of diverse envelope stressors. Strains harboring in-frame unmarked deletions (D) of *cenR, essR, essS*, carrying integrated empty vectors (EV) or genetic complementation vectors (::*gene locus number*) were plated in $\log_{10}$ dilution series on plain TSA blood agar (untreated), TSA-B containing 2.75mM EDTA (+EDTA), TSA-B containing 215 mM NaCl (+NaCl), or were cells treated with 1 mg/mL polymyxin B for 80 minutes before being plated on TSA-B (polymyxin B treated). Dilution plating experiments were repeated three times for all strains, and one representative experiment is shown.

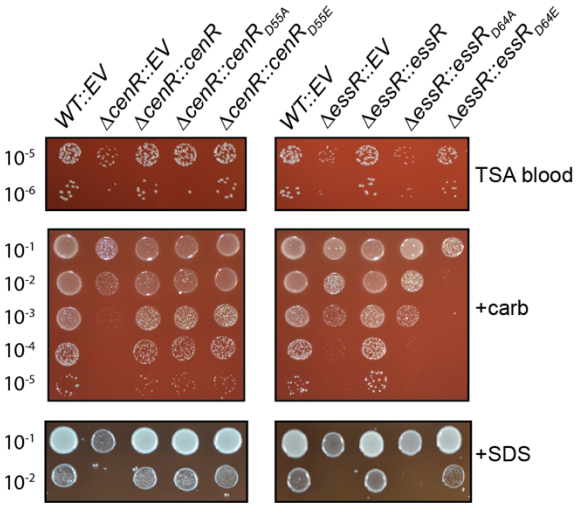

Figure 3.4: **Functional analysis of the conserved aspartyl phosphorylation sites of the CenR and EssR response regulators.** Test for genetic complementation of D*cenR* and D*essR* envelope stress phenotypes by expression of either non-phosphorylatable alleles of *cenR* (D55A) and *essR* (D64A) or putative phosphomimetic alleles (D55E / D64E). Conditions and dilution plating as in Figure 1; Plain TSA blood (TSAB) plates, TSAB + 2 µg/ml carbenicillin (+carb) and TSAB + 0.0045% SDS (+SDS). D*cenR* and D*essR* each carry an empty vector as control (EV). Experiments were repeated at least three times for all strains and one representative experiment is shown.

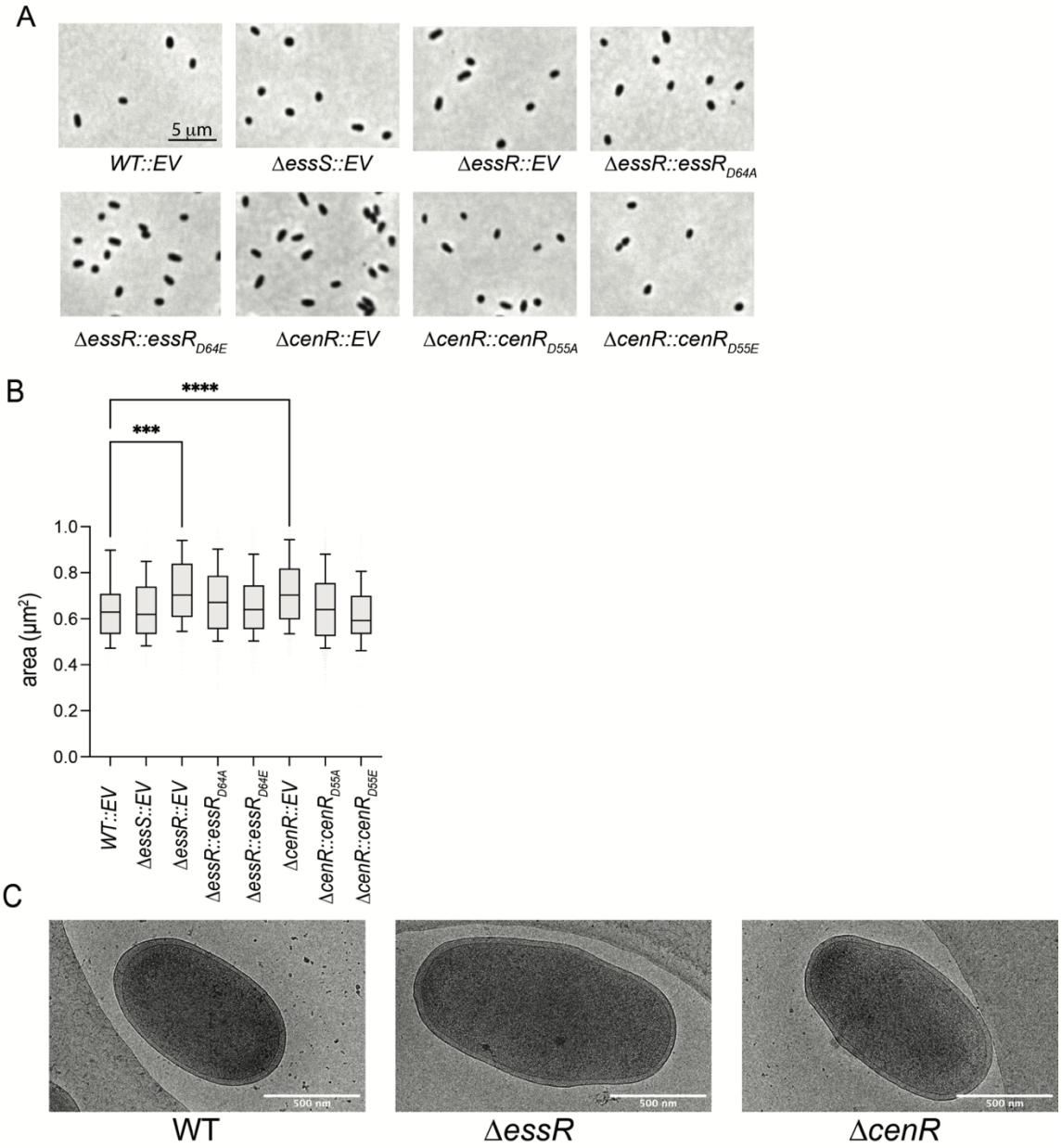

Figure 3.5: Deletion of *cenR* and *essR* results in increased cell area. A) Phase-contrast micrographs (630x magnification) of WT *B. ovis*, D*essS*, D*essR*, and D*cenR* in-frame deletion mutants; D*essR* complemented with *essR*$_{D64A}$ and *essR*$_{D64E}$; D*cenR* complemented with *cenR*$_{D55A}$ and cen*R*$_{D55E}$. B) Cell area analysis of WT (n=113), D*essS* (n=173), D*essR* (n=242), and D*cenR* (n=535) empty vector control strains (EV), D*essR* complemented with *essR*$_{D64A}$ (n=478) and *essR*$_{D64E}$ (n=466) alleles and D*cenR* complemented with *cenR*$_{D55A}$ (n=908) and cen*R*$_{D55E}$ (n=180) alleles. Mean is shown as a horizontal line in the box (25th-75th percentile); whiskers capture from 10th-90th percentile. Statistical significance was calculated using one-way ANOVA, followed by Dunnett's multiple comparison test to WT empty vector control (WT::EV) ($p < 0.001$, ***; $p < 0.0001$, ****). C) Representative cryo-EM images of WT *B. ovis*, Δ*essR*, and Δ*cenR* in-frame deletion mutants.

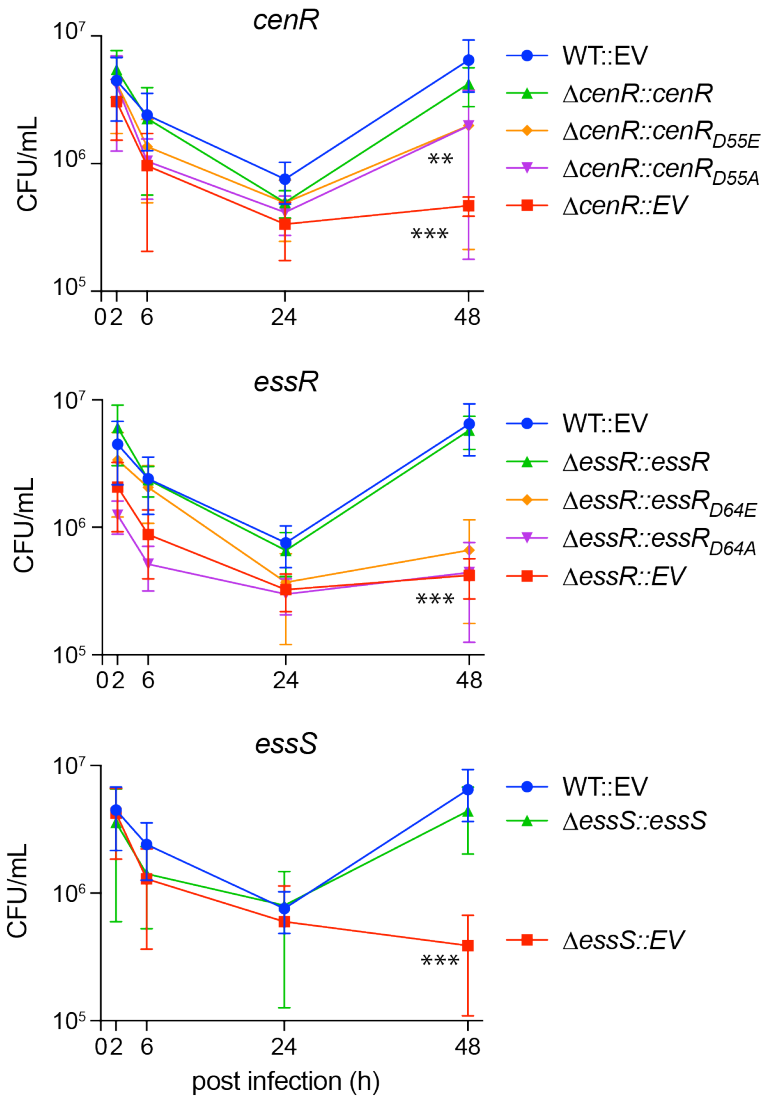

Figure 3.6: *B. ovis* Δ*cenR,* Δ*essR*, and Δ*essS* deletion strains have reduced fitness in the intracellular niche of mammalian macrophage-like cells; intact CenR and EssR aspartyl phosphorylation sites contribute to *B. ovis* fitness in the intracellular niche. Log_{10} colony forming units (CFU) per well of wild-type *B. ovis* carrying an integrated empty vector (WT::EV) (blue), Δ*cenR*, Δ*essR*, and Δ*essS* carrying an EV (red), or Δ*cenR*, Δ*essR*, and Δ*essS* expressing the missing gene from an integrated vector *(*green). Brucellae were isolated from infected THP-1 cells and enumerated at 2, 6, 24 and 48 hours (h) post infection. The contribution of the conserved aspartyl phosphorylation sites of CenR and EssR to intracellular fitness was assessed by testing for genetic complementation of D*cenR* and D*essR* phenotypes by integration of either non-phosphorylatable alleles of *cenR* (D55A) and *essR* (D64A) (purple) or putative phosphomimetic alleles (D55E / D64E) (orange). Infections were repeated 3 times; error bars represent standard deviation of the three biological replicates. Statistical significance was calculated at 48h p.i. using one-way ANOVA, followed by Dunnett's multiple comparisons test to WT::EV control ($p < 0.001$, **; $p < 0.0001$, ***).

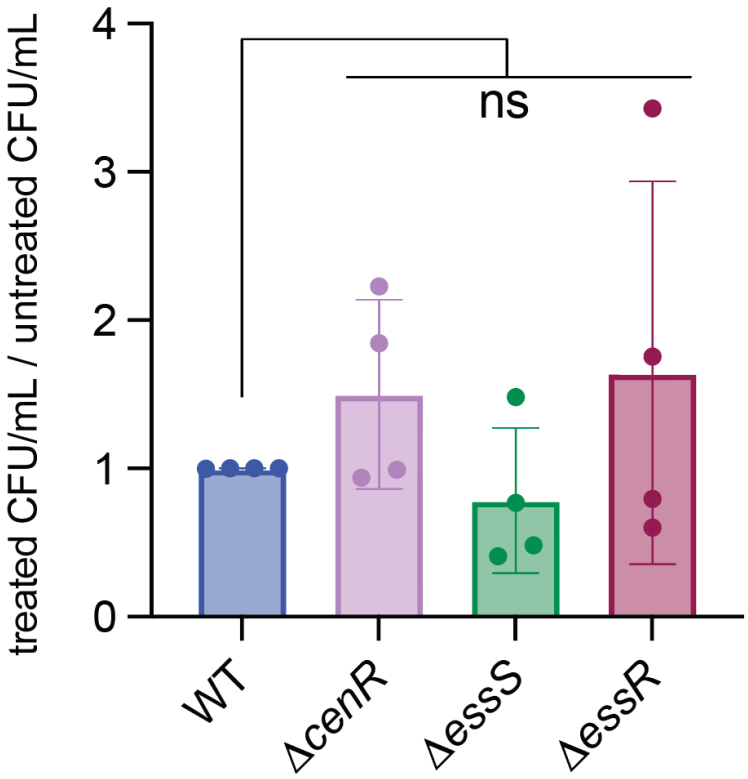

Figure 3.7: Δ*cenR,* Δ*essS*, and Δ*essR* are not sensitive to acidic pH. Strains harboring in-frame deletions of *cenR, essS*, and *essR* were incubated in Brucella broth at pH 7.0 or Brucella broth at pH 4.2 for 2 h before being serially diluted and plated on TSAB. CFU of treated cultures (pH 4.2) were normalized to CFU of untreated cultures (pH 7). Error bars represent the mean ± standard deviation of the four replicates. Statistical significance was calculated using one-way ANOVA, followed by Dunnett's multiple comparisons test to WT (n.s. = non-significant, $p > 0.05$).

Figure 3.8: CenR and EssRS regulate an overlapping set of genes and have a correlated ChIP-seq profile. (A) Heat map of $\log_2$ fold change in gene expression in Δ*cenR* and Δ*essRS* deletion strains relative to wildtype (WT). Genes presented have a fold change ³ |2| with an FDR p-value < 10^{-4}. Genes highlighted in orange are adjacent on the chromosome. (B) EssR and CenR chromatin immunoprecipitation (ChIP)-seq peaks (q-value £ 0.05; minimum AUC = 20) along chromosomes 1 and 2. Red lines mark significant DNA peaks that are immunoprecipitated by CenR and EssR. Blue lines indicate peaks that are unique to either CenR or EssR.

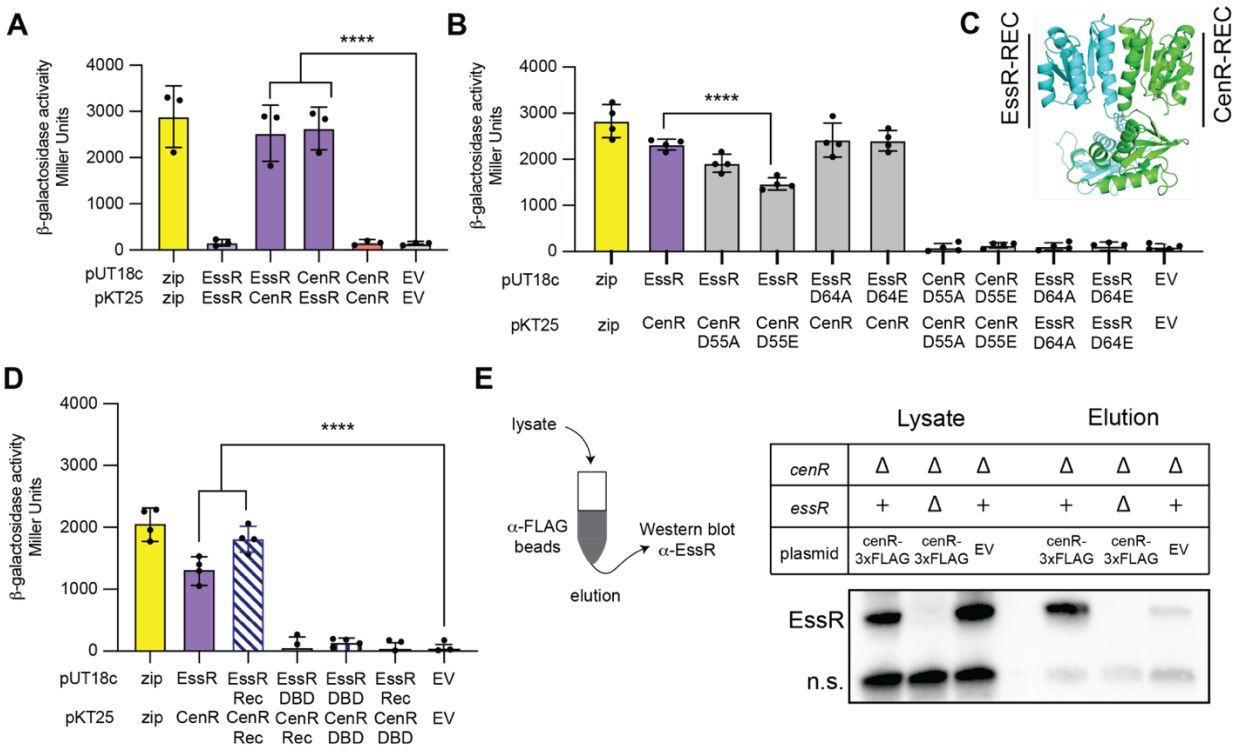

Figure 3.9: CenR and EssR physically interact in a heterologous system and in *B. ovis*. (A,B) Measurement of homomeric and heteromeric interactions between EssR and CenR (and their aspartyl phosphorylation site mutants; D®A & D®E) using an *E. coli* bacterial two-hybrid assay. Proteins were fused to split adenylate cyclase fragments in vectors pUT18c and pKT25. Positive control (zip) and empty vector (EV) negative controls are shown. (C) CenR:EssR heterodimer structure showing interaction at the α4-β5-α5 structural face of each protein as predicted by AFComplex2 (126); CenR (green) and EssR (blue) (D) Test for interactions between DNA-binding domain (DBD) and receiver domain (Rec) fragments of EssR and CenR by bacterial two-hybrid. Error bars represent the standard deviation of 4 biological replicates. Statistical significance was calculated using one-way ANOVA, followed by Dunnett's multiple comparisons test ($p < 0.0005$, ***; $p < 0.0001$, ****) to EV control or WT CenR-EssR interaction. (E) Co-immunoprecipitation of EssR and CenR-3xFLAG from *B. ovis* lysate. (left) CenR-3xFLAG was captured using anti-FLAG beads, which were washed before elution. (right) EssR association with CenR-3xFLAG in the eluate was monitored by Western blot using polyclonal antiserum to EssR (a-EssR). Non-specific (n.s.) cross-reactive band is shown as an indicator of loading. Representative blot from three biological replicates.

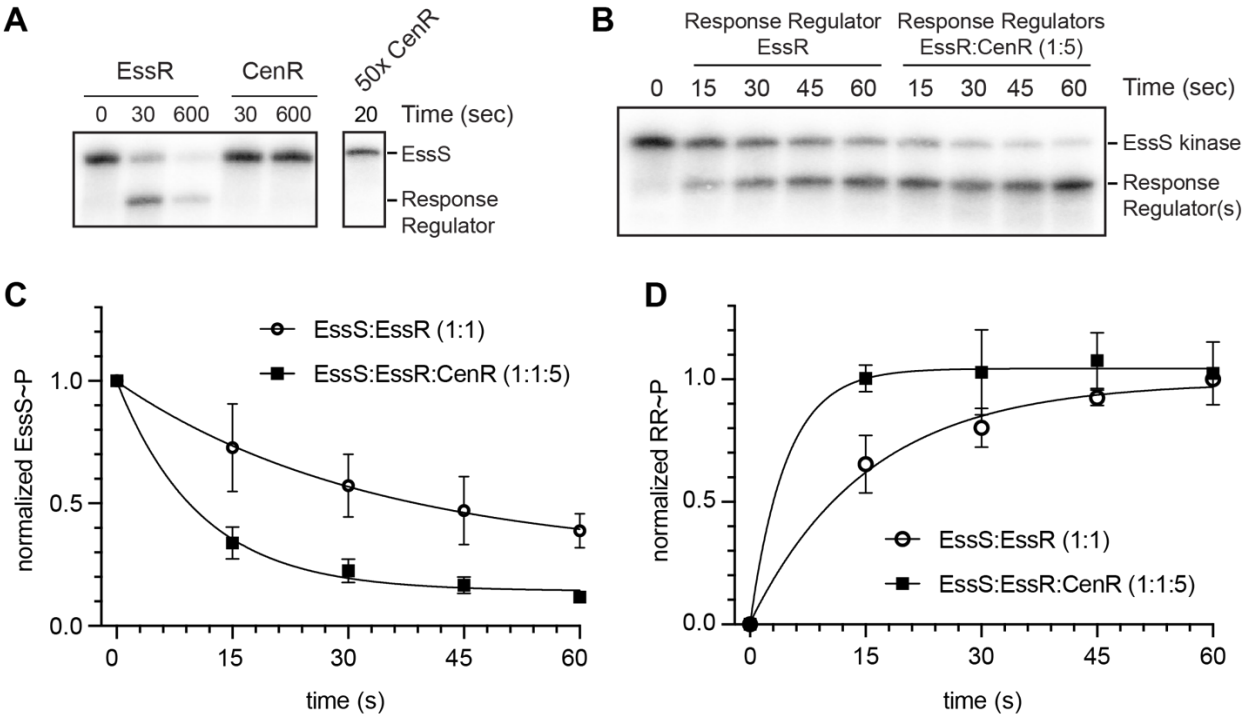

Figure 3.10: EssS specifically phosphorylates EssR; CenR stimulates phosphoryl transfer from EssS to EssR. (A) EssS autophosphorylation and phosphoryl transfer assay. Phosphoryl transfer from EssS to either EssR or CenR was assessed at 30s and 600s timepoints. 50x molar excess of CenR was added to phospho-EssS to test kinase specificity. Lower molecular weight band corresponds to phospho-EssR. B) Phosphoryl transfer kinetics from EssS to EssR at a 1:1 molar ratio and at a 1:1:5 (EssS:EssR:CenR) molar ratio. C) Normalized EssS-P dephosphorylation kinetics at a 1:1 molar ratio of EssS to EssR and at a 1:1:5 (EssS:EssR:CenR) ratio. D) Normalized EssR phosphorylation kinetics at the same molar ratios as panel C. Points and error bars represent the mean ± standard deviation of three replicates.

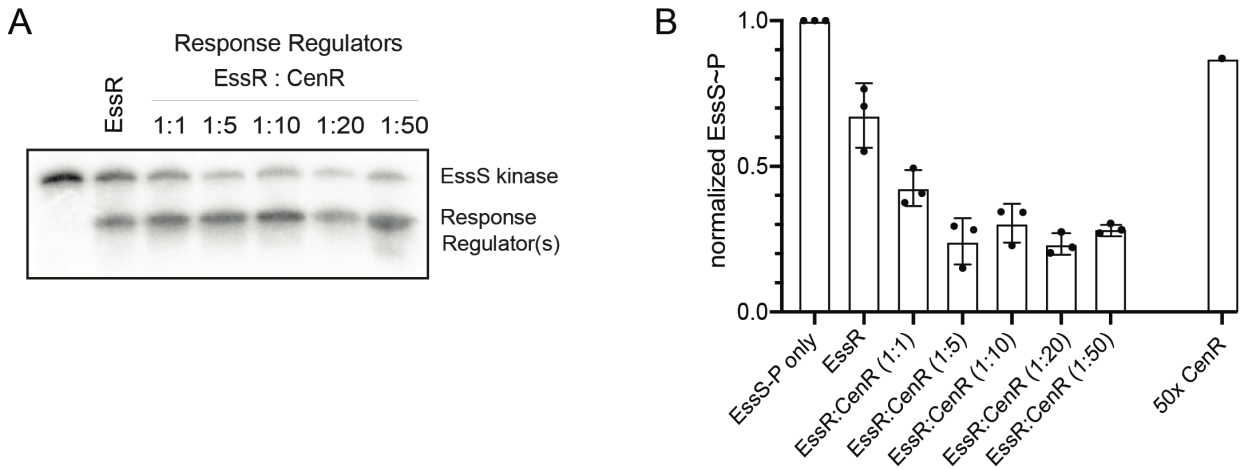

Figure 3.11: CenR enhances dephosphorylation of EssS~P in the presence of EssR. A) *In vitro* phosphoryl transfer assay with purified EssS kinase domain and EssR (1:1) and increasing ratiometric amounts of CenR. All reactions were stopped after 20s. B) Quantification of EssS~P levels; mean EssS~P band intensity is set to 1 in the EssS~P only reaction. Normalized EssS~P levels 20s after addition of EssR and CenR in varying ratios is plotted. Error bars represent the standard deviation of three biological replicates.

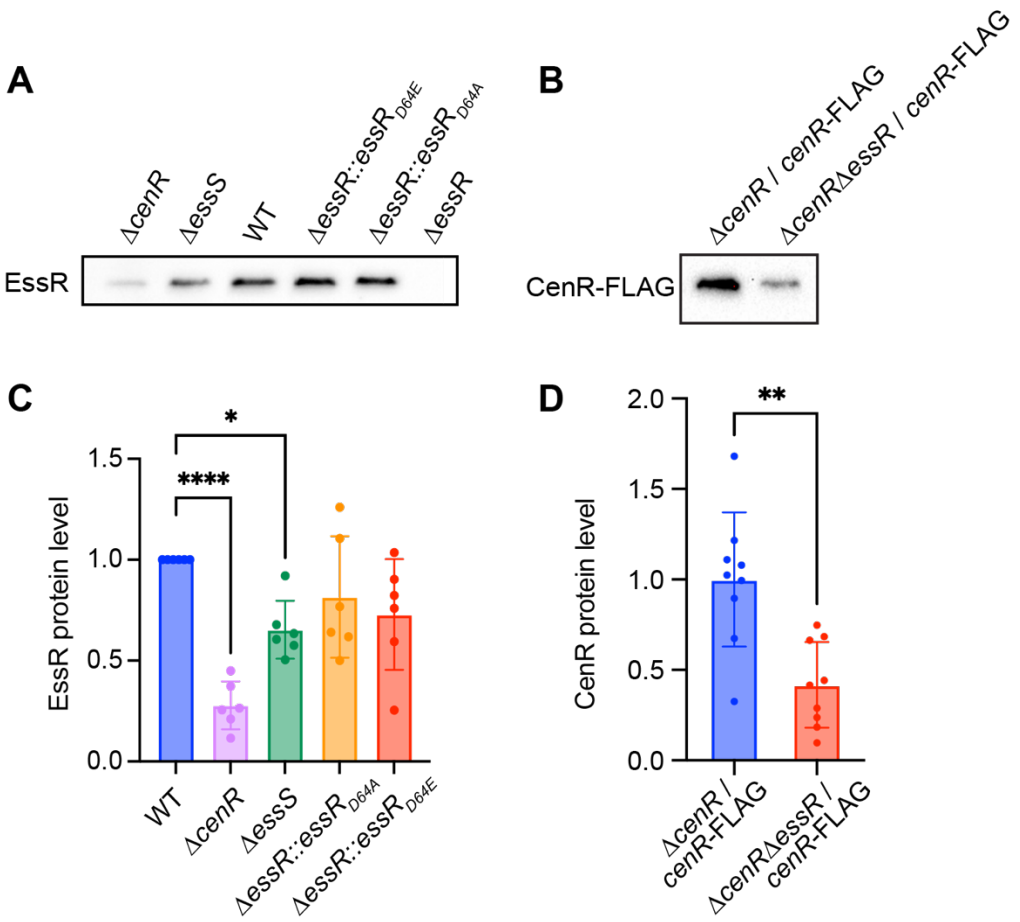

Figure 3.12: CenR and EssR proteins levels are influenced by each other. (A) a-EssR Western blot of lysate from WT *B. ovis* and *B. ovis* expressing EssR(D64A), EssR(D64E), and in strains lacking *essS* (D*essS*), *cenR* (D*cenR*) or *essR (*Δ*essR*). (B) a-FLAG Western blot of lysate from *B. ovis* strains lacking *cenR* (Δ*cenR*) or *cenR* and *essR (*Δ*cenR* Δ*essR*) and expressing *cenR-3xFLAG* from pQF plasmid. (C) Quantification of EssR band intensities normalized to the EssR intensity from WT on each blot. Error bars represent the mean ± standard deviation of six replicates. Statistical significance was calculated using one-way ANOVA, followed by Dunnett's multiple comparisons test to WT ($p < 0.05$, *; $p < 0.0001$, ****). (D) Quantification of CenR-3xFLAG band intensities normalized to the average intensity from Δ*cenR / cenR-3xFLAG* on each blot. Error bars represent the mean ± standard deviation of nine samples assayed on three independent blots. Statistical significance was calculated using an unpaired t test ($p < 0.005$, **).

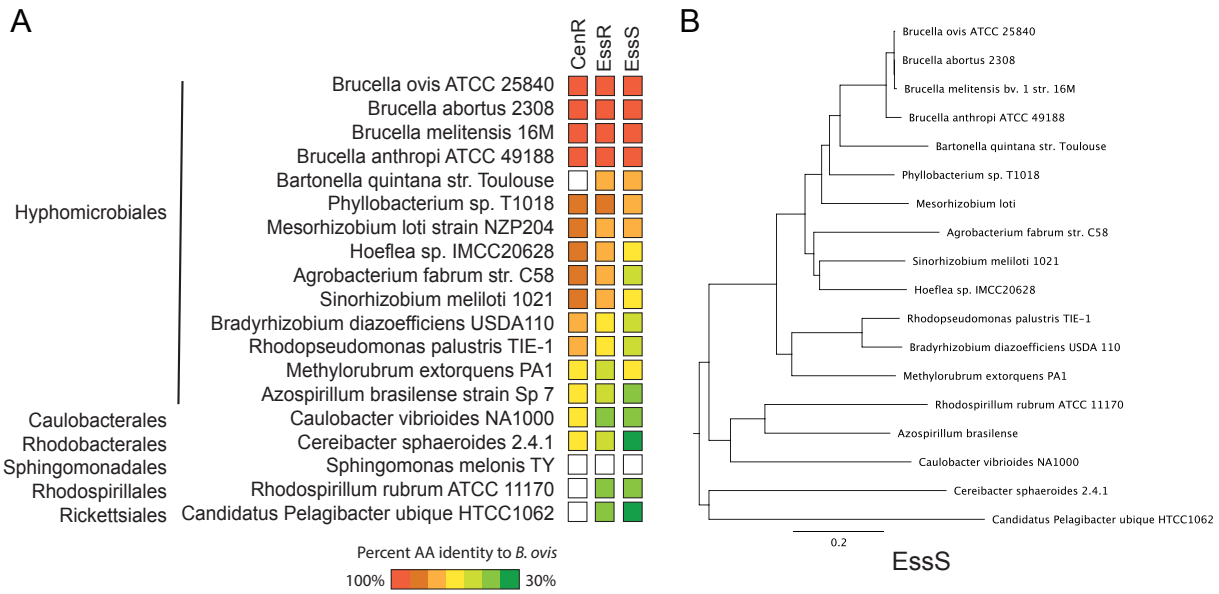

Figure 3.13: CenR, EssR, and EssS are widely distributed in the class Alphaproteobacteria. A) Representative Alphaproteobacterial genomes were queried for reciprocal top BLAST hits of CenR, EssR, and EssS. A gene was determined as present (colored box) if a reciprocal top-hit pair was found, and as absent (white) if no such pair was found. The color of the boxes reflects the percent amino acid (AA) identity (over the full protein length) to the corresponding *B. ovis* sequences. B) A phylogenetic tree based on the amino acid sequence of EssS orthologs. Global alignment with free end gaps was used as the alignment type and Blosum62 as the cost matrix. Jukes-Cantor was used as the genetic distance model and neighbor-joining was the tree build method with no outgroup.

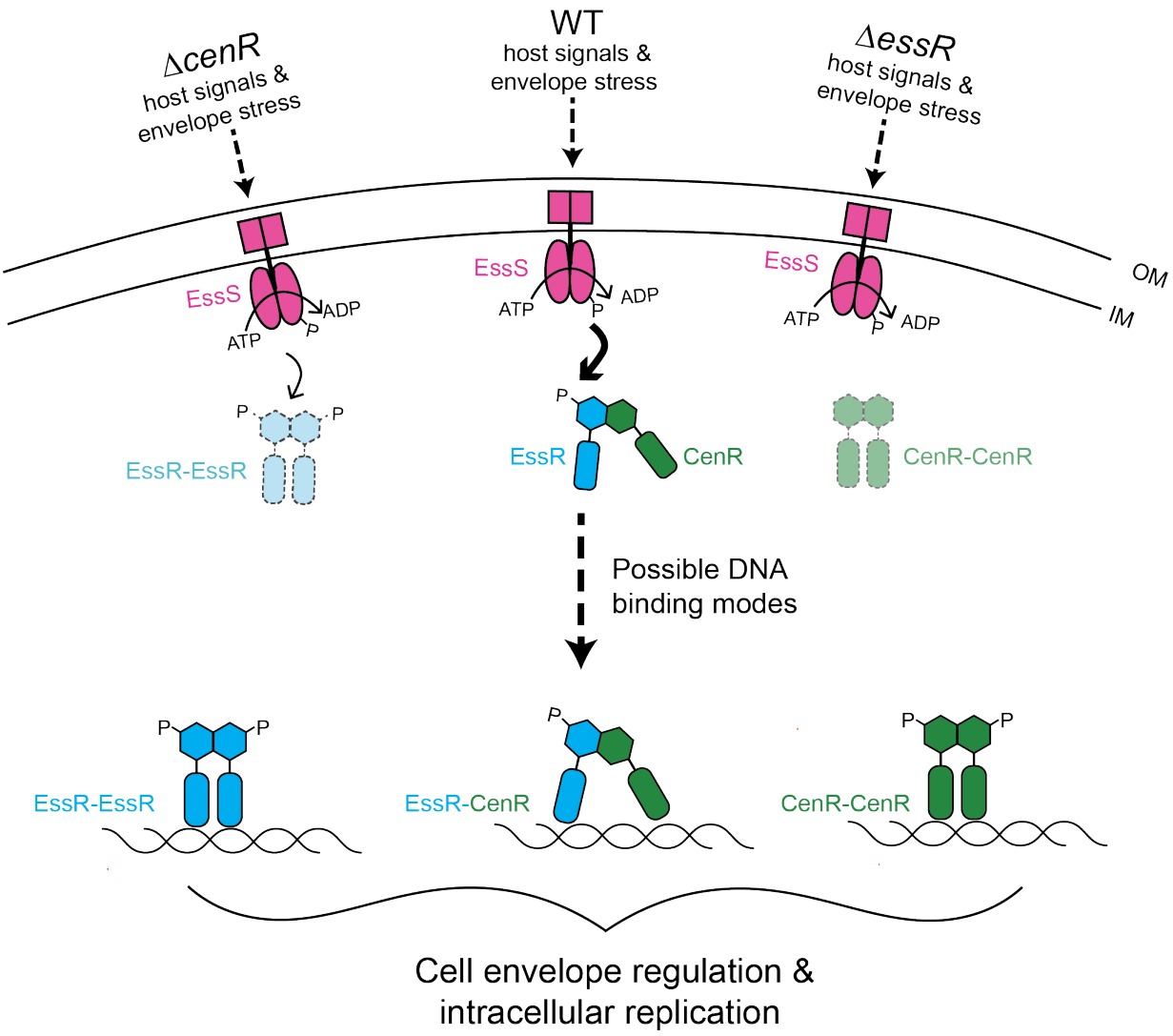

Figure 3.14: Model of EssS-EssR-CenR-dependent gene regulation in *B. ovis*. Upon detection of host signals, EssS (pink) autophosphorylates and transfers a phosphoryl group (P) to EssR (blue). CenR (green) supports EssS-EssR signal transduction by directly stimulating phosphoryl transfer from EssS and EssR via a receiver domain interaction. Loss of CenR results in diminished EssR levels (light blue with dashed outlines) and loss of EssR results in diminished CenR levels (light green with dashed outlines), via a post-transcriptional mechanism. CenR and EssR directly interact with an overlapping set of promoters, and three possible modes of transcriptional regulation by EssR and CenR are shown: EssR-EssR homodimer, EssR-CenR heterodimer, and/or CenR-CenR homodimers binding to target promoters. Genes regulated by the EssS-EssR-CenR system impact *B. ovis* cell size, contribute to growth/survival during cell envelope stress *in vitro*, and support intracellular replication in a macrophage infection model.

Chapter 4: *B. ovis* HWE kinase is important for detergent resistance

Introduction

In the initial system-level screen presented in Chapter 2, Δ*BOV_1602* was the only mutant that was more resistant to SDS than WT. Since little is known about BOV_1602 and to better understand the mechanism of this resistance phenotype, I used genetic and biochemical approaches to explore the impact of BOV_1602 in resistance to other detergents and membrane stressors, regulation of cell size, and intracellular survival inside macrophages. In this chapter, I demonstrate that deletion of *BOV_1602* leads to an altered outer membrane protein composition through its effects on gene regulation, both transcriptionally and post-transcriptionally. I also provide a partial mechanism of the detergent resistance phenotype of Δ*BOV_1602* through a connection with the type IV secretion system and a SPFH (stomatin/prohibitin/flotillin/HflKC) protein.

Results

The sensor histidine kinase gene BOV_1602 influences detergent resistance in Brucella ovis

BOV_1602 encodes a cytoplasmic HWE kinase. As mentioned earlier, HWE kinases are a group of kinases that possess the unique sequence HWE motif, and that are reported to form unusual oligomeric complexes (53, 54). Many HWE kinases in Alphaproteobacteria are involved in general stress response (58, 134). *BOV_1602* is not encoded adjacent to a response regulator and no studies have shown its interacting partners. Therefore, BOV_1602 is considered an orphan HK. Notably, *BOV_1602* is adjacent to the *nepR-ecfG-phyR* general stress response (GSR) locus (59) in *B. ovis*. Although it was reported that orthologs of *BOV_1602* do not regulate *Brucella* spp. GSR *in vitro* or *in vivo* (64, 135), the GSR regulation is complex and there may be conditions where BOV_1602 is involved. As presented in Chapter 2, deletion of *BOV_1602* leads to significant increase in resistance to the detergent, SDS. SDS is an anionic detergent, and I

sought to test whether *BOV_1602* also influenced resistance to detergents with different chemical properties. To do this, I performed the same agar stress assay with four additional detergents: the anionic bile acid detergent deoxycholate, the non-ionic detergent Triton, the cationic detergent cetyltrimethylamonium bromide (CTAB), and the zwitterionic detergent 3-((3-cholamidopropyl) dimethylammonio)-a-propanesulfonate (CHAPS). Similar to SDS, the Δ*BOV_1602* strain was also highly resistant to deoxycholate, Triton, and CHAPS (**Figure 4.1A**). Specifically, this strain was approximately 4-$\log_{10}$ units more resistant to deoxycholate, 3-$\log_{10}$ units more resistant to Triton, and 4-$\log_{10}$ units more resistant to CHAPS. Conversely, Δ*BOV_1602* was more sensitive to CTAB than WT. There is no apparent similarity between the chemical structures of all the detergents that Δ*BOV_1602* is resistant to (**Figure 4.1B**). However, CTAB is the only detergent with a positive charge. To test whether Δ*BOV_1602* is sensitive to other cationic molecules, I tested the mutant against polymyxin B, which is a cationic antibiotic that targets the outer membrane of Gram-negative bacteria (**Figure 4.2**). Similarly, Δ*BOV_1602* is more sensitive to polymyxin B than WT. This suggests that Δ*BOV_1602* may be more sensitive to positively charged compounds than WT.

Deletion of BOV_1602 does not impact the growth rate of B. ovis in broth culture

One hypothesis as to why Δ*BOV_1602* is resistant to SDS, deoxycholate, Triton, and CHAPS is that the mutant has a different growth rate than WT under no stress or detergent-stress conditions. Indeed, slow growth can often enhance survival of bacteria under stress conditions (136, 137). To test this hypothesis, I grew WT and mutant strains in Brucella broth and calculated the growth rate of each strain. Over the course of 24 hours, I did not observe any significant differences in growth rate or terminal culture density between Δ*BOV_1602* and WT (**Figure 4.3A**). These results provide evidence that the detergent-resistant phenotype is not a consequence of differences in growth rate between strains.

SDS treatment induces large transcriptional changes in WT but not in ΔBOV_1602

BOV_1602 encodes a sensor histidine kinase and is therefore predicted to impact detergent resistance through its effects on the regulation of gene expression. To uncover possible mechanisms underlying Δ*BOV_1602* SDS resistance, I therefore used RNA-seq to define transcriptional differences between Δ*BOV_1602* and WT that may explain the agar detergent resistance phenotype. To compare the transcriptome of WT to that of Δ*BOV_1602* mutant in unstressed and SDS stressed conditions, I grew strains on both TSAB and TSAB supplemented with SDS and extracted RNA from cells cultured in both conditions.

The transcriptional profile of the *ΔBOV_1602* strain differed significantly from that of the wild type (WT). When considering a fold change threshold of at least |2| and a false discovery rate (FDR) P-value < 0.0001, over 800 genes showed differential expression as a result of *BOV_1602* deletion in conditions without stress (**Table S6**). Notably, the transcriptional profiles of Δ*BOV_1602* cultivated on plain TSAB agar versus SDS agar are remarkably similar; only 261 genes exhibit differential expression between these conditions using the same criteria. In contrast, for WT, over 1000 genes are differentially expressed when comparing growth on SDS agar to growth on plain agar. This constitutes approximately one-third of all genes in the *B. ovis* genome. Many of the most highly differentially regulated genes upon *BOV_1602* deletion (in unstressed conditions) are also highly ranked in WT cultivated on SDS agar relative to plain agar, (**Figure 4.4; Table S6**). In fact, the set of genes dysregulated upon *BOV_1602* deletion contains over 400 of the same genes that change expression upon treatment of WT with SDS. In other words, the transcriptional profile of Δ*BOV_1602* in plain media strongly parallels that of WT under SDS stress conditions. From these results, one may infer that *BOV_1602* deletion transcriptionally "pre-adapts" *B. ovis* to SDS stress conditions. Specific classes of dysregulated genes that may be functionally relevant for the detergent resistance phenotype are described in the next sections below.

ΔBOV_1602 does not have stationary phase survival defect

Several genes encoding ribosomal proteins had reduced transcript levels in Δ*BOV_1602* relative to WT (**Table S6**). Downregulation of ribosomal proteins expression is a hallmark of the stringent response, which is a highly conserved starvation response in bacteria (138) that can impact cell survival in stationary phase (139). To test whether *BOV_1602* deletion influences *B. ovis* fitness in stationary phase, I measured cell viability in stationary phase. To do this, I grew WT and Δ*BOV_1602* in Brucella broth and plated for CFU/mL every 12 hours for 60 hours. I observed no difference in CFU between the mutant and WT at any time during the 60 hours (**Figure 4.3B**).

SDS treatment induces expression of Type IV secretion system genes

The *virB* operon encodes the *Brucella* type IV secretion system, which is a trans-envelope protein complex required for survival inside mammalian hosts(14, 140, 141). There are 12 genes in the *virB* operon, each encodes a component of the T4SS apparatus. In WT and Δ*BOV_1602* cells grown on SDS plates, all 12 *virB* genes were upregulated. Expression of most of these genes remain unchanged in Δ*BOV_1602* on plain TSAB agar, with the exception of *virB2, virB3*, and *virB4* which had increased expression upon *BOV_1602* deletion (**Table 4.1**). Many of the known regulators of the *virB* operon are also differentially expressed in all three groups, though *virB* operon itself did not show major changes in Δ*BOV_1602* grown on plain plates. For example, both the alpha and beta subunits of integration host factor (IHF) are upregulated in all three groups. IHF is known to bind to the promoter of *virB* operon and activate its transcription (142). The quorum sensing protein *vjbR* – a major type IV regulator (143, 144) - is also upregulated in all three groups. BlxR/BabR, another quorum sensing protein and a repressor of the *virB* operon (145), is downregulated in WT and Δ*BOV_1602* grown on SDS plates while being upregulated in Δ*BOV_1602* grown on plain plates.

Deletion of BOV_1602 leads to dysregulation of several outer membrane protein genes

Outer membrane proteins (OMPs) are important for cell membrane stability and changes in OMP composition could lead to differences in sensitivity to cell membrane disturbance. Since SDS is a detergent that targets the membrane, I postulated that *BOV_1602* deletion may result in compositional changes in OMPs as a result of transcriptional and/or post-transcriptional dysregulation. Indeed, my RNA-seq data revealed several genes encoding outer membrane proteins that were differentially expressed in Δ*BOV_1602* compared to WT (**Table 4.2**), regardless of treatment, as well as in WT cultured on SDS agar plates. For example, *omp25 (BOV_0692), omp31 (BOV_A0366), omp2a (BOV_0632), omp2b (BOV_0634),* and *ompW (BOV_1510)* were all downregulated in Δ*BOV_1602* grown on plain agar plates. On the other hand, *omp22 (BOV_1247), omp28 (BOV_1430),* and *omp1/bamA (BOV_1112)* were upregulated in Δ*BOV_1602*. Δ*BOV_1602* cultured on plain plates and WT cultured on SDS plates have similar transcriptional changes of these *omp* genes.

Outer membrane proteins and transporters protein levels are different in Δ**BOV_1602

Given the changes in transcript levels of outer membrane protein genes, I predicted that the protein levels of some of these regulated OMPs may also differ in Δ*BOV_1602* relative to WT. To measure changes in protein levels, I isolated outer membranes from both Δ*BOV_1602* and WT grown on plain TSAB plates and used mass spectrometry (LC/MS/MS) to identify and quantify the proteins. The most abundant protein in the WT *B. ovis* outer membrane was Omp2b (BOV_0634). Levels of this protein were reduced by approximately 50% in Δ*BOV_1602* (**Table S7**). Omp1/BamA (BOV_1112) was another abundant outer membrane protein in WT and, similar to Omp2b, its levels were lower in Δ*BOV_1602*. Omp28, as mentioned previously, had higher transcript levels in Δ*BOV_1602* (plain). Congruent with this observation, protein levels of Omp28 were approximately 50% higher in Δ*BOV_1602*.

BhuA, a TonB-dependent transporter encoded by the gene *BOV_A1093*, is yet another abundant OMP that has reduced levels in the Δ*BOV_1602* mutant (**Table S7**). Among the three

TonB-dependent transporters in *Brucella*, BhuA is unique as the sole heme transporter, crucial for sourcing iron, which Palluey et al. have demonstrated to be essential for sustaining chronic infections in mice (146). The TonB-dependent transporter, Cir (BOV_1306), showed a 40% decrease in abundance in *ΔBOV_1602*. Cir functions as an iron transporter, specifically mediating the uptake of iron chelated by *Brucella*-produced catechol siderophores, namely 2,3-dihydroxybenzoic acid (DHBA) and brucebactin (147). ExbB (*BOV_1612*) forms part of the membrane proton channel complex that powers TonB-dependent transporters using the proton motive force (148). In contrast to BhuA and Cir, the protein levels of ExbB were increased by approximately 60% in Δ*BOV_1602*. Likewise, the lipoprotein chaperone, LolA (BOV_1926), was also elevated in ∆*BOV_1602*. The complete list of differently synthesized OMPs in ∆*BOV_1602* are presented in Table S7.

Proteins involved in cell division and envelope biosynthesis are dysregulated in ∆BOV_1602

Approximately 20 proteins involved in cell division or cell envelope biosynthesis were differentially expressed in ∆*BOV_1602*. These include three proteins from the Tol-Pal system, TolB, TolQ, and Pal. This multi-protein complex spans the periplasm to the outer membrane, and it is essential for constricting the outer membrane and cell division in Gram-negative bacteria. The core components of Tol-Pal are made of TolA, TolB, TolQ, TolR, and Pal. My proteomic data show that TolB, TolQ, and Pal proteins are significantly elevated in ∆*BOV_1602* though the transcript levels were unchanged. This result provides evidence that post-transcriptional layers of regulation impact envelope composition when *BOV_1602* is deleted. There are six proteins in a 20-kb cell division/PG synthesis region on chromosome 1 that have different expression levels in ∆*BOV_1602* compared to WT.

Proteins associated with detergent resistant membranes are differentially expressed in ∆BOV_1602

Detergent-resistant membranes (DRMs) are lipid rafts on the cell membrane that are resistant to non-ionic detergent. They differ in lipid and protein composition from the rest of the cell membrane. Czolkoss et al. (149) reported proteins that are associated with DRMs in *Agrobacterium tumefaciens*, which is closely related to *Brucella* spp. Several proteins in *A. tumefaciens* DRMs were differentially expressed in ∆*BOV_1602*. SPFH (stomatin/prohibitin/flotillin/HflKC) proteins are markers of DRMs as they often co-purify with DRMS. Two SPFH proteins, HflC (BOV_1352) and SPFH/band 7/PHB domain protein (BOV_A0070), both have significantly higher protein expression levels in ∆*BOV_1602* than WT (**Table S7**). Both proteins are reported to be modulators of the zinc metalloprotease, FtsH (150). PpiD, peptidyl-prolyl cis-trans isomerase (BOV_0675), is a periplasmic chaperon for outer membrane proteins (151) and is a substrate of FtsH (152) and it also has an elevated protein level in ∆*BOV_1602* (**Table S7**).

T4SS (Type IV secretion system) components were also reported to be enriched in DRMs in *A. tumefaciens*. I observed upregulation of VirB3 (2.4-fold +), VirB4 (1.6-fold +), VirB9 (5-fold +), VirB10 (3-fold +), and VirB11(2-fold +) in ∆*BOV_1602*. VirB9 and VirB10 are part of the outer membrane core while VirB3 and VirB4 are on the inner membrane (**Figure 4.5**). VirB4 and VirB11 are the ATPases that supply energy for the system. Notably, levels of type IV proteins were not entirely congruent with transcripts: transcript levels of *virB3* and *virB4* were upregulated in ∆*BOV_1602* while there were slightly lower levels of *virB9*, *virB10*, and *virB11*. Other possible detergent resistance proteins include TatB (BOV_0874), a twin-arginine-targeting protein translocase, SipF (BOV_0653), signal peptidase I, and MotB (BOV_1656). All of these proteins were found exclusively in DRMs in *A. tumefaciens* and all have increased expression in ∆*BOV_1602*. The cell division protein FtsA (BOV_0803) was only found in DSM (detergent-sensitive membranes) in *A. tumefaciens* and its protein level is lower in ∆*BOV_1602* than in WT.

Elevated VirB and SPFH contribute to detergent resistance

Considering the notably enhanced levels of proteins known to be present in DRMs in *B. ovis* Δ*BOV_1602*, I next sought to test whether the changes in these DRM-associated proteins play a role in the detergent resistance phenotype of Δ*BOV_1602*. To this end, I constructed in-frame deletions of the Type IV secretion system (T4SS) membrane components, specifically *virB8-virB11*, since they are in an operon, as well as one SPFH protein, *BOV_A0070*, in the Δ*BOV_1602* background. These mutants were then subjected to the same agar stress assay to assess their phenotypes. The double deletion strains, Δ*BOV_1602* Δ*virB8-12* and Δ*BOV_1602* Δ*BOV_A0070*, were more sensitive to Triton, CHAPS, and deoxycholate compared to the Δ*BOV_1602* single mutant, though these strains remained more resistant to detergent than the WT. The Δ*BOV_1602* Δ*BOV_A0070* double mutant is more sensitive to Triton and CHAPS than Δ*BOV_1602* Δ*virB8-11.* I conclude that the VirB system and BOV_A0070 contribute to the Triton, CHAPS, and deoxycholate resistance phenotype of Δ*BOV_1602*. However, both double mutants had detergent resistance profiles similar to that of the Δ*BOV_1602* single mutant in SDS and CTAB (**Figure 4.6**). This indicates that factors other than VirB or BOV_A0070 contribute to the SDS resistance and CTAB sensitivity in Δ*BOV_1602*. Additionally, Δ*BOV_1602* appears to have denser colony than the double and triple mutants on TSAB containing Triton, CHAPS, deoxycholate, and SDS, even though all four mutants have similar CFU on SDS agar plate. Notably, the deletion of *virB8-12* and *BOV_A0070* in the Δ*BOV_1602* background resulted in a pronounced increase in sensitivity to NaCl. I also made a triple mutant, deleting *BOV_1602, virB8-virB11,* and *BOV_A0070*. The triple mutant phenocopied the double mutant Δ*BOV_1602* Δ*virB8-1* in all the tested conditions (**Figure 4.6**).

ΔBOV_1602 has cell size defect

Given the changes in levels of proteins associated with cell division processes in Δ*BOV_1602*, I hypothesized that the mutant cells would have morphological differences from WT. I inspected the mutant cells by phase contrast microscopy and did not observe major

defects/differences in cell shape (**Figure 4.7A**). However, careful measurements of cell size showed that deletion of *BOV_1602* results in longer and wider cells compared to WT (**Figure 4.7B**). Interestingly, though Δ*BOV_1602* Δ*virB8-11* and Δ*BOV_1602* Δ*BOV_A0070* partially rescued the detergent resistance phenotype, they did not complement the cell size defect phenotype. Similar to the single mutant Δ*BOV_1602*, the double mutants Δ*BOV_1602* Δ*virB8-11* and Δ*BOV_1602* Δ*BOV_A0070* also have bigger cell size than WT.

ΔBOV_1602 does not display differences in fitness in macrophage infection

The Type IV secretion system (T4SS) is an important virulence determinant for *Brucella* spp. Given my observations of transcriptional upregulation and increased protein levels in of the Type IV (VirB) system in Δ*BOV_1602*, I tested whether Δ*BOV_1602* displayed any fitness differences relative to the wild type (WT) in a macrophage infection model. However, deletion of *BOV_1602* did not result in any significant defect or advantage in fitness or survival following entry (2 hours post-infection), during the early stages of infection (6 and 24 hours post-infection), or throughout the later stages of infection (48 and 72 hours post-infection) as compared to WT (**Figure 4.8**).

Conclusion

Maintaining cell envelope integrity is critical for bacterial survival. Regulating the outer membrane composition is important for resistance to different envelope stressors. In this chapter, I have provided experimental evidence that the orphan HWE HK, BOV_1602, impacts resistance to different cell envelope stressors, especially detergents. RNA-seq, mass spectrometry of outer membrane fractions and cell size analysis revealed that BOV_1602 regulates composition of membrane proteins, cell size, and cell shape in *B. ovis*. My analysis of RNA-seq data from Δ*BOV_1602* revealed that deletion of BOV_1602 primes the cells to a “detergent-ready” state (**Figure 4.9**), where the cells are transcriptionally primed to resist detergent assault. Lastly, combining proteomic data and genetic manipulation, I have shown that deletion of BOV_1602 led to elevated protein levels of type IV secretion system and SPFH proteins, which both contribute

to the detergent resistance phenotype. Overall, this study sheds light on a previously unknown regulatory role of a HWE HK and a link between T4SS and SPFH and detergent resistance.

Figures

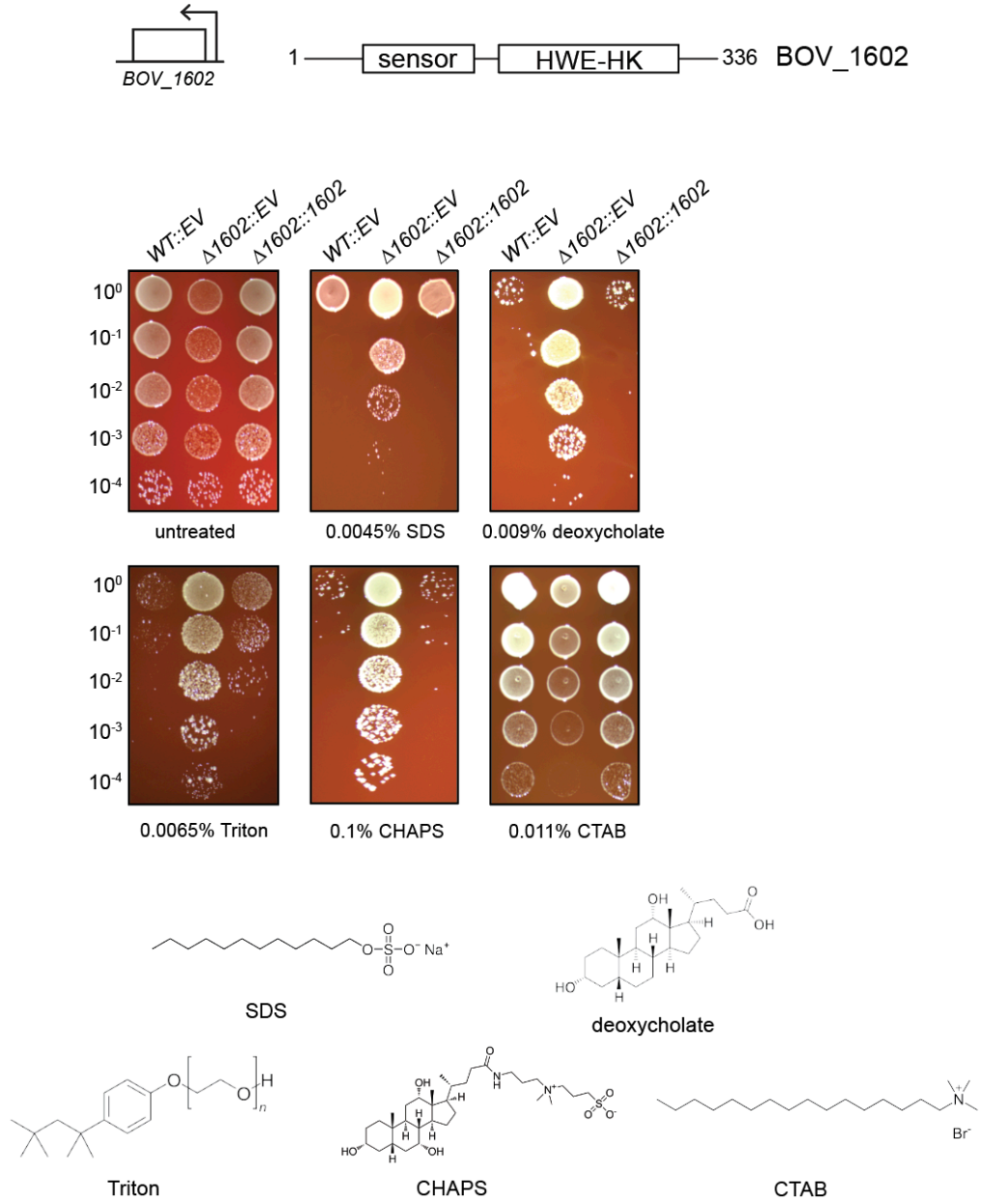

Figure 4.1: Analysis of *BOV_1602* deletion strain to different detergents. (A) (left) Cartoon of the *BOV_1602 S* genetic locus. (right) Protein domain models of BOV_1602 with number of amino acid residues in each protein. Domains are labeled as follows: sensor - extracellular sensor domain, HWE-HK – HWE histidine kinase domain. (B) Strains harboring an in-frame deletion of *BOV_1602*, carrying integrated empty vector (EV) or genetic complementation vector (::1602) were plated in log10 dilution series on plain TSA blood agar (TSAB), TSAB containing SDS, sodium deoxycholate, Triton X-100, CHAPS, or CTAB. Dilution plating experiments were repeated at least three times, and one representative experiment is shown. (C) Chemical structures of each detergent used in panel B.

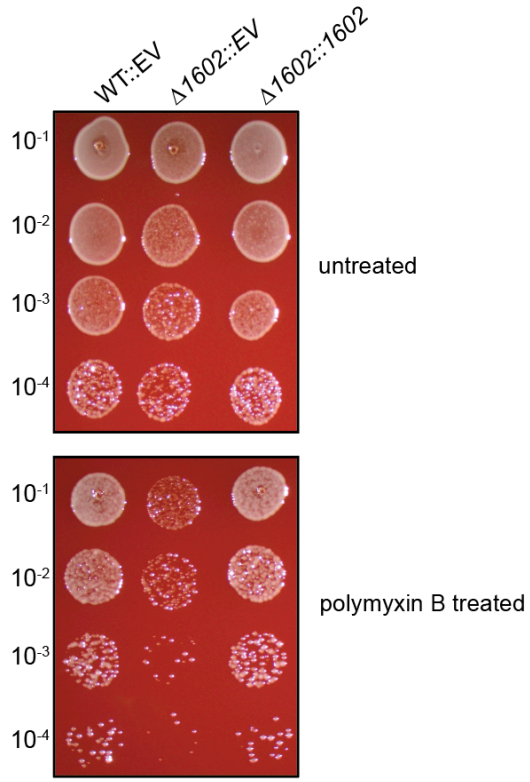

Figure 4.2: Δ*BOV_1602* is sensitive to polymyxin B treatment. Strains harboring in-frame unmarked deletions (Δ) of *BOV_1602*, carrying integrated empty vectors (EV) or genetic complementation vectors (::*1602*) were plated in $\log_{10}$ dilution series on plain TSA blood agar (untreated), or cells treated with 1 mg/mL polymyxin B for 80 minutes before being plated on TSA-B (polymyxin B treated). Dilution plating experiments were repeated three times for all strains, and one representative experiment is shown.

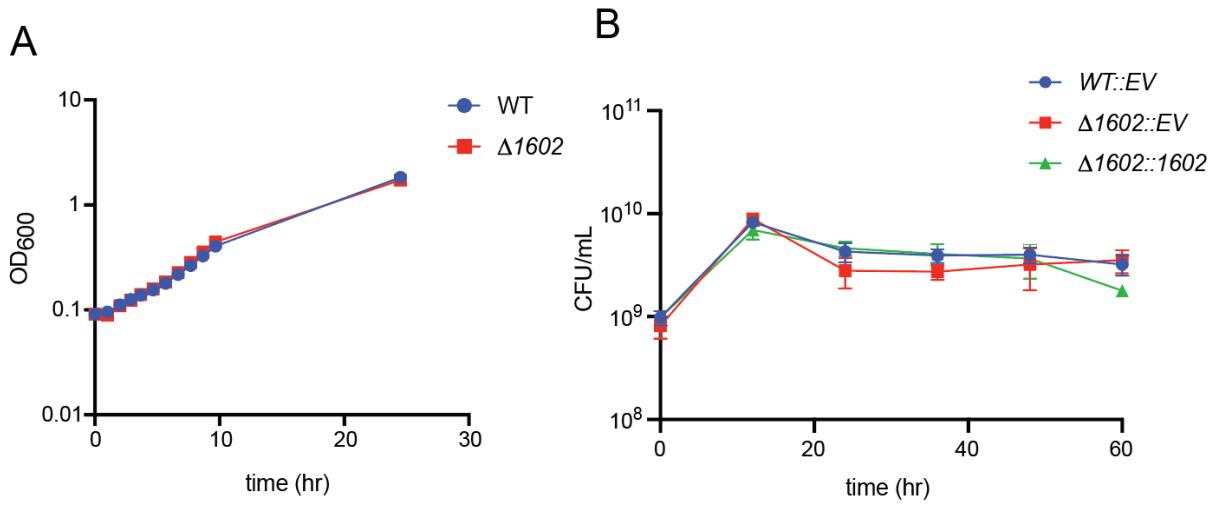

Figure 4.3: deletion of BOV_1602 does not lead to growth rate defect or long-term stationary survival defect. (A) Growth curve of WT and Δ*BOV_1602* in Brucella broth over the course of 24h. The growth rate of Δ*BOV_1602* is 0.00307 min^{-1} and of WT is 0.002775 min^{-1}. (B) Recovered CFU/mL of cultures grown in Brucella broth over the course of 60h. All experiments were repeated three times; error bars represent standard deviation of the three biological replicates.

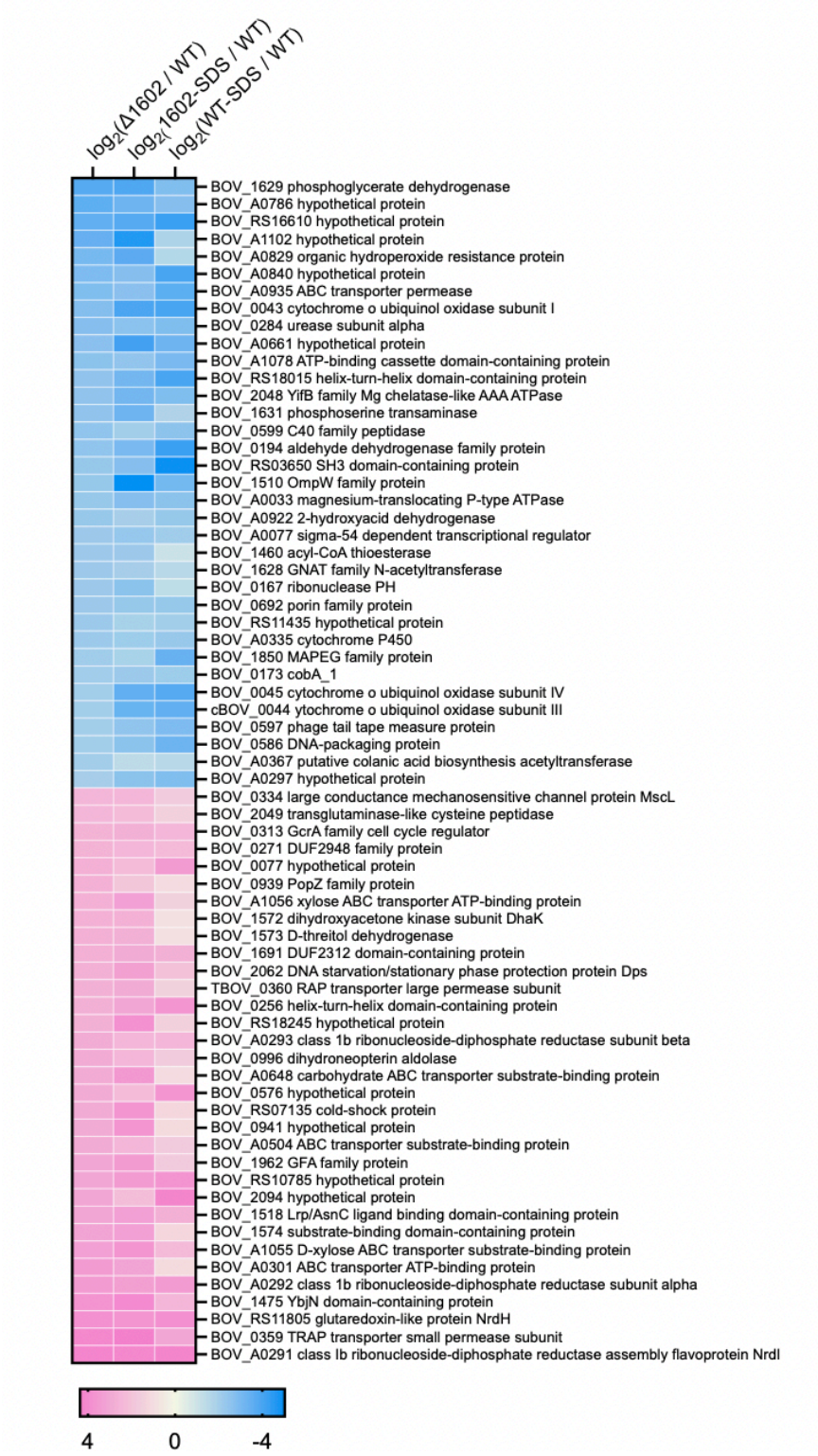

Figure 4.4: deletion of BOV_1602 with or without SDS treatment leads to similar transcriptional changes as WT treated with SDS. Genes presented have a $\log_2$ fold change either > 2.5 or < -2; all genes have an FDR P-value < 10^{-4}.

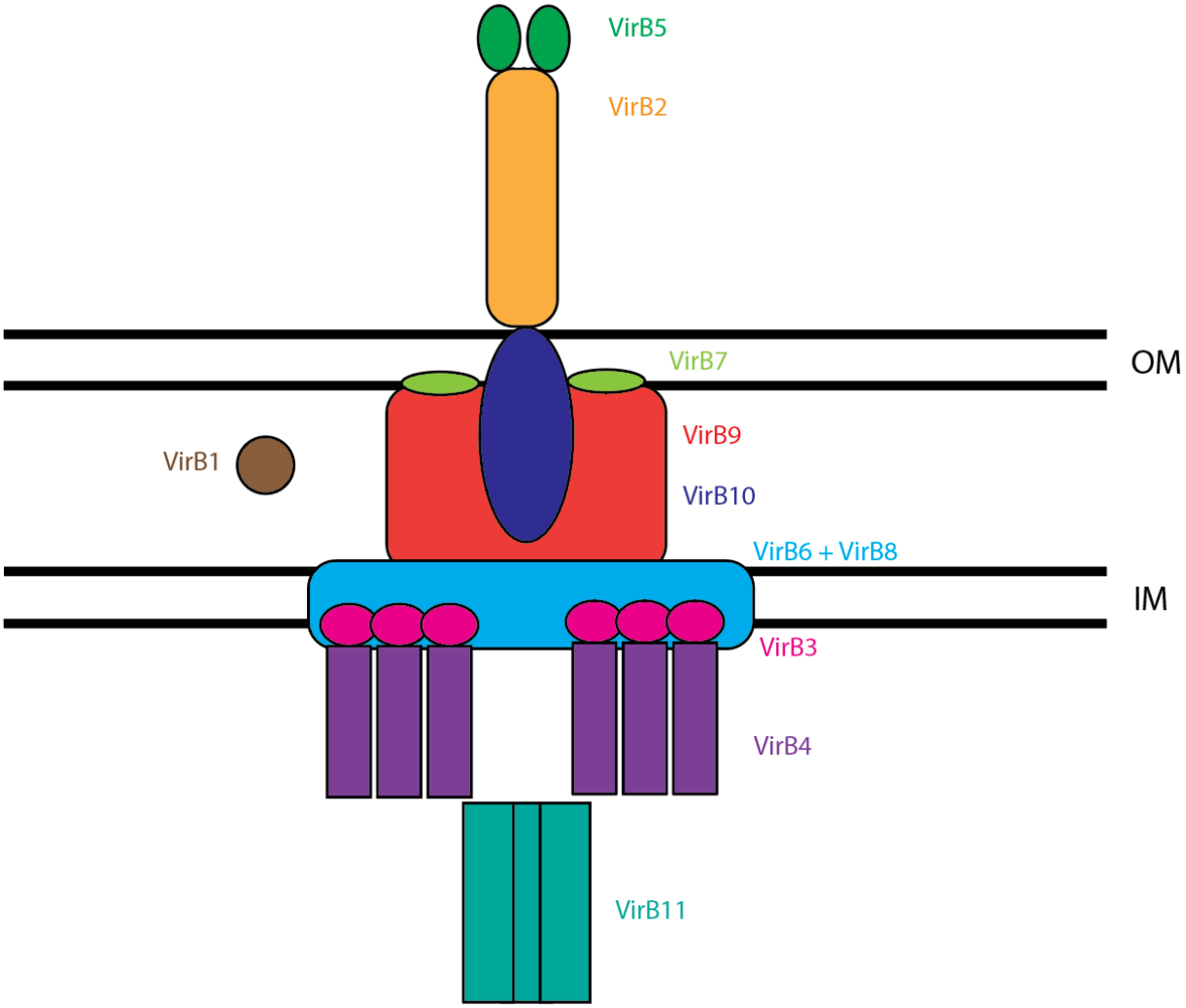

Figure 4.5: cartoon model of the T4SS in Brucella. Figure is adapted from published figures (153, 154). The external pilus is composed of VirB2 (orange) and VirB5 (green). The outer membrane core is composed of VirB7 9 (lime green), VirB9 (red), and VirB10 (dark blue). VirB1 (brown) locates in the periplasm. The inner membrane core is composed of VirB6 (light blue), VirB8 (light blue), VirB3 (pink), and VirB4 (purple). VirB11 (teal) is in the cytoplasm but its exact interaction with the rest of the T4SS apparatus is still unclear.

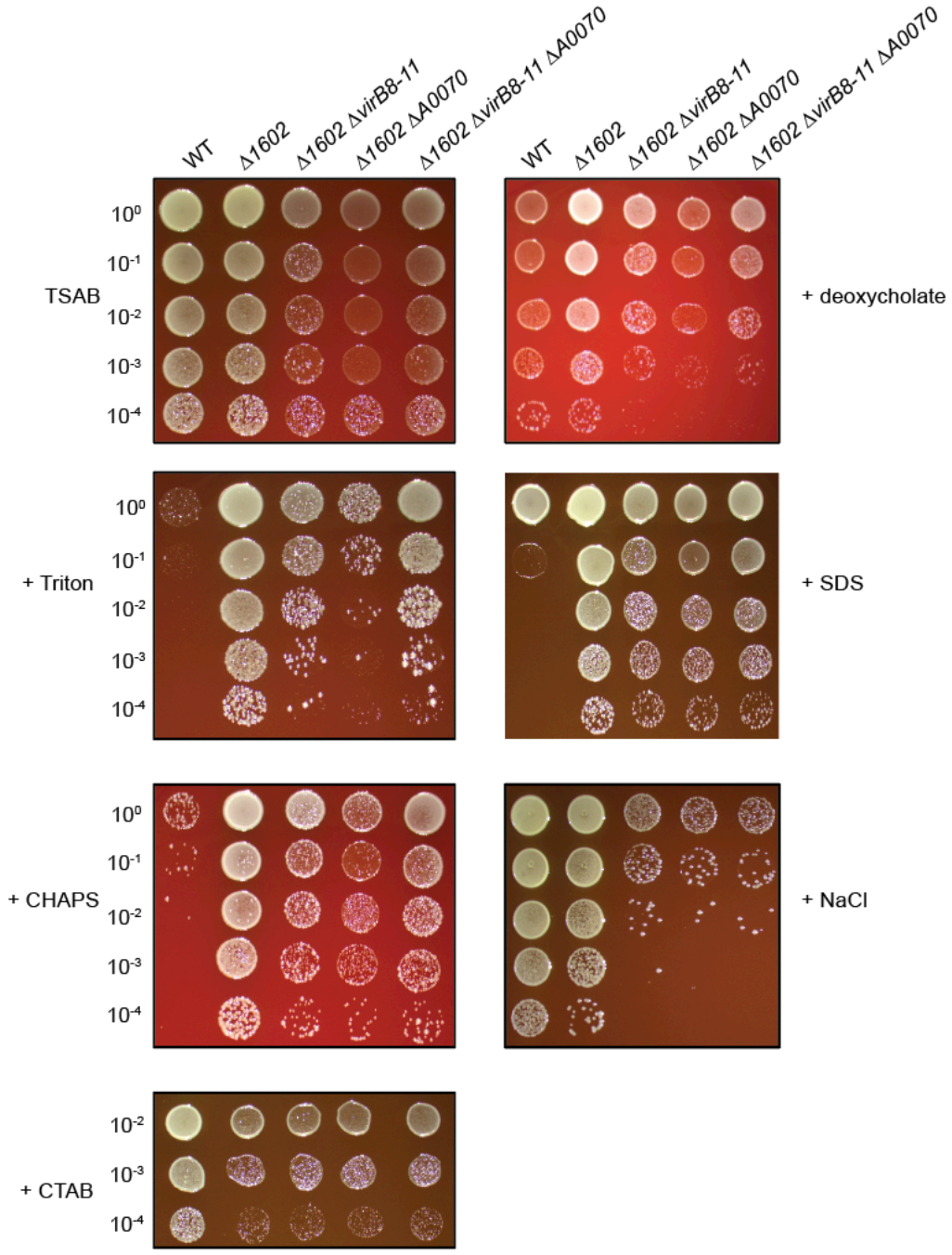

Figure 4.6: VirB8-11 and BOV_A0070 are important for detergent resistance. Strains harboring in-frame unmarked deletions of *B. ovis* TCS gene loci *BOV_1602* (*Δ1602*) alone and in combination of *BOV_A0054-A0057 (ΔvirB8-11),* and *BOV_A0070 (ΔA0070)* were plated in $\log_{10}$ dilution series on plain TSA blood agar (TSAB), TSAB containing 0.09% Triton (+Triton), 0.1% CHAPS (+CHAPS), 0.11% CTAB (+CTAB), 0.08% deoxycholate (+deoxycholate), 0.045% SDS (+SDS), or 215 mM NaCl (+NaCl). Dilution plating experiments were repeated at least three times, and one representative experiment is shown.

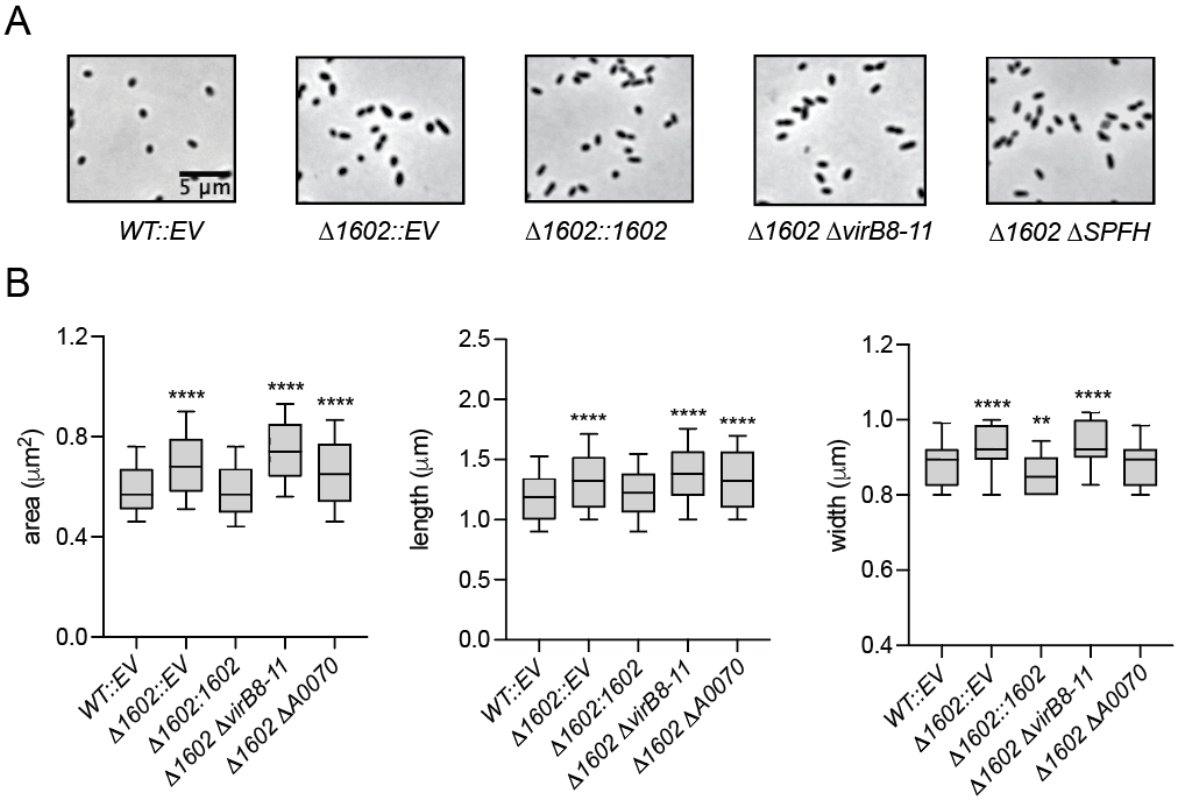

Figure 4.7: cell size analysis of *B. ovis* Δ*1602,* Δ*1602* Δ*virB8-11*, and Δ*1602* Δ*A0070*. (A) Representative phase contrast micrographs (630x magnification) of WT *B. ovis*, Δ*1602,* Δ*1602* Δ*virB8-11,* Δ*1602* Δ*A0070* in-frame deletion mutants. (B) Cell area, length and width analysis of WT (n=267), Δ*1602* (n=425) empty vector control strains (EV), Δ*1602* complementation strain (n=522), Δ*1602* Δ*virB8-11* (n=230), Δ*1602* Δ*A0070* (n=403). Mean is shown as a horizontal line in the box (25th-75th percentile); wiskers capture from 10th-90th percentile. Statistical significance was calculated using one-way ANOVA, followed by Dunnett's multiple comparison test to WT empty vector control (*WT::EV*) ($p<0.005$, **; $p<0.0001$, ****).

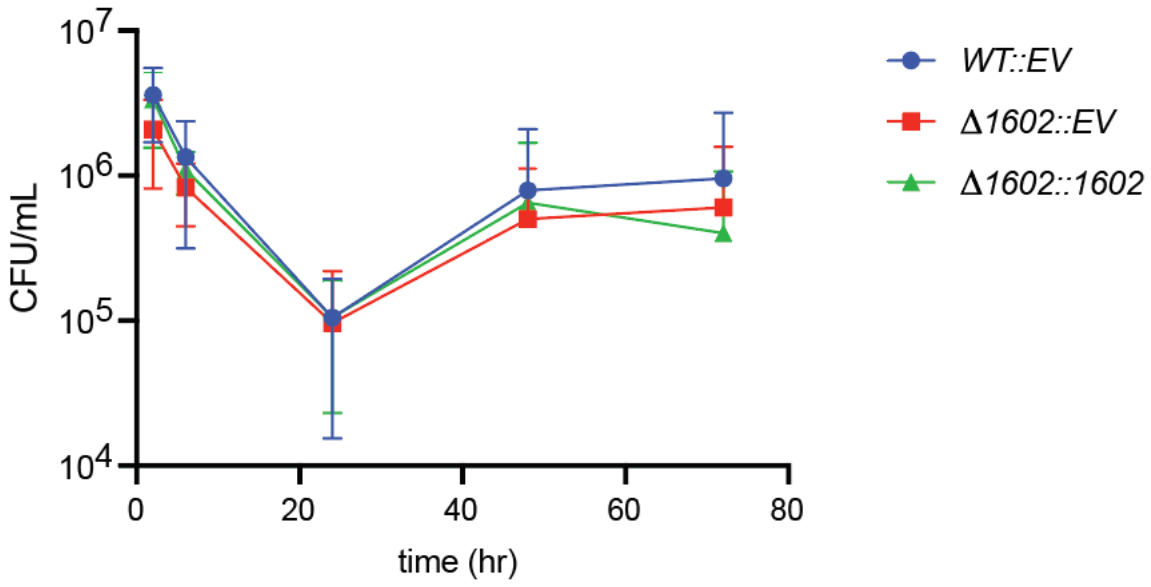

Figure 4.8: deletion of 1602 does not affect fitness during infection in human macrophage-like cells. Log10 CFU per well of wild-type *B. ovis* carrying an integrated empty vector (*WT::EV*) (blue, circle), Δ*1602* carrying an EV *(Δ1602::EV*) (red, square), and Δ*1602* carrying an integrated vector with 1602 under its native promoter (green, triangle). *Brucellae* were isolated from THP-1 cells and enumerated at 2, 6, 24, 48, and 72 h post-infection. Infections were repeated four times; error bars represent standard deviation of four biological replicates.

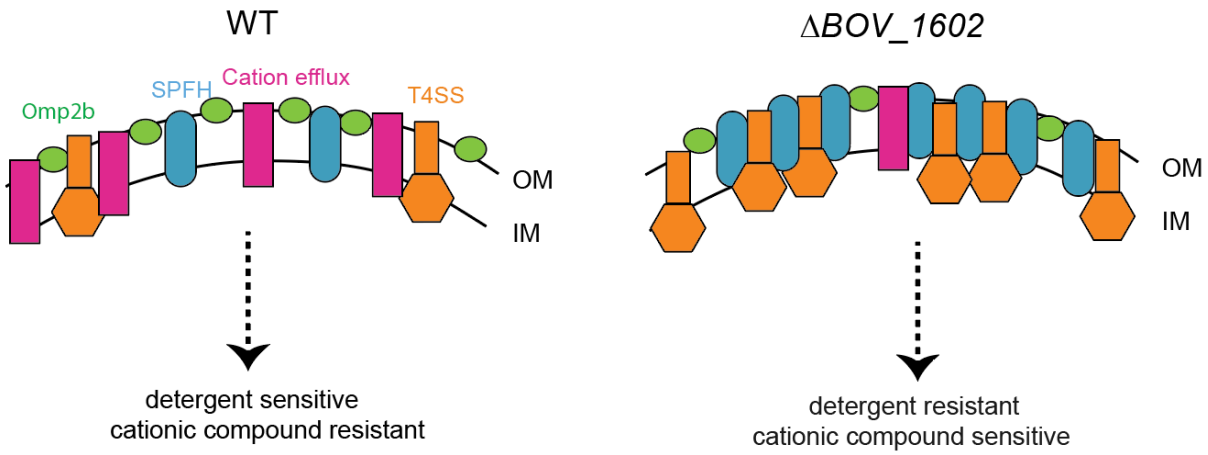

Figure 4.9: model of Δ*BOV_1602* detergent resistant mechanism. In WT *Brucella* cells, there are more Omp2b (green) and cation efflux (pink) proteins and less SPFH (blue) and T4SS (orange) proteins on the cell membrane. In Δ*BOV_1602* mutant cells, there are more T4SS and SPFH proteins and less Omp2b and cation efflux proteins. This differences in outer membrane protein composition may lead to the difference in sensitivity to detergents and cationic compounds.

Tables

Table 4.1: transcriptional changes of *virB* operon and its regulators

Gene name	Locus tag	Log_2 (Δ1602 / WT)	Log_2 (Δ1602-SDS / WT)	Log_2 (WT-SDS / WT)
virB1	BOV_A0063	-0.17	-0.59	1.21
virB2	BOV_A0062	1.26	1.98	3.00
virB3	BOV_A0061	1.84	3.00	3.75
virB4	BOV_A0060	0.92	2.31	3.37
virB5	BOV_A0059	-0.52	0.40	0.67
virB6	BOV_A0058	-0.66	0.73	1.38
virB7	BOV_RS10630	-0.14	2.13	2.66
virB8	BOV_A0057	0.07	1.58	2.81
virB9	BOV_A0056	-0.87	0.37	1.68
virB10	BOV_A0055	-0.87	0.36	2.07
virB11	BOV_A0054	-0.58	1.04	2.05
virB12	BOV_A0053	-0.06	1.24	1.90
vjbR	BOV_A0110	0.90	2.04	1.53
hutC	BOV_A0869	0.06	0.32	-0.09
IHF a subunit	BOV_0771	1.47	1.18	1.91
IHF b subunit	BOV_0148	1.77	1.06	1.15
BvrR	BOV_2010	-0.22	-0.38	-0.99
BlxR	BOV_0183	0.73	-0.85	-2.44

Table 4.2: transcriptional changes of outer membrane protein genes

gene name	locus tag	Log_2 (Δ1602 / WT)	Log_2 (Δ1602-SDS / WT)	Log_2 (WT-SDS / WT)
omp25	BOV_0692	-2.22	-2.34	-2.36
omp25c	BOV_0115	-0.29	-0.42	-0.26
omp25d	BOV_0116	0.29	-0.07	-0.30
omp31	BOV_A0366	-1.15	-1.62	-0.52
omp22	BOV_1247	1.16	2.15	3.82
omp19	BOV_1858	-0.40	-0.70	0.44
omp10	BOV_A0072	-0.74	-0.59	-1.13
omp16 (pal)	BOV_1638	0.07	0.32	1.35
omp1 (bamA)	BOV_1112	1.65	1.66	1.65
Putative outer membrane protein	BOV_A0863	0.19	-0.11	0.31
Putative outer membrane protein	BOV_1633	0.03	0.66	0.27
omp2a	BOV_0632	-1.00	-0.28	-1.15
omp2b	BOV_0634	-0.70	-0.51	-0.98
omp28	BOV_1430	1.00	1.00	1.40
ompW	BOV_1510	-2.35	-5.03	-3.11

Material & Methods

Chromosomal deletion strain construction and complementation strain construction

Same as described in Chapters 2 and 3.

Agar plate growth/stress assays

After 2 days of growth on TSAB or TSAB supplemented with kanamycin, *B. ovis* cells were collected and resuspended in sterile phosphate-buffered saline (PBS) to an OD_{600} = 0.3. Each strain was serially diluted in PBS using a 10^{-1} dilution factor. 5 µl of each dilution was plated onto either TSAB, TSAB containing 0.0045% SDS, 0.008-0.009% deoxycholate, 0.0065-0.008% Triton, 0.1% CHAPS, 0.011% CTAB, or 215 mM NaCl. After 3 days of incubation for TSAB, 4 days for TSAB + 0.0045% SDS, 0.008-0.009% deoxycholate, 0.0065-0.008% Triton, 0.1% CHAPS, 0.011% CTAB, and 5 days for TSAB + 215 mM NaCl, growth was documented photographically.

Polymyxin B stress assay

Same was previously described in Chapter 3.

Growth curve

Strains were grown on TSAB plates for two days. Cells were inoculated in 8 mL Brucella broth and incubated on rotor overnight. The next day, cells were back diluted to OD_{600} = 0.05 in 9 mL Brucella broth at time = 0 h. Optical density at 600 was measured every hour for the first 9 hours and once at 24 h.

Long-term stationary survival assay

After 2 days of growth on on TSAB supplemented with kanamycin, *B. ovis* cells were collected and resuspended in 8 mL Brucella broth and incubated on rotor overnight. The next day, cells were back diluted to OD_{600} = 0.05 in 9 mL Brucella broth at time = 0 h. 100 µL of culture was taken to be serially diluted in PBS using a 10^{-1} dilution factor. 5 µl of each dilution was plated onto TSAB. Plates were incubated for 3 days and CFU were enumerated. The same step was repeated every 12 h for 60 h.

RNA extraction and sequencing

B. ovis strains were grown on either TSAB for 2 days. Cells were collected in Brucella broth and OD600 was adjusted to 0.3 x 10^-3. 200 uL of cells were plated onto either TSAB or TSAB + 0.004% SDS and spread evenly with sterile cotton swabs. WT and ∆*BOV_1602* grown on TSAB and ∆*BOV_1602* grown on TSAB + 0.004% SDS were incubated for 3 days. WT grown on TSAB + 0.004% SDS were incubated for 4 days. Cells were collected from plates and resuspended in 1 mL TRIzol. Samples were stored at -80˚C until RNA extraction. The extraction process was the same as described in Chapter 3.

RNA-seq analysis

All RNA-seq analyses were conducted the same as described in Chapter 3. Raw and processed RNA-seq data are publicly available in the NCBI GEO database at accession GSE262183.

Outer membrane preparation

B. ovis strains were grown on TSAB for 3 days. Cells were collected in Tris 7.3 and OD600 was adjusted to 40 in 40 mL of Tris pH7.4. Cells were centrifuged at 7197 x g for 10 minutes at 4˚C. Pellets were collected and suspended in 1mL 10 mM Tris pH 7.4 and stored at -80˚C overnight to weaken the cell wall and membrane. Pellets were thawed on ice. 1 µL DNase, 10 mg/mL lysozyme, and 1 mM PMSF were added to each sample. Samples were sonicated on ice for 5 cycles (20% magnitude, 20 s on/off) and centrifuged at 17,000 x g for 10 minutes at 4˚C. The supernatants were transferred to an ultra tube and centrifuged at 100,000 x g for 1h at 4˚C to separate the cytoplasm and the membranes. The supernatants were removed, and the pellets were resuspended in 1.5 mL 10 mM Tris pH 7.4 + 2% Triton x-100. Samples were mixed at room temperature for 30 minutes and centrifuged at 100,000 x g for 1h at 4˚C to separate the inner membrane and the outer membrane. The supernatants were removed, and the pellets were resuspended in 1.5 mL 10 mM Tris pH 7.4 + 2% Triton x-100. Samples were mixed at room temperature for 30 minutes and centrifuged at 100,000 x g for 1h at 4˚C. Supernatants were

removed and the pellets were resuspended in 1.5 mL 10mM Tris pH 7.4. Samples were centrifuged at 100,000 x g for 1h at 4˚C. The supernatants were removed, and the pellets were resuspended in 50 µL SDS loading buffer.

Proteolytic Digestion

Two biological replicates of outer membrane isolation samples from *B. ovis WT* and *B. ovis* Δ*BOV_1602* were heated at 95˚C for 5 minutes before resolving on a 12% mini-PROTEAN precast gel (BioRad) at 180V for 5 minutes. About 5 mm area around the dye front was cut out and added to 100 µL 5% acetic acid. Gel bands were digested in gel according to Shevchenko, et. al. with modifications (155). Briefly, gel bands were dehydrated using 100% acetonitrile and incubated with 10mM dithiothreitol in 100mM ammonium bicarbonate, pH ~8, at 56˚C for 45 minutes, dehydrated again and incubated in the dark with 50 mM chloroacetamide in 100 mM ammonium bicarbonate for 20 minutes. Gel bands were then washed with ammonium bicarbonate and dehydrated again. Sequencing grade modified trypsin was prepared to 0.005 µg/µL in 50 mM ammonium bicarbonate and ~100 µL of this was added to each gel band so that the gel was completely submerged. Bands were then incubated at 37˚C overnight. Peptides were extracted from the gel by water bath sonication in a solution of 60% Acetonitrile (ACN) /1% Trifluoroacetic acid (TFA) and vacuum dried to < 2 µL.

DIA (Data independent acquisition) LC/MS/MS sample analysis

An injection of 5 µL was automatically made using a Thermo (www.thermo.com) EASYnLC 1000 onto a Thermo Acclaim PepMap RSLC 0.1 mm x 20 mm C18 trapping column and washed for ~ 5 minutes with buffer A [99.9% Water/0.1% Formic Acid]. Bound peptides were then eluted over 35 minutes onto a Thermo Acclaim PepMap RSLC 0.075 mm x 250 mm resolving column with a linear gradient of 5% buffer B [80% Acetonitrile/0.1% Formic Acid/19.9% Water] to 28% buffer B in 24 minutes. After the gradient the column was washed with 90% buffer B for the duration of the run at a constant flow rate of 300 nL/min. Column temperature was maintained at

a constant temperature of 50˚C using an integrated column oven (PRSO-V1, Sonation GmbH, Biberach, Germany).

Eluted peptides were sprayed into a ThermoScientific Q-Exactive mass spectrometer for data independent acquisition (www.thermo.com) using a FlexSpray spray ion source. Survey scans were taken in the Orbi trap (35000 resolution, determined at m/z 200) over mass range of 395-905 m/z. Fixed windows of 30 m/z (50 total) were sequentially scanned and fragmented by HCD acquired in the Orbitrap at a resolution of 35,000 (determined at 200 m/z).

LC/MS/MS DIA Data Analysis

Acquired spectra were processed using DIA-NN (156), v1.8.1, using the Robust LC (high precision) quantitation strategy with RT-dependent cross-referencing and Deep Learning enabled in library-free mode against a FASTA of all *B.ovis* protein sequences available from NCBI (downloaded 2023-04-20 from www.ncbi.nlm.nih.gov). Search parameters were optimized by DIA-NN and results filtered at a precursor FDR of 1%.

Only proteins that were identified in both biological replicates of both strains were selected. The average spectra count of each protein in each strain was calculated. The fold change of *(ΔBOV_1602* / WT) for each protein was calculated using the average spectra counts. Proteins have a fold change of ≤ 0.9 or ≥ 1.1 were selected and presented in Table S7.

Macrophage infection assay

Same as previously described in Chapter 3.

Phase contrast microscopy

Same as previously described in Chapter 3.

Chapter 5: Discussion and future direction

Preface

The content of this session was modified and adapted from its published form:

Chen X, Alakavuklar MA, Fiebig A, Crosson, S. *mBio* (2023).

Discussion

Discovery of a cell envelope regulatory system in Brucella

TCS proteins play a key role in the regulation of cell envelope biogenesis and homeostasis in the bacterial kingdom (157-159). The function of the EssR-EssS TCS protein pair had not been defined in any species prior to this study, though this system is conserved in many *Alphaproteobacteria*. Our data provide evidence that these two proteins play an important role in *Brucella* resistance to cell envelope disruptors *in vitro*, and in regulating processes important for intracellular replication in a macrophage infection model. Apparent orthologs of the sensor kinase, EssS, are present in select genera across the orders *Hyphomicrobiales*, *Caulobacterales, Rhodobacterales, Rhodospirillales*, and *Rickettsiales*; EssR has a similar phylogenetic distribution (**Figure 3.13**). The functional importance of EssR-EssS in *Alphaproteobacteria* is evidenced by the fact that it is 1 of only 5 TCS signaling pairs (NtrXY, PhoBR, RegBA, ChvGI/BvgRS, & EssRS) in the highly streamlined SAR11 genome (*Pelagibacter ubique*). The HK domain of EssS has low sequence identity to other well-studied Gram-negative envelope regulators (e.g. CpxA and EnvZ), but multiple sequence alignment models in the conserved domain database (CDD) (109) suggest that the EssS, CpxA, and EnvZ HKs have common ancestry (e-value < 10^{-40}). Likewise, EssR is most closely related to the OmpR sequence family in the CDD (e-value < 10^{-70}). OmpR functions as the cognate regulator of the EnvZ kinase in enteric bacteria (89).

EssS and EssR clearly form a cognate signaling pair *in vitro* as evidenced by specific phosphoryl transfer from the EssS kinase domain to EssR on a fast time scale (**Figure 3.10**). However, the phenotypes of the Δ*essS* and Δ*essR* strains are not equivalent in an *in vitro* model

of cell envelope stress. Under most challenges (SDS, carbenicillin, EDTA, and polymyxin B) the defect of Δ*essR* was more severe than Δ*essS* (Figure 1, S1 and S2), and these mutants have opposite phenotypes when exposed to high NaCl: the *essR* mutant is NaCl resistant while the *essS* mutant is sensitive compared to WT (**Figure 3.3**). The mechanism underlying the opposing NaCl phenotypes of these strains merits further investigation. The phenotypes of Δ*essS* and Δ*essR* are equivalent in a macrophage infection model (**Figure 3.6**). This result provides evidence that EssS-dependent phosphorylation (or dephosphorylation) of EssR is more important for system function in the complex environment of the intracellular niche than it is in a simple *in vitro* agar plate assay.

An unexpected functional role for the conserved cell envelope regulator, CenR

The result that *B. ovis* CenR confers resistance to SDS and carbenicillin (**Figures 3.1 & 3.4**) was not unexpected considering the phenotypes of *cenR* mutants in other Alphaproteobacteria. CenR was first described as an essential RR in *C. crescentus*, where it functions to regulate cell envelope structure (93), and is now known to be conserved in many alphaproteobacterial orders (92). Recent work has shown that *cenR* is essential in *R. sphaeroides*, where it controls transcription of the Tol-Pal outer membrane complex and other cell envelope genes (92), and in *Sinorhizobium meliloti* where it mediates osmotolerance and oxidative stress resistance (96). In all three of these species, CenR is regulated by a cognate histidine kinase, CenK. Our data show that *cenR* is not essential for *B. ovis* growth or division under standard culture conditions and indicate that it may be an orphan response regulator, which is consistent with a previous report in *B. melitensis* (106). *B. ovis cenR* (and *essR*-*essS*) do not function to mitigate acid stress *in vitro*. Though a *B. melitensis cenR* mutant was previously reported to be acid sensitive (105), the treatment protocol and measured pH range differ substantially between our *B. ovis* study and the *B. melitensis* study. The possibility that a *Brucella* HK phosphorylates (or dephosphorylates) CenR under certain conditions cannot be conclusively ruled out from our data. Indeed, there is some evidence that the conserved CenR aspartyl phosphorylation site can

impact CenR-EssR interaction (**Figure 3.9**) and replication in the intracellular niche (**Figure 3.6**). Nonetheless, both $cenR_{D55A}$ and $cenR_{D55E}$ alleles fully complement the agar plate stress phenotypes of Δ*cenR*. And unlike *R. sphaeroides* and *C. crescentus*, where *cenR* depletion results in major defects in cell envelope structure, the impact of *cenR* deletion on *B. ovis* cell morphology is small: *B. ovis* Δ*cenR* mutants are slightly (but significantly) larger than WT (**Figure 3.5**), but the morphology of the mutant cells otherwise appears normal. These results indicate that CenR function in *Brucella ovis* differs somewhat from *Caulobacter*, *Rhodobacter*, and *Sinorhizobium*.

CenR is a post-transcriptional regulator of the EssS-EssR two-component system

Cross-regulation between TCSs is uncommon, though there is experimental support for direct interactions between otherwise distinct TCS HK-RR protein pairs for limited number of systems (122). For example, the NarXL and NarQP systems of *Escherichia coli* cross-phosphorylate to tune nitrate and nitrite respiratory processes (160), and in *C. crescentus*, a consortium of sensor kinases that coordinately regulate cell adhesion in response to a range of environmental cues physically interact in cells (161). In chapter 3, we present evidence for a mode of TCS cross-regulation in which a non-cognate RR (CenR) directly stimulates the phosphoryl transfer activity of a cognate HK-RR protein pair (EssS-EssR) (**Figure 3.10 and Figure 3.14**). We further demonstrate that CenR and EssR reciprocally regulate their protein levels in *B. ovis* cells via a post-transcriptional mechanism (**Figure 3.12**). EssR and CenR physically interact via their receiver domains (**Figure 3.9**), and it seems most likely that CenR and EssR protect each other from proteolytic degradation in the *Brucella* cell though we cannot rule out other post-transcriptional models at this time. The positive effect of CenR on EssS-EssR phosphoryl transfer activity and the positive effect of EssR and CenR protein levels on each other are consistent with the congruent phenotypes of strains lacking *cenR* and *essR*.

However, CenR does not simply control the activity and levels EssS-EssR. CenR is itself a DNA binding protein, and we have presented evidence that EssR and CenR both directly and

indirectly regulate transcription of a highly correlated set of genes that includes multiple transporters and cell wall metabolism genes (**Figure 3.8**). These two transcriptional regulators directly bind shared and unique sets of sites on *B. ovis* chromosomes 1 and 2. It is possible that CenR and EssR bind DNA as heterodimers, which has been described for the BldM and WhiI response regulators of *Streptomyces* (162), and the RcsB regulator of *E. coli* with GadE (163) and BglJ (164). These heterodimeric regulators are competent to control different classes of promoters depending on oligomeric state; a similar mechanism may exist for EssR and CenR though we have not identified distinct promoter classes in our data. It is plausible that CenR and EssR bind as homodimers and heterodimers considering the pattern of unique and overlapping genes/promoters in the transcriptomic and ChIP-seq datasets. Future studies aimed at deciphering molecular features of environmental signal detection by the EssS sensor kinase, allosteric regulation of TCS activity by CenR, and transcriptional control by the CenR and EssR regulators will generally inform our understanding of the evolution of cell envelope regulatory systems in bacteria. More specifically, investigation of these proteins will illuminate mechanisms by which *Brucella* replicate in the intracellular niche and spread from cell to cell in face of harsh immune stresses encountered within the host.

Discovery of a HWE histidine kinase that impacts B. ovis detergent resistance

Deletion of the HWE-family sensor histidine kinase, *BOV_1602,* results in resistance to anionic and zwitterionic detergents and sensitivity to cationic detergent (**Figure 4.1 and 4.6**). Δ*BOV_1602* also is more sensitive to another positively charged peptide, polymyxin B (**Figure 4.2**). It is possible that deletion of *BOV_1602* results in sensitivity to positive charged compounds in general, and not just CTAB and polymyxin B. Additionally, Δ*BOV_1602* is slightly sensitive to high NaCl and carbenicillin treatment (**Figure 2.1 and Figure 4.6**). The sensitivity and resistance profile of Δ*BOV_1602* to different cell envelope disruptors suggests that the cell envelope of this mutant differs from WT. Indeed, RNA-seq and proteomic studies provides support that deletion of *BOV_1602* leads to an altered outer membrane protein composition. In my proteomic data,

Omp2b was the most abundant outer membrane protein in WT and deletion of BOV_1602 resulted in a 50% reduction of its protein levels. Even though *omp2b* is considered not essential according to our Tn-seq data, I was not able to make a deletion mutant of Δ*omp2b* in WT *B.ovis* after several attempts. Since Omp2b is a highly abundance protein in WT *B. ovis* (**Table S7**), deletion of the gene may lead to drastic changes in the cell. Additionally, since the processes of transposon insertion and making a deletion mutation are different, it is possible that omp2b is important during the counter selection step in generating the mutant. Even though I did not examine the effect of Omp2b on the resistance to cell envelope stressors specifically, it seems likely that it contributes to one or more of the cell envelope phenotypes of Δ*BOV_1602*. Since deletion of *virB* genes and SPFH gene partial restored the detergent phenotypes of Δ*BOV_1602* to WT levels, it is possible that the altered levels of Omp2b also play a role in detergent interactions with the cell.

Several cell envelope proteins with predicted resistance/sensitivity functions that have altered protein levels in my proteomic data set. For example, LptA (BOV_1874) is the lipid A phosphate-ethanolamine transferase and is known to be important for resistance against polymyxin B (165). Deletion of *BOV_1602* led to reduced protein levels of LptA and downregulation of its transcript, which could explain the polymyxin B sensitivity phenotype.

Other proteins known to be associated with detergent resistant membranes also have increase expression in Δ*BOV_1602*, such as signal peptidase I (SipF, BOV_0653), TatB (BOV_0874), and peptidyl-prolyl cis-trans isomerase (BOV_0676) (**Table S7**). Although the exact mechanism remains unclear, I have confirmed that T4SS and an SPFH protein contribute to the resistance phenotype of Δ*BOV_1602* on TSAB containing Triton, CHAPS, and deoxycholate. Though the double mutants have similar CFU on SDS agar plates, colonies of Δ*BOV_1602* are denser and whiter than that of the double mutants. Whether this difference represents a difference in response to SDS requires further investigation. The fact that deleting *virB8-virB11* and

BOV_A0070 in Δ*BOV_1602* resulted in significant increase in sensitivity to NaCl suggests that these proteins are important for cell envelope maintenance and stress response.

Transcription and detergent resistance

The RNA-seq analysis surprisingly revealed that SDS treatment has less of an effect on the transcriptome of Δ*BOV_1602* than WT. Approximately 200 genes were differentially expressed in Δ*BOV_1602* cultured on unsupplemented agar plates compared to cells cultured on plates supplemented with SDS. In contrast, in WT, transcript levels of over 800 genes were affected by SDS treatment. These results provide evidence that WT is transcriptionally more sensitive to SDS treatment than Δ*BOV_1602*. This is an interesting phenomenon given that Δ*BOV_1602* mutant is highly resistant to SDS and other detergents. It is plausible that deletion of *BOV_1602* primes the cells to be "detergent-ready."

Proteomic data collected on outer membrane tractions also provided evidence of altered protein levels of around 400 proteins. However, with few exceptions, the protein level changes did not correspond with the transcript level changes. For example, VirB8-VirB11 protein levels were elevated in Δ*BOV_1602*, though the transcript level were either slightly repressed or unchanged. This could be due to autorepressive regulation where the increased protein levels repress the transcription of the genes. The impact of post-transcriptional regulatory processes on *Brucella* outer membrane regulation is an interesting area of future investigation.

Future Directions

CenR, EssRS, and BOV_1602

This thesis focused on three TCSs in *B. ovis* – CenR, EssRS, and BOV_1602. There are still many features that we do not understand regarding how these signaling systems function. For example, I have not explored what signals regulates the activation of EssS. Also, it remains undetermined whether CenR has a HK partner or if CenR is phosphorylated by EssS in the presence of EssR. In Chapter 4, I provided the first genetic and physiological analysis of BOV_1602, but there are still many things to be learned about this HWE-family sensor histidine

kinase. We do not know the exact signals that BOV_1602 senses or its mechanism of activation, nor do we know which response regulator(s) or other proteins that BOV_1602 interacts with. Though macrophage infection assays show that deletion of *BOV_1602* does not result in an intracellular survival defect, it remains undetermined whether deletion of *BOV_1602* will result in any fitness defect in an animal model. All of these unanswered questions will need further investigation for better understanding of these important cell envelope regulatory TCSs that I have characterized.

Other TCSs

My system-level genetic analysis defined 9 TCS genes to be important for cell envelope regulation in *B. ovis, which are BOV_0577 (divJ), BOV_0615 (pleC), BOV_1602, BOV_0311, BOV_0611-0612, BOV_1472-1472 (essRS), and BOV_1929 (cenR)* (**Figure 2.1**). This thesis only focused on four of these genes and the other five will need more detailed research to understand their direct or indirect roles in cell envelope regulation in *B. ovis*. For example, even though DivJ and PleC have been studied in the context of cell cycle regulation, little is known about their cell envelope regulatory functions in *Brucella*. BOV_0611-0612 is another previously uncharacterized system that deserves more investigation.

Utilizing the genetic libraries for future studies

During my thesis work, I have generated two useful genetic resources: the library of non-essential TCS mutants and the barcoded transposon TCS mutant library. Mutant libraries are a robust and reliable genetic tool for screening TCSs that are important for sensing different signals and responding to different stressors. The majority of the mutants did not have different phenotypes that differed from WT in my initial cell envelope screen. This calls for future studies to use this library to identify different signals that these TCS may sense and respond to. Additionally, further effort may be required on generating mutants of the few non-essential TCS genes that I was not able to/ did not attempt to generate.

The barcoded transposon library as mentioned in Chapter 2, requires more optimization for better results. However, I believe that once the library is optimized for more even amplification of the barcodes and better recovery after freezing, this library will be a powerful tool for high throughput screening. It can be used for identifying TCS genes that are important for many more conditions and discovering potential connections between different TCSs.

REFERENCES

1. Bruce D. 1887. note on the discovery of a microorganism in malta fever, p 170.

2. Whatmore AM, Foster JT. 2021. Emerging diversity and ongoing expansion of the genus Brucella. Infect Genet Evol 92:104865.

3. Tsolis RM, Seshadri R, Santos RL, Sangari FJ, Lobo JM, de Jong MF, Ren Q, Myers G, Brinkac LM, Nelson WC, Deboy RT, Angiuoli S, Khouri H, Dimitrov G, Robinson JR, Mulligan S, Walker RL, Elzer PE, Hassan KA, Paulsen IT. 2009. Genome degradation in Brucella ovis corresponds with narrowing of its host range and tissue tropism. PLoS One 4:e5519.

4. Suarez-Esquivel M, Baker KS, Ruiz-Villalobos N, Hernandez-Mora G, Barquero-Calvo E, Gonzalez-Barrientos R, Castillo-Zeledon A, Jimenez-Rojas C, Chacon-Diaz C, Cloeckaert A, Chaves-Olarte E, Thomson NR, Moreno E, Guzman-Verri C. 2017. Brucella Genetic Variability in Wildlife Marine Mammals Populations Relates to Host Preference and Ocean Distribution. Genome Biol Evol 9:1901-1912.

5. Suarez-Esquivel M, Chaves-Olarte E, Moreno E, Guzman-Verri C. 2020. Brucella Genomics: Macro and Micro Evolution. Int J Mol Sci 21.

6. Feng Y, Peng X, Jiang H, Peng Y, Zhu L, Ding J. 2017. Rough brucella strain RM57 is attenuated and confers protection against Brucella melitensis. Microb Pathog 107:270-275.

7. Jain-Gupta N, Waldrop SG, Tenpenny NM, Witonsky SG, Boyle SM, Sriranganathan N. 2019. Rough Brucella neotomae provides protection against Brucella suis challenge in mice. Vet Microbiol 239:108447.

8. Munoz PM, Conde-Alvarez R, Andres-Barranco S, de Miguel MJ, Zuniga-Ripa A, Aragon-Aranda B, Salvador-Bescos M, Martinez-Gomez E, Iriarte M, Barberan M, Vizcaino N, Moriyon I, Blasco JM. 2022. A Brucella melitensis H38DeltawbkF rough mutant protects against Brucella ovis in rams. Vet Res 53:16.

9. Boschiroli ML, Foulongne V, O'Callaghan D. 2001. Brucellosis: a worldwide zoonosis. Curr Opin Microbiol 4:58-64.

10. Whatmore AM. 2009. Current understanding of the genetic diversity of Brucella, an expanding genus of zoonotic pathogens. Infect Genet Evol 9:1168-84.

11. Seleem MN, Boyle SM, Sriranganathan N. 2010. Brucellosis: a re-emerging zoonosis. Vet Microbiol 140:392-8.

12. Varesio LM, Willett JW, Fiebig A, Crosson S. 2019. A Carbonic Anhydrase Pseudogene Sensitizes Select Brucella Lineages to Low CO(2) Tension. J Bacteriol 201.

13. Roop RM, 2nd, Barton IS, Hopersberger D, Martin DW. 2021. Uncovering the Hidden Credentials of Brucella Virulence. Microbiol Mol Biol Rev 85.

14. Celli J. 2015. The changing nature of the Brucella-containing vacuole. Cell Microbiol 17:951-8.

15. Boschiroli ML, Ouahrani-Bettache S, Foulongne V, Michaux-Charachon S, Bourg G, Allardet-Servent A, Cazevieille C, Liautard JP, Ramuz M, O'Callaghan D. 2002. The Brucella suis virB operon is induced intracellularly in macrophages. Proc Natl Acad Sci U S A 99:1544-9.

16. Celli J. 2019. The Intracellular Life Cycle of Brucella spp. Microbiol Spectr 7.

17. Raetz CR, Whitfield C. 2002. Lipopolysaccharide endotoxins. Annu Rev Biochem 71:635-700.

18. Moreno E, Stackebrandt E, Dorsch M, Wolters J, Busch M, Mayer H. 1990. Brucella abortus 16S rRNA and lipid A reveal a phylogenetic relationship with members of the alpha-2 subdivision of the class Proteobacteria. J Bacteriol 172:3569-76.

19. Stranahan LW, Arenas-Gamboa AM. 2021. When the Going Gets Rough: The Significance of Brucella Lipopolysaccharide Phenotype in Host-Pathogen Interactions. Front Microbiol 12:713157.

20. Duenas AI, Orduna A, Crespo MS, Garcia-Rodriguez C. 2004. Interaction of endotoxins with Toll-like receptor 4 correlates with their endotoxic potential and may explain the proinflammatory effect of Brucella spp. LPS. Int Immunol 16:1467-75.

21. Erridge C, Bennett-Guerrero E, Poxton IR. 2002. Structure and function of lipopolysaccharides. Microbes Infect 4:837-51.

22. Monreal D, Grillo MJ, Gonzalez D, Marin CM, De Miguel MJ, Lopez-Goni I, Blasco JM, Cloeckaert A, Moriyon I. 2003. Characterization of Brucella abortus O-polysaccharide and core lipopolysaccharide mutants and demonstration that a complete core is required for rough vaccines to be efficient against Brucella abortus and Brucella ovis in the mouse model. Infect Immun 71:3261-71.

23. Conde-Alvarez R, Arce-Gorvel V, Iriarte M, Mancek-Keber M, Barquero-Calvo E, Palacios-Chaves L, Chacon-Diaz C, Chaves-Olarte E, Martirosyan A, von Bargen K, Grillo MJ, Jerala R, Brandenburg K, Llobet E, Bengoechea JA, Moreno E, Moriyon I, Gorvel JP. 2012. The lipopolysaccharide core of Brucella abortus acts as a shield against innate immunity recognition. PLoS Pathog 8:e1002675.

24. Gil-Ramirez Y, Conde-Alvarez R, Palacios-Chaves L, Zuniga-Ripa A, Grillo MJ, Arce-Gorvel V, Hanniffy S, Moriyon I, Iriarte M. 2014. The identification of wadB, a new glycosyltransferase gene, confirms the branched structure and the role in virulence of the lipopolysaccharide core of Brucella abortus. Microb Pathog 73:53-9.

25. Mancilla M. 2015. Smooth to Rough Dissociation in Brucella: The Missing Link to Virulence. Front Cell Infect Microbiol 5:98.

26. Godfroid F, Taminiau B, Danese I, Denoel P, Tibor A, Weynants V, Cloeckaert A, Godfroid J, Letesson JJ. 1998. Identification of the perosamine synthetase gene of

Brucella melitensis 16M and involvement of lipopolysaccharide O side chain in Brucella survival in mice and in macrophages. Infect Immun 66:5485-93.

27. McQuiston JR, Vemulapalli R, Inzana TJ, Schurig GG, Sriranganathan N, Fritzinger D, Hadfield TL, Warren RA, Lindler LE, Snellings N, Hoover D, Halling SM, Boyle SM. 1999. Genetic characterization of a Tn5-disrupted glycosyltransferase gene homolog in Brucella abortus and its effect on lipopolysaccharide composition and virulence. Infect Immun 67:3830-5.

28. Gonzalez D, Grillo MJ, De Miguel MJ, Ali T, Arce-Gorvel V, Delrue RM, Conde-Alvarez R, Munoz P, Lopez-Goni I, Iriarte M, Marin CM, Weintraub A, Widmalm G, Zygmunt M, Letesson JJ, Gorvel JP, Blasco JM, Moriyon I. 2008. Brucellosis vaccines: assessment of Brucella melitensis lipopolysaccharide rough mutants defective in core and O-polysaccharide synthesis and export. PLoS One 3:e2760.

29. Zygmunt MS, Blasco JM, Letesson JJ, Cloeckaert A, Moriyon I. 2009. DNA polymorphism analysis of Brucella lipopolysaccharide genes reveals marked differences in O-polysaccharide biosynthetic genes between smooth and rough Brucella species and novel species-specific markers. BMC Microbiol 9:92.

30. Fernandez-Prada CM, Nikolich M, Vemulapalli R, Sriranganathan N, Boyle SM, Schurig GG, Hadfield TL, Hoover DL. 2001. Deletion of wboA enhances activation of the lectin pathway of complement in Brucella abortus and Brucella melitensis. Infect Immun 69:4407-16.

31. Porte F, Naroeni A, Ouahrani-Bettache S, Liautard JP. 2003. Role of the Brucella suis lipopolysaccharide O antigen in phagosomal genesis and in inhibition of phagosome-lysosome fusion in murine macrophages. Infect Immun 71:1481-90.

32. Tian M, Qu J, Han X, Ding C, Wang S, Peng D, Yu S. 2014. Mechanism of Asp24 upregulation in Brucella abortus rough mutant with a disrupted O-antigen export system and effect of Asp24 in bacterial intracellular survival. Infect Immun 82:2840-50.

33. Martin-Martin AI, Sancho P, Tejedor C, Fernandez-Lago L, Vizcaino N. 2011. Differences in the outer membrane-related properties of the six classical Brucella species. Vet J 189:103-5.

34. Mancilla M, Marin CM, Blasco JM, Zarraga AM, Lopez-Goni I, Moriyon I. 2012. Spontaneous excision of the O-polysaccharide wbkA glycosyltranferase gene is a cause of dissociation of smooth to rough Brucella colonies. J Bacteriol 194:1860-7.

35. Turse JE, Pei J, Ficht TA. 2011. Lipopolysaccharide-Deficient Brucella Variants Arise Spontaneously during Infection. Front Microbiol 2:54.

36. Alakavuklar MA, Fiebig A, Crosson S. 2023. The Brucella Cell Envelope. Annu Rev Microbiol 77:233-253.

37. Martin-Martin AI, Caro-Hernandez P, Sancho P, Tejedor C, Cloeckaert A, Fernandez-Lago L, Vizcaino N. 2009. Analysis of the occurrence and distribution of the Omp25/Omp31 family of surface proteins in the six classical Brucella species. Vet Microbiol 137:74-82.

38. Martin-Martin AI, Caro-Hernandez P, Orduna A, Vizcaino N, Fernandez-Lago L. 2008. Importance of the Omp25/Omp31 family in the internalization and intracellular replication of virulent B. ovis in murine macrophages and HeLa cells. Microbes Infect 10:706-10.

39. Manterola L, Guzman-Verri C, Chaves-Olarte E, Barquero-Calvo E, de Miguel MJ, Moriyon I, Grillo MJ, Lopez-Goni I, Moreno E. 2007. BvrR/BvrS-controlled outer membrane proteins Omp3a and Omp3b are not essential for Brucella abortus virulence. Infect Immun 75:4867-74.

40. Caro-Hernandez P, Fernandez-Lago L, de Miguel MJ, Martin-Martin AI, Cloeckaert A, Grillo MJ, Vizcaino N. 2007. Role of the Omp25/Omp31 family in outer membrane properties and virulence of Brucella ovis. Infect Immun 75:4050-61.

41. Cloeckaert A, Vergnaud G, Zygmunt MS. 2020. Omp2b Porin Alteration in the Course of Evolution of Brucella spp. Front Microbiol 11:284.

42. Marquis H, Ficht TA. 1993. The omp2 gene locus of Brucella abortus encodes two homologous outer membrane proteins with properties characteristic of bacterial porins. Infect Immun 61:3785-90.

43. Galperin MY. 2005. A census of membrane-bound and intracellular signal transduction proteins in bacteria: bacterial IQ, extroverts and introverts. BMC Microbiol 5:35.

44. Bretl DJ, Kirby JR. 2016. Molecular Mechanisms of Signaling in Myxococcus xanthus Development. J Mol Biol 428:3805-30.

45. Capra EJ, Laub MT. 2012. Evolution of two-component signal transduction systems. Annu Rev Microbiol 66:325-47.

46. Esther Chen MA, Aretha Fiebig, Sean Crosson. 2022. Brucella ovis Tn-himar sequencing dataset, NCBI sequence read archive.

47. Park H, Saha SK, Inouye M. 1998. Two-domain reconstitution of a functional protein histidine kinase. Proc Natl Acad Sci U S A 95:6728-32.

48. Casino P, Rubio V, Marina A. 2010. The mechanism of signal transduction by two-component systems. Curr Opin Struct Biol 20:763-71.

49. Henry JT, Crosson S. 2011. Ligand-binding PAS domains in a genomic, cellular, and structural context. Annu Rev Microbiol 65:261-86.

50. Zhulin IB, Nikolskaya AN, Galperin MY. 2003. Common extracellular sensory domains in transmembrane receptors for diverse signal transduction pathways in bacteria and archaea. J Bacteriol 185:285-94.

51. Kaczmarczyk A, Hochstrasser R, Vorholt JA, Francez-Charlot A. 2015. Two-tiered histidine kinase pathway involved in heat shock and salt sensing in the general stress response of Sphingomonas melonis Fr1. J Bacteriol 197:1466-77.

52. Tagua VG, Molina-Henares MA, Travieso ML, Nisa-Martinez R, Quesada JM, Espinosa-Urgel M, Ramos-Gonzalez MI. 2022. C-di-GMP and biofilm are regulated in

Pseudomonas putida by the CfcA/CfcR two-component system in response to salts. Environ Microbiol 24:158-178.

53. Herrou J, Crosson S, Fiebig A. 2017. Structure and function of HWE/HisKA2-family sensor histidine kinases. Curr Opin Microbiol 36:47-54.

54. Karniol B, Vierstra RD. 2004. The HWE histidine kinases, a new family of bacterial two-component sensor kinases with potentially diverse roles in environmental signaling. J Bacteriol 186:445-53.

55. Rivera-Cancel G, Ko WH, Tomchick DR, Correa F, Gardner KH. 2014. Full-length structure of a monomeric histidine kinase reveals basis for sensory regulation. Proc Natl Acad Sci U S A 111:17839-44.

56. Wojnowska M, Yan J, Sivalingam GN, Cryar A, Gor J, Thalassinos K, Djordjevic S. 2013. Autophosphorylation activity of a soluble hexameric histidine kinase correlates with the shift in protein conformational equilibrium. Chem Biol 20:1411-20.

57. Foreman R, Fiebig A, Crosson S. 2012. The LovK-LovR two-component system is a regulator of the general stress pathway in Caulobacter crescentus. J Bacteriol 194:3038-49.

58. Francez-Charlot A, Kaczmarczyk A, Fischer HM, Vorholt JA. 2015. The general stress response in Alphaproteobacteria. Trends Microbiol 23:164-71.

59. Kim HS, Willett JW, Jain-Gupta N, Fiebig A, Crosson S. 2014. The Brucella abortus virulence regulator, LovhK, is a sensor kinase in the general stress response signalling pathway. Mol Microbiol 94:913-25.

60. Zschiedrich CP, Keidel V, Szurmant H. 2016. Molecular Mechanisms of Two-Component Signal Transduction. J Mol Biol 428:3752-75.

61. Kirby AJ, Nome F. 2015. Fundamentals of phosphate transfer. Acc Chem Res 48:1806-14.

62. Stock AM, Robinson VL, Goudreau PN. 2000. Two-component signal transduction. Annu Rev Biochem 69:183-215.

63. Leicht O, van Teeseling MCF, Panis G, Reif C, Wendt H, Viollier PH, Thanbichler M. 2020. Integrative and quantitative view of the CtrA regulatory network in a stalked budding bacterium. PLoS Genet 16:e1008724.

64. Kim HS, Caswell CC, Foreman R, Roop RM, 2nd, Crosson S. 2013. The Brucella abortus general stress response system regulates chronic mammalian infection and is controlled by phosphorylation and proteolysis. J Biol Chem 288:13906-16.

65. Kato M, Mizuno T, Shimizu T, Hakoshima T. 1997. Insights into multistep phosphorelay from the crystal structure of the C-terminal HPt domain of ArcB. Cell 88:717-23.

66. Varughese KI. 2002. Molecular recognition of bacterial phosphorelay proteins. Curr Opin Microbiol 5:142-8.

67. Varughese KI, Madhusudan, Zhou XZ, Whiteley JM, Hoch JA. 1998. Formation of a novel four-helix bundle and molecular recognition sites by dimerization of a response regulator phosphotransferase. Mol Cell 2:485-93.

68. Blair JA, Xu Q, Childers WS, Mathews, II, Kern JW, Eckart M, Deacon AM, Shapiro L. 2013. Branched signal wiring of an essential bacterial cell-cycle phosphotransfer protein. Structure 21:1590-601.

69. Lima S, Guo MS, Chaba R, Gross CA, Sauer RT. 2013. Dual molecular signals mediate the bacterial response to outer-membrane stress. Science 340:837-41.

70. Mecsas J, Rouviere PE, Erickson JW, Donohue TJ, Gross CA. 1993. The activity of sigma E, an Escherichia coli heat-inducible sigma-factor, is modulated by expression of outer membrane proteins. Genes Dev 7:2618-28.

71. De Las Penas A, Connolly L, Gross CA. 1997. The sigmaE-mediated response to extracytoplasmic stress in Escherichia coli is transduced by RseA and RseB, two negative regulators of sigmaE. Mol Microbiol 24:373-85.

72. Cezairliyan BO, Sauer RT. 2007. Inhibition of regulated proteolysis by RseB. Proc Natl Acad Sci U S A 104:3771-6.

73. Chaba R, Alba BM, Guo MS, Sohn J, Ahuja N, Sauer RT, Gross CA. 2011. Signal integration by DegS and RseB governs the σ E-mediated envelope stress response in Escherichia coli. Proc Natl Acad Sci U S A 108:2106-11.

74. Raivio TL. 2014. Everything old is new again: an update on current research on the Cpx envelope stress response. Biochim Biophys Acta 1843:1529-41.

75. Kohanski MA, Dwyer DJ, Wierzbowski J, Cottarel G, Collins JJ. 2008. Mistranslation of membrane proteins and two-component system activation trigger antibiotic-mediated cell death. Cell 135:679-90.

76. Srinivasan VB, Vaidyanathan V, Mondal A, Rajamohan G. 2012. Role of the two component signal transduction system CpxAR in conferring cefepime and chloramphenicol resistance in Klebsiella pneumoniae NTUH-K2044. PLoS One 7:e33777.

77. Jubelin G, Vianney A, Beloin C, Ghigo JM, Lazzaroni JC, Lejeune P, Dorel C. 2005. CpxR/OmpR interplay regulates curli gene expression in response to osmolarity in Escherichia coli. J Bacteriol 187:2038-49.

78. Danese PN, Silhavy TJ. 1998. CpxP, a stress-combative member of the Cpx regulon. J Bacteriol 180:831-9.

79. Mileykovskaya E, Dowhan W. 1997. The Cpx two-component signal transduction pathway is activated in Escherichia coli mutant strains lacking phosphatidylethanolamine. J Bacteriol 179:1029-34.

80. Hobbs EC, Yin X, Paul BJ, Astarita JL, Storz G. 2012. Conserved small protein associates with the multidrug efflux pump AcrB and differentially affects antibiotic resistance. Proc Natl Acad Sci U S A 109:16696-701.

81. Lopez C, Checa SK, Soncini FC. 2018. CpxR/CpxA Controls scsABCD Transcription To Counteract Copper and Oxidative Stress in Salmonella enterica Serovar Typhimurium. J Bacteriol 200.

82. Raivio TL, Leblanc SK, Price NL. 2013. The Escherichia coli Cpx envelope stress response regulates genes of diverse function that impact antibiotic resistance and membrane integrity. J Bacteriol 195:2755-67.

83. Laubacher ME, Ades SE. 2008. The Rcs phosphorelay is a cell envelope stress response activated by peptidoglycan stress and contributes to intrinsic antibiotic resistance. J Bacteriol 190:2065-74.

84. Majdalani N, Hernandez D, Gottesman S. 2002. Regulation and mode of action of the second small RNA activator of RpoS translation, RprA. Mol Microbiol 46:813-26.

85. Francez-Charlot A, Laugel B, Van Gemert A, Dubarry N, Wiorowski F, Castanie-Cornet MP, Gutierrez C, Cam K. 2003. RcsCDB His-Asp phosphorelay system negatively regulates the flhDC operon in Escherichia coli. Mol Microbiol 49:823-32.

86. DeAngelis CM, Nag D, Withey JH, Matson JS. 2019. Characterization of the Vibrio cholerae Phage Shock Protein Response. J Bacteriol 201.

87. Srivastava D, Moumene A, Flores-Kim J, Darwin AJ. 2017. Psp Stress Response Proteins Form a Complex with Mislocalized Secretins in the Yersinia enterocolitica Cytoplasmic Membrane. mBio 8.

88. Flores-Kim J, Darwin AJ. 2016. The Phage Shock Protein Response. Annu Rev Microbiol 70:83-101.

89. Kenney LJ, Anand GS. 2020. EnvZ/OmpR Two-Component Signaling: An Archetype System That Can Function Noncanonically. EcoSal Plus 9.

90. DeJesus MA, Ambadipudi C, Baker R, Sassetti C, Ioerger TR. 2015. TRANSIT--A Software Tool for Himar1 TnSeq Analysis. PLoS Comput Biol 11:e1004401.

91. Mirabella A, Yanez Villanueva RM, Delrue RM, Uzureau S, Zygmunt MS, Cloeckaert A, De Bolle X, Letesson JJ. 2012. The two-component system PrlS/PrlR of Brucella melitensis is required for persistence in mice and appears to respond to ionic strength. Microbiology (Reading) 158:2642-2651.

92. Lakey BD, Myers KS, Alberge F, Mettert EL, Kiley PJ, Noguera DR, Donohue TJ. 2022. The essential Rhodobacter sphaeroides CenKR two-component system regulates cell division and envelope biosynthesis. PLoS Genet 18:e1010270.

93. Skerker JM, Prasol MS, Perchuk BS, Biondi EG, Laub MT. 2005. Two-component signal transduction pathways regulating growth and cell cycle progression in a bacterium: a system-level analysis. PLoS Biol 3:e334.

94. Shea A, Wolcott M, Daefler S, Rozak DA. 2012. Biolog phenotype microarrays. Methods Mol Biol 881:331-73.

95. Choi KH, Gaynor JB, White KG, Lopez C, Bosio CM, Karkhoff-Schweizer RR, Schweizer HP. 2005. A Tn7-based broad-range bacterial cloning and expression system. Nat Methods 2:443-8.

96. Bensig EO, Valadez-Cano C, Kuang Z, Freire IR, Reyes-Prieto A, MacLellan SR. 2022. The two-component regulatory system CenK-CenR regulates expression of a previously uncharacterized protein required for salinity and oxidative stress tolerance in Sinorhizobium meliloti. Front Microbiol 13:1020932.

97. Sternon JF, Godessart P, Goncalves de Freitas R, Van der Henst M, Poncin K, Francis N, Willemart K, Christen M, Christen B, Letesson JJ, De Bolle X. 2018. Transposon Sequencing of Brucella abortus Uncovers Essential Genes for Growth In Vitro and Inside Macrophages. Infect Immun 86.

98. Chen E, Alakavuklar M, Fiebig A, Crosson S. 2022. Brucella ovis Tn-himar sequencing dataset, NCBI Sequence Read Archive.

99. De Bolle X, Crosson S, Matroule JY, Letesson JJ. 2015. Brucella abortus Cell Cycle and Infection Are Coordinated. Trends Microbiol 23:812-821.

100. Guzman-Verri C, Manterola L, Sola-Landa A, Parra A, Cloeckaert A, Garin J, Gorvel JP, Moriyon I, Moreno E, Lopez-Goni I. 2002. The two-component system BvrR/BvrS essential for Brucella abortus virulence regulates the expression of outer membrane proteins with counterparts in members of the Rhizobiaceae. Proc Natl Acad Sci U S A 99:12375-80.

101. Martin-Martin AI, Sancho P, de Miguel MJ, Fernandez-Lago L, Vizcaino N. 2012. Quorum-sensing and BvrR/BvrS regulation, the type IV secretion system, cyclic glucans, and BacA in the virulence of Brucella ovis: similarities to and differences from smooth brucellae. Infect Immun 80:1783-93.

102. Sola-Landa A, Pizarro-Cerda J, Grillo MJ, Moreno E, Moriyon I, Blasco JM, Gorvel JP, Lopez-Goni I. 1998. A two-component regulatory system playing a critical role in plant pathogens and endosymbionts is present in Brucella abortus and controls cell invasion and virulence. Mol Microbiol 29:125-38.

103. Stein BJ, Fiebig A, Crosson S. 2021. The ChvG-ChvI and NtrY-NtrX Two-Component Systems Coordinately Regulate Growth of Caulobacter crescentus. J Bacteriol 203:e0019921.

104. Liu W, Dong H, Liu W, Gao X, Zhang C, Wu Q. 2012. OtpR regulated the growth, cell morphology of B. melitensis and tolerance to beta-lactam agents. Vet Microbiol 159:90-8.

105. Liu W, Dong H, Li J, Ou Q, Lv Y, Wang X, Xiang Z, He Y, Wu Q. 2015. RNA-seq reveals the critical role of OtpR in regulating Brucella melitensis metabolism and virulence under acidic stress. Sci Rep 5:10864.

106. Zhang X, Ren J, Li N, Liu W, Wu Q. 2009. Disruption of the BMEI0066 gene attenuates the virulence of Brucella melitensis and decreases its stress tolerance. Int J Biol Sci 5:570-7.

107. Burger L, van Nimwegen E. 2008. Accurate prediction of protein-protein interactions from sequence alignments using a Bayesian method. Mol Syst Biol 4:165.

108. Parsons JD, Cocker CR, East AK, Wheatley RM, Ramachandran VK, Kaschani F, Kaiser M, Poole PS. 2022. Factors governing attachment of *Rhizobium leguminosarum* to legume roots. BioRxiv doi:10.1101/2022.11.21.517457.

109. Marchler-Bauer A, Zheng C, Chitsaz F, Derbyshire MK, Geer LY, Geer RC, Gonzales NR, Gwadz M, Hurwitz DI, Lanczycki CJ, Lu F, Lu S, Marchler GH, Song JS, Thanki N, Yamashita RA, Zhang D, Bryant SH. 2013. CDD: conserved domains and protein three-dimensional structure. Nucleic Acids Res 41:D348-52.

110. Vogt SL, Raivio TL. 2012. Just scratching the surface: an expanding view of the Cpx envelope stress response. FEMS Microbiol Lett 326:2-11.

111. Vaara M. 1992. Agents that increase the permeability of the outer membrane. Microbiol Rev 56:395-411.

112. Porte F, Liautard JP, Kohler S. 1999. Early acidification of phagosomes containing Brucella suis is essential for intracellular survival in murine macrophages. Infect Immun 67:4041-7.

113. Starr T, Ng TW, Wehrly TD, Knodler LA, Celli J. 2008. Brucella intracellular replication requires trafficking through the late endosomal/lysosomal compartment. Traffic 9:678-94.

114. Boggiatto PM, Fitzsimmons D, Bayles DO, Alt D, Vrentas CE, Olsen SC. 2018. Coincidence cloning recovery of Brucella melitensis RNA from goat tissues: advancing the in vivo analysis of pathogen gene expression in brucellosis. BMC Mol Biol 19:10.

115. Kleinman CL, Sycz G, Bonomi HR, Rodriguez RM, Zorreguieta A, Sieira R. 2017. ChIP-seq analysis of the LuxR-type regulator VjbR reveals novel insights into the Brucella virulence gene expression network. Nucleic Acids Res 45:5757-5769.

116. Kahl-McDonagh MM, Ficht TA. 2006. Evaluation of protection afforded by Brucella abortus and Brucella melitensis unmarked deletion mutants exhibiting different rates of clearance in BALB/c mice. Infect Immun 74:4048-57.

117. Lin J, Ficht TA. 1995. Protein synthesis in Brucella abortus induced during macrophage infection. Infect Immun 63:1409-14.

118. Cloeckaert A, Vizcaino N, Paquet JY, Bowden RA, Elzer PH. 2002. Major outer membrane proteins of Brucella spp.: past, present and future. Vet Microbiol 90:229-47.

119. Salhi I, Boigegrain RA, Machold J, Weise C, Cloeckaert A, Rouot B. 2003. Characterization of new members of the group 3 outer membrane protein family of Brucella spp. Infect Immun 71:4326-32.

120. Bialer MG, Ferrero MC, Delpino MV, Ruiz-Ranwez V, Posadas DM, Baldi PC, Zorreguieta A. 2021. Adhesive Functions or Pseudogenization of Type Va Autotransporters in Brucella Species. Front Cell Infect Microbiol 11:607610.

121. Abdou E, Deredjian A, Jimenez de Bagues MP, Kohler S, Jubier-Maurin V. 2013. RegA, the regulator of the two-component system RegB/RegA of Brucella suis, is a controller of both oxidative respiration and denitrification required for chronic infection in mice. Infect Immun 81:2053-61.

122. Laub MT, Goulian M. 2007. Specificity in two-component signal transduction pathways. Annu Rev Genet 41:121-45.

123. Hallez R, Mignolet J, Van Mullem V, Wery M, Vandenhaute J, Letesson JJ, Jacobs-Wagner C, De Bolle X. 2007. The asymmetric distribution of the essential histidine kinase PdhS indicates a differentiation event in Brucella abortus. EMBO J 26:1444-55.

124. Karimova G, Ullmann A, Ladant D. 2000. A bacterial two-hybrid system that exploits a cAMP signaling cascade in Escherichia coli. Methods Enzymol 328:59-73.

125. Jumper J, Evans R, Pritzel A, Green T, Figurnov M, Ronneberger O, Tunyasuvunakool K, Bates R, Zidek A, Potapenko A, Bridgland A, Meyer C, Kohl SAA, Ballard AJ, Cowie A, Romera-Paredes B, Nikolov S, Jain R, Adler J, Back T, Petersen S, Reiman D, Clancy E, Zielinski M, Steinegger M, Pacholska M, Berghammer T, Bodenstein S, Silver D, Vinyals O, Senior AW, Kavukcuoglu K, Kohli P, Hassabis D. 2021. Highly accurate protein structure prediction with AlphaFold. Nature 596:583-589.

126. Gao M, Nakajima An D, Parks JM, Skolnick J. 2022. AF2Complex predicts direct physical interactions in multimeric proteins with deep learning. Nat Commun 13:1744.

127. Toro-Roman A, Wu T, Stock AM. 2005. A common dimerization interface in bacterial response regulators KdpE and TorR. Protein Sci 14:3077-88.

128. Herrou J, Willett JW, Fiebig A, Varesio LM, Czyz DM, Cheng JX, Ultee E, Briegel A, Bigelow L, Babnigg G, Kim Y, Crosson S. 2019. Periplasmic protein EipA determines envelope stress resistance and virulence in Brucella abortus. Mol Microbiol 111:637-661.

129. Wetmore KM, Price MN, Waters RJ, Lamson JS, He J, Hoover CA, Blow MJ, Bristow J, Butland G, Arkin AP, Deutschbauer A. 2015. Rapid quantification of mutant fitness in diverse bacteria by sequencing randomly bar-coded transposons. mBio 6:e00306-15.

130. Hartmann R, van Teeseling MCF, Thanbichler M, Drescher K. 2020. BacStalk: A comprehensive and interactive image analysis software tool for bacterial cell biology. Mol Microbiol 114:140-150.

131. Langmead B, Salzberg SL. 2012. Fast gapped-read alignment with Bowtie 2. Nat Methods 9:357-9.

132. Ramirez F, Ryan DP, Gruning B, Bhardwaj V, Kilpert F, Richter AS, Heyne S, Dundar F, Manke T. 2016. deepTools2: a next generation web server for deep-sequencing data analysis. Nucleic Acids Res 44:W160-5.

133. Freese NH, Norris DC, Loraine AE. 2016. Integrated genome browser: visual analytics platform for genomics. Bioinformatics 32:2089-95.

134. Fiebig A, Herrou J, Willett J, Crosson S. 2015. General Stress Signaling in the Alphaproteobacteria. Annu Rev Genet 49:603-25.

135. Gourley CR, Petersen E, Harms J, Splitter G. 2015. Decreased in vivo virulence and altered gene expression by a Brucella melitensis light-sensing histidine kinase mutant. Pathog Dis 73:1-8.

136. Biselli E, Schink SJ, Gerland U. 2020. Slower growth of Escherichia coli leads to longer survival in carbon starvation due to a decrease in the maintenance rate. Mol Syst Biol 16:e9478.

137. Kolter R, Balaban N, Julou T. 2022. Bacteria grow swiftly and live thriftily. Curr Biol 32:R599-R605.

138. Boutte CC, Crosson S. 2013. Bacterial lifestyle shapes stringent response activation. Trends Microbiol 21:174-80.

139. Jaishankar J, Srivastava P. 2017. Molecular Basis of Stationary Phase Survival and Applications. Front Microbiol 8:2000.

140. Celli J, de Chastellier C, Franchini DM, Pizarro-Cerda J, Moreno E, Gorvel JP. 2003. Brucella evades macrophage killing via VirB-dependent sustained interactions with the endoplasmic reticulum. J Exp Med 198:545-56.

141. Comerci DJ, Martinez-Lorenzo MJ, Sieira R, Gorvel JP, Ugalde RA. 2001. Essential role of the VirB machinery in the maturation of the Brucella abortus-containing vacuole. Cell Microbiol 3:159-68.

142. Sieira R, Comerci DJ, Pietrasanta LI, Ugalde RA. 2004. Integration host factor is involved in transcriptional regulation of the Brucella abortus virB operon. Mol Microbiol 54:808-22.

143. Altamirano-Silva P, Meza-Torres J, Castillo-Zeledon A, Ruiz-Villalobos N, Zuniga-Pereira AM, Chacon-Diaz C, Moreno E, Guzman-Verri C, Chaves-Olarte E. 2018. Brucella abortus Senses the Intracellular Environment through the BvrR/BvrS Two-Component System, Which Allows B. abortus To Adapt to Its Replicative Niche. Infect Immun 86.

144. Delrue RM, Deschamps C, Leonard S, Nijskens C, Danese I, Schaus JM, Bonnot S, Ferooz J, Tibor A, De Bolle X, Letesson JJ. 2005. A quorum-sensing regulator controls expression of both the type IV secretion system and the flagellar apparatus of Brucella melitensis. Cell Microbiol 7:1151-61.

145. Rambow-Larsen AA, Rajashekara G, Petersen E, Splitter G. 2008. Putative quorum-sensing regulator BlxR of Brucella melitensis regulates virulence factors including the type IV secretion system and flagella. J Bacteriol 190:3274-82.

146. Paulley JT, Anderson ES, Roop RM, 2nd. 2007. Brucella abortus requires the heme transporter BhuA for maintenance of chronic infection in BALB/c mice. Infect Immun 75:5248-54.

147. Roop RM, 2nd. 2012. Metal acquisition and virulence in Brucella. Anim Health Res Rev 13:10-20.

148. Lamontagne J, Forest A, Marazzo E, Denis F, Butler H, Michaud JF, Boucher L, Pedro I, Villeneuve A, Sitnikov D, Trudel K, Nassif N, Boudjelti D, Tomaki F, Chaves-Olarte E, Guzman-Verri C, Brunet S, Cote-Martin A, Hunter J, Moreno E, Paramithiotis E. 2009. Intracellular adaptation of Brucella abortus. J Proteome Res 8:1594-609.

149. Czolkoss S, Safronov X, Rexroth S, Knoke LR, Aktas M, Narberhaus F. 2021. Agrobacterium tumefaciens Type IV and Type VI Secretion Systems Reside in Detergent-Resistant Membranes. Front Microbiol 12:754486.

150. Kihara A, Akiyama Y, Ito K. 1996. A protease complex in the Escherichia coli plasma membrane: HflKC (HflA) forms a complex with FtsH (HflB), regulating its proteolytic activity against SecY. EMBO J 15:6122-31.

151. Maddalo G, Stenberg-Bruzell F, Gotzke H, Toddo S, Bjorkholm P, Eriksson H, Chovanec P, Genevaux P, Lehtio J, Ilag LL, Daley DO. 2011. Systematic analysis of native membrane protein complexes in Escherichia coli. J Proteome Res 10:1848-59.

152. Bittner LM, Westphal K, Narberhaus F. 2015. Conditional Proteolysis of the Membrane Protein YfgM by the FtsH Protease Depends on a Novel N-terminal Degron. J Biol Chem 290:19367-78.

153. Christie PJ, Whitaker N, Gonzalez-Rivera C. 2014. Mechanism and structure of the bacterial type IV secretion systems. Biochim Biophys Acta 1843:1578-91.

154. Jiao H, Zhou Z, Li B, Xiao Y, Li M, Zeng H, Guo X, Gu G. 2021. The Mechanism of Facultative Intracellular Parasitism of Brucella. Int J Mol Sci 22.

155. Shevchenko A, Wilm M, Vorm O, Jensen ON, Podtelejnikov AV, Neubauer G, Shevchenko A, Mortensen P, Mann M. 1996. A strategy for identifying gel-separated proteins in sequence databases by MS alone. Biochem Soc Trans 24:893-6.

156. Demichev V, Messner CB, Vernardis SI, Lilley KS, Ralser M. 2020. DIA-NN: neural networks and interference correction enable deep proteome coverage in high throughput. Nat Methods 17:41-44.

157. Cardona ST, Choy M, Hogan AM. 2018. Essential Two-Component Systems Regulating Cell Envelope Functions: Opportunities for Novel Antibiotic Therapies. J Membr Biol 251:75-89.

158. Macritchie DM, Raivio TL. 2009. Envelope Stress Responses. EcoSal Plus 3.

159. Saha S, Lach SR, Konovalova A. 2021. Homeostasis of the Gram-negative cell envelope. Curr Opin Microbiol 61:99-106.

160. Stewart V. 2003. Biochemical Society Special Lecture. Nitrate- and nitrite-responsive sensors NarX and NarQ of proteobacteria. Biochem Soc Trans 31:1-10.

161. Reyes Ruiz LM, Fiebig A, Crosson S. 2019. Regulation of bacterial surface attachment by a network of sensory transduction proteins. PLoS Genet 15:e1008022.

162. Al-Bassam MM, Bibb MJ, Bush MJ, Chandra G, Buttner MJ. 2014. Response regulator heterodimer formation controls a key stage in Streptomyces development. PLoS Genet 10:e1004554.

163. Castanie-Cornet MP, Cam K, Bastiat B, Cros A, Bordes P, Gutierrez C. 2010. Acid stress response in Escherichia coli: mechanism of regulation of gadA transcription by RcsB and GadE. Nucleic Acids Res 38:3546-54.

164. Venkatesh GR, Kembou Koungni FC, Paukner A, Stratmann T, Blissenbach B, Schnetz K. 2010. BglJ-RcsB heterodimers relieve repression of the Escherichia coli bgl operon by H-NS. J Bacteriol 192:6456-64.

165. Conde-Alvarez R, Palacios-Chaves L, Gil-Ramirez Y, Salvador-Bescos M, Barcena-Varela M, Aragon-Aranda B, Martinez-Gomez E, Zuniga-Ripa A, de Miguel MJ, Bartholomew TL, Hanniffy S, Grillo MJ, Vences-Guzman MA, Bengoechea JA, Arce-Gorvel V, Gorvel JP, Moriyon I, Iriarte M. 2017. Identification of lptA, lpxE, and lpxO, Three Genes Involved in the Remodeling of Brucella Cell Envelope. Front Microbiol 8:2657.

APPENDIX

Script for counting barcode sequencing reads

Note: this script is written as a bash file and all the fasta files from Illumina sequencing should be in the same directory.

```
read -p "Enter the directory:" directory

if [ -d "$directory" ]; then
        for file in "$directory"/*; do
                echo "Processing file:$file"
                count_barcode19=$(grep -o 'CATTTTCACAGTCGAGACACGTCATGCGAT' $file
| wc -w)
                count_barcode5=$(grep -o 'GGAAACATTCTACGCAAGTCTTCCTCCCCA' $file |
wc -w)
                count_barcode37=$(grep -o 'TCTAAAGTTTGTCATTCCTACTCGTACTGC' $file |
wc -w)
                count_barcode24=$(grep -o 'GAAACATTTGGTGCATTTTGTGCCCCTCGG' $file
| wc -w)
                count_barcode15=$(grep -o 'ACCAGCTAATGGACCGGTGCCGAGTCGATT'
$file | wc -w)
                count_barcode13=$(grep -o 'TAGGGCTCTCCGGCAGTCGCGCTGTATCCC'
$file | wc -w)
                count_barcode30=$(grep -o 'CCTTGATTGGCGTTGCGCGCTTACATCTTA' $file
| wc -w)
                count_barcode25=$(grep -o 'TACGGCGTACCACGACCATGTAATTCCACT' $file
| wc -w)
                count_barcode10=$(grep -o 'CTTATATCTCAGTTCGCGGTGGCTAACCTC' $file
| wc -w)
                count_barcode20=$(grep -o 'GCGTCCGTCGCGCTGCCCCCTTATTAACTC'
$file | wc -w)
                count_barcode9=$(grep -o 'CTCGGTGATGTCTCGAATATGGGCGCTTGG' $file
| wc -w)
                count_barcode27=$(grep -o 'AGCGTCTAAGGTTTGACTTGGTGATTACTC' $file
| wc -w)
                count_barcode11=$(grep -o 'TCCCATCGTCATTTCCGGTTAAGGTCTCTA' $file
| wc -w)
                count_barcode18=$(grep -o 'GACTTAGCGAATCGACGCGATTGCGGATGC'
$file | wc -w)
                count_barcode14=$(grep -o 'CCGATGGTCTCCTAGTCCTTGCCCCGGAGC'
$file | wc -w)
                count_barcode16=$(grep -o 'CTTAACCCCGTCGGTATGGCCATTTCGATT' $file
| wc -w)
                count_barcode23=$(grep -o 'ACTTTAACAGCCATGGGCTTCTCGATTCAT' $file
| wc -w)
                count_barcode26=$(grep -o 'ACTTCACGTAAAGGCGACTCCGGTGCTCCG'
$file | wc -w)
                count_barcode8=$(grep -o 'GGATTTTTTTCAATCTGCACGGGGATTTTT' $file |
wc -w)
```

```
                count_barcode28=$(grep -o 'CTATCGCTTTCTTGCCCCGCCGTCTGTCTG' $file
| wc -w)
                count_barcode22=$(grep -o 'TTCTTATGTGACTGTCACTACCTTCGCGTC' $file
| wc -w)
                count_barcode21=$(grep -o 'TCTTCATGACTCATGGTCAAGGAGAATCC' $file |
wc -w)
                count_barcode17=$(grep -o 'CCTATCTCTACCGCGATAAACTCCTGTCTA' $file
| wc -w)
                count_barcode3=$(grep -o 'TGCGTAACTAGTTTAGTGGTCATGTTTTAA' $file |
wc -w)
                count_barcode33=$(grep -o 'CGTATCTCGAATCTGCCAATATGTGCTAAG' $file
| wc -w)
                count_barcode34=$(grep -o 'TGCTGCTCGCAATCATACTCGCGGTACCCT' $file
| wc -w)
                count_barcode36=$(grep -o 'ACTTAATATGGTTCTCCGCATATGCCCTAA' $file
| wc -w)
                echo "the results for $file are:" >> result.txt
                echo "$count_barcode19" >> result.txt
                echo "$count_barcode5" >> result.txt
                echo "$count_barcode37" >> result.txt
                echo "$count_barcode24" >> result.txt
                echo "$count_barcode15" >> result.txt
                echo "$count_barcode13" >> result.txt
                echo "$count_barcode30" >> result.txt
                echo "$count_barcode25" >> result.txt
                echo "$count_barcode10" >> result.txt
                echo "$count_barcode20" >> result.txt
                echo "$count_barcode9" >> result.txt
                echo "$count_barcode27" >> result.txt
                echo "$count_barcode11" >> result.txt
                echo "$count_barcode18" >> result.txt
                echo "$count_barcode14" >> result.txt
                echo "$count_barcode16" >> result.txt
                echo "$count_barcode23" >> result.txt
                echo "$count_barcode26" >> result.txt
                echo "$count_barcode8" >> result.txt
                echo "$count_barcode28" >> result.txt
                echo "$count_barcode22" >> result.txt
                echo "$count_barcode21" >> result.txt
                echo "$count_barcode17" >> result.txt
                echo "$count_barcode3" >> result.txt
                echo "$count_barcode33" >> result.txt
                echo "$count_barcode34" >> result.txt
                echo "$count_barcode36" >> result.txt
        done
else
        echo "Directory doesn't exist"
fi
```